5-2010

Pulsed-Laser Excited Photothermal Study of Glasses and Nanoliter Cylindrical Sample Cell Based on Thermal Lens Spectroscopy

Prakash Raj Joshi
Utah State University

PULSED-LASER EXCITED PHOTOTHERMAL STUDY OF GLASSES AND NANOLITER CYLINDRICAL SAMPLE CELL BASED ON THERMAL LENS SPECTROSCOPY

by

Prakash Raj Joshi

A dissertation submitted in partial fulfillment
of the requirements for the degree

of

DOCTOR OF PHILOSOPHY

in

Chemistry

Approved:

----------	----------
Dr. Stephen E. Bialkowski Major Professor	Dr. Robert S. Brown Committee Member
----------	----------
Dr. Alexander I. Boldyrev Committee Member	Dr. T. C. Shen Committee Member
----------	----------
Dr. David Farrelly Committee Member	Dr. Byron R. Burnham Dean of Graduate Studies

UTAH STATE UNIVERSITY
Logan, Utah

2010

ABSTRACT

Pulsed-laser Excited Photothermal Study of Glasses and Nanoliter Cylindrical Sample Cell Based on Thermal Lens Spectroscopy

by

Prakash Raj Joshi, Doctor of Philosophy

Utah State University, 2010

Major Professor: Stephen E. Bialkowski
Department: Chemistry and Biochemistry

The research in this dissertation presents Pulsed-Laser Excited photothermal studies of optical glasses and cylindrical sample cell.

First, a study of a photothermal lens experiment and the finite element analysis modeling for commercial colored glass filters is done. The ideal situation of a semi-infinite cylinder approximate model used to describe the photothermal lens experiment requires the boundary condition that there is no transfer of heat from the glass to surrounding when the glass is excited with a laser. The finite element analysis modeling for photothermal signal with coupling heat with surrounding shows the thermal heat transfer between the glass surface and the coupling fluid. This work shows that the problem can be resolved by using pulsed laser excitation where the signal decay is faster than the heat diffusion to the surrounding, and finite element analysis modeling to correct the likely deviation from semi-infinite cylinder approximate models.

Second, finite element analysis modeling of a photothermal lens signal also shows that there are slow and fast components of signals, which are detected by using a fast response detector and is explained to be due to the axial and radial transfer of heat. A semi-analytical theoretical description of the mode-mismatched continuous and pulsed-laser excitation thermal lens effect that accounts for heat coupling both within the sample and out to the surrounding is presented. The results are compared with the finite element analysis solution and found to be an excellent agreement. The analytical model is then used to quantify the effect of the heat transfer from the sample surface to the air coupling fluid on the thermal lens signal. The results showed that the air signal contribution to the total photothermal lens signal is significant in many cases.

Third, surface deformation phenomena are quite common when glasses are excited by laser. Finite element analysis modeling of a surface deformation phenomenon is done. A thermal lens reflection experiment is carried out and results are compared with modeling. The effect of coupling fluid on sample is taken in to account to make more accurate measurement of thermophysical properties of solid sample.

Fourth, a novel apparatus for performing photothermal lens spectroscopy is described which uses a low-volume cylindrical sample cell with a pulsed excitation laser. Finite element analysis modeling is used to examine the temperature profile and the photothermal signal. The result of finite element analysis is compared with the experimental result. The experimental photothermal lens enhancement has been found to be that predicted from theory within experimental error.

(176 Pages)

DEDICATION

In memory of my Iza (Mom)

ACKNOWLEDGMENTS

First of all I would like to record my deepest gratitude to my major advisor, Professor Stephen E. Bialkowski, for his supervision, advice, and guidance from the very early stage of this research as well as giving me extraordinary experiences throughout the work. Above all and the most needed, he provided me unflinching encouragement and support in various ways. His truly scientist intuition has made him as a constant oasis of ideas and passions in science, which exceptionally inspire and enrich my growth as a student, a researcher, and a scientist want-to-be. I am indebted to him more than he knows.

I gratefully acknowledge all of my advisory committee members, Dr. Robert S. Brown, Dr. Alexander I. Boldyrev, Dr. David Farrelly, and Dr. T. C. Shen, for their time, advice, and supervision during my education at Utah State University. I am also grateful to my former advisory committee member, Dr. Philip Silva, for his guidance during his stay at Utah State University.

I would especially thank Dr. Brown for his suggestions and readiness to help during my education at USU whenever I needed it.

There are no words to express my appreciation to my wife, Paban, whose dedication, love, and persistent confidence in me has taken the load off my shoulder. I owe her for being unselfish, loving, and such a caring mom of our beautiful kids Vinayak, Gargee, and Vitaraag.

Many thanks go in particular to my co-graduate students in the Department of Chemistry and Biochemistry, especially to Oluwatosin O. Dada and Mark Erupe for their companionship and nice time we spent together.

I would like to thank the USU Department of Chemistry and Biochemistry for giving me an opportunity to pursue my graduate study and support in the form of a teaching assistantship and research assistantship through 2005 to 2010.

Finally, I would like to thank everybody who was important to the successful realization of this dissertation, as well as expressing my apology that I could not mention each one personally.

Prakash Raj Joshi

CONTENTS

Page

LIST OF TABLES

LIST OF FIGURES

LIST OF ABBREVIATIONS

Abbreviations	Definition
AU	Spectroscopic Absorbance Unit
cw	Continuous Wave
FEA	Finite Element Analysis
$FeCp_2$	Iron (II) Dicyclopentadine
HeNe	Helium Neon
PDE	Partial Differential Equation
TEM	Transverse Electromagnetic Mode
TL	Thermal Lens
TLS	Thermal Lens Spectrometry

CHAPTER 1

INTRODUCTION

Realizing that, it would be easy to compare the measurement results of different laboratories if all researchers share the same standard calibration materials for photothermal lens apparatus, our laboratory started experimenting on colored glass filters, which could serve as such a standard instead of using liquid sample. Colored glass or volume-absorbing neutral density filters are ubiquitous, stable over time, and easy to handle. Thermal lens experiments in reflection mode and thermal deflection confirmed the induced thermal expansion in the sample and the heat transfer to the coupling fluid. After carrying out the experiments and finite element analysis (FEA) of continuous laser-excited photothermal spectrometry of CdS_xSe_{1-x} doped glasses, two problems were realized.[1]

First, the colored glass and neutral density filters that we examined had anomalous physical properties. In particular, we find that these optical glasses have a positive temperature-dependent refractive index change coefficient. Second, heat transfer from a glass plate excited with a laser is far from the ideal situation described by the semi-infinite cylinder approximate models that are most often used to describe the photothermal lens experiment.

The problems have been resolved, first, by using pulsed laser excitation which creates a temperature change on timescales short compared to heat transfer, and second by using FEA to model heat transfer to the surroundings to take account of the likely deviation from the semi-infinite cylinder approximate models. FEA modeling is

particularly useful to account for surface heat transfer that will occur in glasses and other samples where the absorbing material is in direct contact with the coupling fluid surroundings.

In pulsed laser excitation, the temperature change is produced almost instantly or at least in an amount of time during which little heat has diffused to the surroundings. In this regard, pulsed laser excitation can be advantageous for measuring absorbance. Photothermal signals are modeled for heat transfer from glass to air after laser excitation and the FEA model results are subsequently compared to the experimental signals. FEA model results for colored glass filters with and without boundary conditions and the experimental investigations of thermal lensing in colored glass filters and liquid sample cells are presented. Thermal lens experiments and FEA modeling are presented to investigate the temperature profile, change in refractive index of CdS_xSe_{1-x}-doped glass, and to determine the thermo-optical coefficient, dn/dT.[2]

The FEA modeling of colored silica glass, of absorption coefficient 3.8 $m^{-1}$with the surrounding environment being air shows that there are slow and fast signal decay component in glass. And time constants varies with square of the excitation beam width according to the equation, $t_c = w^2/4D_t$, The fast and slow decay of signals are interpreted to be due to the fast transfer of heat in axial and slow transfer of heat in radial direction of the excitation laser beam. After realizing the fact of fast and slow components in glass, transmission and reflection photothermal experiments were carried out using fast response detector to detect the event. And that fast and slow decay of signal were found. Works done in collaboration with Nelson G. C. Astrath, Luis C. Malacarne, Paulo R. B.

Pedreira, Marcos P. Belancon, and Mauro L. Baesso from Departamento de Física, Universidade Estadual de Maringá, Maringá-PR, 87020-900, Brazil, have been presented. In which a analytical theoretical description of the mode-mismatched continuous and pulsed-laser excitation thermal lens effect, by taking into account the coupling of heat both within the sample and out to the surroundings, is presented. The results are compared with finite elemental analysis solution and found to be an excellent agreement. The analytical model is then used to quantify the effect of the heat transfer from the sample surface to the air coupling fluid on the thermal lens signal. The results showed that the air signal contribution to the total photothermal lens signal is significant in many cases.

When focused excitation laser beam shines on a solid material, one of the most ordinary observed effects is the surface displacement or deformation. The absorbed energy converts to heat, resulting in expansion and then local surface displacement of the solid sample.

The FEA modeling shows that there is surface deformation due to pulse laser heating of colored glass filters, and consequently the optical path length of them changed. The modeling also shows that the extent of deformation increases with absorption coefficient of glass. It has been found that the photothermal lens signals are affected due to surface deformation phenomenon.

The photothermal expansion is modeled for glasses by FEA modeling with and without heat coupling environment. Comsol Multiphysics,3.4, thermal-structural interaction module was used to model. Time resolved reflection photothermal lens experiment is carried out using silica glass and thermoelastic surface displacement is

measured. An experimentally monitored thermoelastic surface displacement result is compared with that of modeling and are found to be very close.

A low volume cylindrical sample cell made of silica glass having an internal diameter 240 and external diameter 1 cm, fitted in 1 cm^3 steel block, for performing photothermal lens spectroscopy with pulsed-laser excitation is described. Experiments to verify the operation of the apparatus are performed with dicyclopentadienyl iron ($FeCp_2$) in ethanol. The results were compared with that of standard conventional cell of 2 mm size. The whole sample cell volume is irradiated with pulsed excitation laser. The photothermal lens element is formed by thermal diffusion from the irradiated sample volume through the sample cell walls. The apparatus has been found to work with cells designed to contain sample volumes to 361 nL. Larger and smaller volume cells are practical. FEA modeling has been also used for the better understanding of temperature profile and for the comparison of the experimental results.

Photothermal lens signals processed in the usual fashion are found to be relatively linear, reproducible, and consistent with the model based on heat conduction through the sample cell walls. The experimental photothermal lens enhancement is found to be that predicted from theory within experimental error.

GLASSES

A glass, whether in bulk, fiber, or film form, is a non-crystalline (or amorphous) solid. Glasses are typically brittle and often optically transparent commonly used for windows, bottles, or eyewear. In principle, any substance can be vitrified by quenching it

from the liquid state, while preventing crystallization, into a solid glass. Cooling a viscous liquid fast enough to avoid crystallization most commonly forms a glass.[3-4]

Most commercially available glasses prepared by melting and quenching, available in large bulk shapes, are silicates of one type or another. Besides common silica-based glasses, many other inorganic and organic materials may also form glasses, including plastics (e.g., acrylic glass), carbon, metals, carbon dioxide, phosphates, borates, chalcogenides, fluorides, germanates (glasses based on GeO_2), tellurites (glasses based on TeO_2), antimonates (glasses based on Sb_2O_3), arsenates (glasses based on As_2O_3), titanates (glasses based on TiO_2), tantalates (glasses based on Ta_2O_5), nitrates, carbonates, and many other substances.[5-6]

Some glasses that do not include silica as a major constituent may have physico-chemical properties useful for their application in fibre optics and other specialized technical applications. These include fluoride glasses (fluorozirconates, fluoroaluminates), aluminosilicates, phosphate glasses, and chalcogenide glasses.

Glass plays an essential role in science and industry. The optical and physical properties of glass make it suitable for applications such as flat glass, container glass, optics and optoelectronics material, laboratory equipment, thermal insulator, reinforcement fiber, and art. It is important to realize that some materials, which have a very strong glassy appearance under the naked eye, or even under a laser beam, may actually contain a fine dispersion of very minute crystals with dimensions well below 100 nm, *i.e.*, nanocrystals.

Although most industrial glasses are based on the SiO_2, many other compounds are normally added to modify it. Cadmium sulfoselenide is the pigment currently used for

making red glasses. The color is due to colloidal particles of the semiconductor cadmium sulfoselenide; photons with energies greater than the band gap of the semiconductor undergo absorption and consequently the optical absorption spectra have a sharp transmission cut-off. The color can be controlled by the ratio of cadmium sulfide and cadmium selenide in the pigment, and can vary from yellow to dark red.

Semiconductor-doped glass consists of microcrystallites of II-VI semiconductor randomly scattered in a glass host. The semiconductor crystallite can be a binary or ternary compound giving a widely tunable band-gap. This property has lead to the application of the glass as short wavelength cut-off filters. There has been a great deal of interest in the glass for use as a nonlinear optical material. In order to enhance nonlinear optical effects by increasing interaction lengths, the glass has been fabricated in both waveguide and optical fiber form.

Glasses doped with semiconductor nanocrystals are candidates for resonant non-linear optical materials. They show rapid response times of a few tens of ps. One such glass has been available for many years as a sharp cut color filter; it contains a very fine (diameter ~ 10 nm) CdS_xSe_{1-x} microcrystalline phase dispersed in the glass matrix.

PHOTOTHERMAL SPCTROSCOPY

Photothermal spectroscopy is a group of high sensitivity methods used to measure optical absorption and thermal characteristics of a sample. The basis of photothermal spectroscopy is a *photo*-induced change in the *thermal* state of the sample. Light energy absorbed and not lost by subsequent emission results in sample heating. This heating results in a temperature change as well as changes in thermodynamic parameters of the

sample which are related to temperature. Measurements of the temperature, pressure, or density changes that occur due to optical absorption are ultimately the basis for photothermal spectroscopic methods.[7]

Photothermal spectroscopy is more sensitive than optical absorption measured by transmission methods. The high sensitivity of the photothermal spectroscopy methods has led to applications for analysis of low absorbance samples.

The basic processes responsible for photothermal spectroscopy signal generation is optical radiation, usually from a laser is used to excite a sample. Absorption of radiation from the excitation source followed by non-radiative excited state relaxation results in sample temperature, and density changes. The density change is primarily responsible for the refractive index change, which can be probed by a variety of methods.[7]

In a generic apparatus used for photothermal spectroscopy the excitation light heats the sample. The probe light monitors changes in the refractive index of the sample resulting from heating. The spatial and propagation characteristics of the probe light will be altered by the refractive index. The spatial filter selects those components of the altered probe light that change with the samples' refractive index. The optical detector monitors changes in the probe light power past the spatial filter. In some apparatuses, a spatial filter and a single channel detector are combined using an image detector. Signals generated by the photodetector are processed to enhance the signal to noise ratio.

There are several methods and techniques used in photothermal spectroscopy. Each of these has a name indicating the specific physical effect measured. Photothermal deflection spectroscopy, photothermal diffraction spectroscopy and photothermal lensing spectroscopy are most commonly used techniques.[7]

The first photothermal spectroscopic method to be applied for sensitive chemical analysis was photothermal lens spectroscopy. The photothermal lens results from optical absorption and heating of the sample in regions localized to the extent of the excitation source. The lens is created through the temperature dependence of the sample refractive index. The lens usually has a negative focal length since most materials expand upon heating and the refractive index is proportional to the density. This negative lens causes beam divergence and the signal is detected as a time dependent decrease in power at the center of the beam. Measurements of the change in divergence of a laser beam after formation of the thermal lens allows determination of the absorbances of $10^{-7} – 10^{-6}$, which correspond to analyte concentrations of $10^{-11} – 10^{-10}$ mole/L. Thus, thermal lens spectrometry is 100 — 1000 times more sensitive than conventional spectrophotometry.

There are two main types of optical apparatus used in photothermal lens spectroscopy. The simplest is the single-laser apparatus. The second type of apparatus commonly used is the two-laser design. In this design one beam is used to excite the sample, and the second beam is used to probe the resulting photothermal lens.

Thermal lens spectrometry was first reported by Gordon *et al*.[8] It can measure very low optical absorption coefficients of transparent samples,[9] and has been used in a wide range of applications such as trace analyses, flowing streams, flow injection, quantum yields and chemical reaction kinetics.[10] There are very good review papers on the subject. [10-12] This is a topic, which has been receiving a great deal of attention especially in the case of some silicate, [13, 14] calcium aluminate, [15, 16] fluoride, [17] chalcogenide, and chalcohalides glasses. Time-resolved TL technique has been shown to be a useful method to measure the thermal diffusivity of transparent samples as well as the temperature

coefficient of optical path length change.[13, 14, 17, 18] Needless to say; these studies are of great interest for glass laser designers and researchers.

The knowledge of the thermo-optical properties is essential for evaluating the figures of merit of optical glasses. Photothermal lens spectroscopy is one of the best methods to measure these properties.

FINITE ELEMENT ANALYSIS MODELING OF PHOTOTHERMAL PHENOMNON

The finite element analysis (FEA) is a numerical technique for finding approximate solutions of partial differential equations (PDE) as well as of integral equations. The solution approach is based either on eliminating the differential equation completely (steady state problems), or rendering the PDE into an approximating system of ordinary differential equations, which are then numerically integrated using standard techniques such as Euler's method, Runge-Kutta, etc.

FEA is a fairly recent discipline that allows the numerical solution of governing physical equations over complicated geometric domains. The method is regularly applied to the structural analysis of designs with complex geometries. The part being analyzed is divided into many small regions called "finite elements." The physical behavior within each element is understood in concise mathematical terms. Assemblage of all elements' behavior produces a large matrix equation, which is solved for the quantity of interest, such as the deformation due to a maximum loading condition. Additional quantities, such as stresses, are then computed.[19]

FEA is a fairly recent discipline crossing the boundaries of mathematics, physics, and engineering and computer science. The method has wide application and enjoys

extensive utilization in the structural, thermal and fluid analysis areas. The finite element method is comprised of three major phases: (1) pre-processing, in which the analyst develops a finite element mesh to divide the subject geometry into subdomains for mathematical analysis, and applies material properties and boundary conditions, (2) solution, during which the program derives the governing matrix equations from the model and solves for the primary quantities, and (3) post-processing, in which the analyst checks the validity of the solution, examines the values of primary quantities (such as displacements and stresses), and derives and examines additional quantities (such as specialized stresses and error indicators).

COMSOL Multiphysics is a finite element analysis, solver and simulation software package for various physics and engineering applications, especially coupled phenomena. It is excellent, state-of-the-art software for the solution of many types of partial differential equations (PDEs). Both stationary and time-dependent analysis can be performed by numerical techniques based on the finite element method for the spatial discretization.[20]

COMSOL Multiphysics also offers an extensive interface to MATLAB and its toolboxes for a large variety of programming, preprocessing and postprocessing possibilities. The packages are cross-platform (Windows, Mac, Linux, and UNIX.) In addition to conventional physics-based user-interfaces, COMSOL Multiphysics also allows for entering coupled systems of partial differential equations (PDEs). The PDEs can be entered directly or using the so-called weak form.

The software runs FEA together with adaptive meshing and error control using a variety of numerical solver to solve the PDEs. Models of different possible type can be

built in the COMSOL Multiphysics user interface. Models of heat transfer module and the thermal structural interaction module of Comsol Multiphysics v 3.3 and 3.5 (Comsol Inc.) in various samples are performed in this dissertation.

The analysis steps in finite element modeling are: [21]

1. Defining multiphysics: Definition of the desired physics mode (heat transfer by conduction, convection, and/or radiation) and types of solution (steady state or transient).
2. Geometry modeling: Definition of sample geometry and materials, boundary conditions, and heat sources and sinks.
3. Meshing: Breaking the geometry into sub-domains or element meshing.
4. Solve the model: Solving the model by choosing appropriate solver parameters.
5. Post-processing: The solution is plotted using a variety of visualization techniques. The data from these plots can also be exported for further analysis in spreadsheet software such as Excel.

ORGANIZATION OF THE REMAINING CHAPTERS

The rest of the chapters in this dissertation present the detailed research documents of pulsed –laser excited photothermal lens spectroscopic method of study of glasses and nanolitre cylindrical sample cell. FEA modeling, simulating the experimental samples, has been done to compare and correct the experimental measurements with the help of Comsol Multiphysics software.

Chapter 2 explains how the pulsed-laser excited photothermal lens spectrometry of low absorbing colored glass filters overcome the problem encountered of coupling of heat

with the surrounding fluid while doing continues laser excited photothermal spectroscopy. Details of thermal lens experiments and FEA modeling are presented to investigate change in refractive index of cadmium sulfoselenium doped glass, and to determine the thermo-optical coefficient. It turns out that the glass produce positive refractive index change contrary to the expected negative index of refraction change.

Chapter 3 contains photothermal experiments (transmission and reflection) and the FEA modeling details of the fast and slow signal decay component in glass. The fast and slow decay of signals are interpreted to be due to the fast transfer of heat in axial and slow transfer of heat in radial direction of the excitation laser beam.

In Chapter 4 details of FEA modeling of surface displacement or deformation phenomenon observed due to photothermal heating of glass are presented. And the effects of coupling fluids on thermal expansion and the photothermal signal are discussed.

Experiments and the FEA modeling, to verify the operation of a nanoliter cylindrical sample cell apparatus for performing photothermal lens spectroscopy with pulsed-laser excitation, are discussed described in chapter 5.The apparatus has been found to work with cells designed to contain sample volumes to 361 nL
A theoretical description of the mode-mismatched thermal lens effect by taking into account the coupling of heat both within the sample and out to the surroundings medium is presented in chapter 6.And the chapter 7 discuses the analytical and finite element analysis modeling methods of the pulsed laser excited photothermal lens signal of solids samples surrounded by air. Chapter 8 is a brief summary of the results in Chapters 2-7. All figures data are available in Appendix A.

REFERENCES

1. Oluwatosin Dada, Matthew R. Jorgensen, and Stephen E. Bialkowski *Applied Spectroscopy* **61**, 1373-1378 (2007).
2. Prakash R. Joshi, Oluwatosin O. Dada, and Stephen E. Bialkowski *Applied Spectroscopy* **63**, 815 (2009).
3. Douglas, R. W. *A History of Glassmaking* (G T Foulis & Co Ltd., Henley-on-Thames, 1972).
4. Zallen, R. *The Physics of Amorphous Solids* (Wiley, New York, 1983).
5. Elliot, S. R., *Physics of Amorphous Materials* (Longman Group Ltd., London, 1984).
6. Horst Scholze, *Glass – Nature, Structure, and Properties* (Springer-Verlag, New York, 1991).
7. S. E. Bialkowski, *Photothermal Spectroscopy Methods for Chemical Analysis* (Wiley, New York, 1996).
8. J.P. Gordon, R.C.C. Leite, R.S. More, S.P.S. Porto, and J.R. Whinnery, J. Appl. Phys. **36**, 3 (1965).
9. J. Shen, and R.D. Snook, Anal. Proc. **26,** 403 (1989).
10. R.D. Snook, and R.D. Lowe, Analyst **120,** 2051 (1995).
11. K.L. Jansen, and J.M. Harris, Anal. Chem. **57**, 1698 (1985).
12. H.L. Fang, and R.L. Swofford, in: D.S. Kliger (Ed.), *Ultrasensitive Laser Spectroscopy* (Academic Press, New York, 1983).
13. M.L. Baesso, J. Shen, and R.D. Snook, J. Appl. Phys. **75**, 3733 (1994).

14. M.L. Baesso, J. Shen, and R.D. Snook, Chem. Phys. Lett. **197**, 255 (1992).

15. M.L. Baesso, A.C. Bento, A.A. Andrade, T. Catunda, J.A. Sampaio, and S. Gama, J. Non-Cryst. Solids **219**, 165 (1997).

16. M.L. Baesso, A.C. Bento, A.A. Andrade, T. Catunda, E. Pecoraro, L.A.O. Nunes, J.A. Sampaio, and S. Gama, Phys. Rev. B. **57**,10545 (1998).

17. S.M. Lima, T. Catunda, R. Lebullenger, A.C. Hernandes, M.L. Baesso, A.C. Bento, and L.C.M. Miranda, Phys. Rev. B **60**, 15173 (1999).

18. M.L. Baesso, A.C. Bento, A.R. Duarte, A.M. Neto, L.C. Miranda, J.A. Sampaio, T. Catunda, S. Gama, and F.C.G. Gandra, J. Appl. Phys. **85**, 8112 (1999).

19. G. Strang, and G. Fix, *An Analysis of The Finite Element Method* (Prentice Hall, Englewood Cliffs, N.J., 1973).

20. Comsol Inc. *Comsol multiphysics 3.3 user's Guide*.

21. Oluwatosin O Dada and Stephen E Bialkowski , *Applied Spectroscopy* **62**, 1336 (2008).

CHAPTER 2

PULSED LASER EXCITED PHOTOTHERMAL LENS SPECTROMETRY OF CdS_XSe_{1-X} DOPED SILICA GLASSES[a]

ABSTRACT

Experimental results for photothermal lens measurements are compared to finite elemental analysis models for commercial colored glass filters. Finite elemental analysis software is used to model the photothermal effect by simulating the coupling of heat both within the sample and out to the surroundings. Modeling shows that heat transfer between the glass surface and the air coupling fluid has a significant effect on the predicted time dependent photothermal lens signals. For comparison with experimental signals, a simple equation based on the finite element analysis result is proposed for accounting for the variance of experimental data where this type of heat coupling situation occurs. The colored glass filters are found to have positive thermo-optical coefficients. The net positive dn/dT of CdS_xSe_{1-x} doped glass filters is considered to be the consequence of counteracting factors: optical nonlinearity, stress-induced birefringence, and the structural network of glass. Finite element analysis modeling results are also used to correlate experimental measurements of different sample geometries. In particular, the glass samples are compared to ethanol solutions of iron (II) dicylopentadiene in a sample cuvette even though heat transfer is different for these two samples.

---

[a]COAUTHORED BY PRAKASH RAJ JOSHI, OLUWATOSIN O. DADA, AND STEPHEN E. BIALKOWSKI.

INTRODUCTION

Thermal lens spectrometry (TLS) can measure very low optical absorption coefficients of transparent samples.[1] Time resolved TLS has been shown to be a useful method for measuring the thermal diffusivity of transparent samples as well as the temperature coefficient of the optical path length, s, change, ds/dT.[2–5] The knowledge of the thermo-optical properties is essential for evaluating the figures of merit of optical glasses. They can readily be used to determine the working glass conditions[6,7] such as thermal shock, thermal stress resistance,[8] and thermal lens effect.[6,7,9–17] Therefore, considering the importance of determining the thermo-optical properties of laser glass materials, a simple and accurate method to determine these properties quantitatively is of utmost importance.

Glasses doped with semiconductor microcrystals are candidates for resonant nonlinear optical materials. The colored glass cut-off filters that have been commercially available for many years contain semiconductor microcrystals on the order of 10 nm and by today's standards these microcrystals would be called nanoparticles.[18-21]The semiconductor nanoparticles are responsible for the optical absorption in these colored glass filters. The chemical composition, size, and method of synthesis of the nanoparticles affect the optical properties of the glass filters, most of which are high-pass wavelength cut-off filters used in spectroscopy and other optical technologies.[22]

The changes in absorption of the semiconductor crystallites relative to the bulk semiconductor lead to refractive index changes through the Kramers–Kronig transformation. The value of $\chi^{(3)}$ will be proportional to the reciprocal of the confinement

volume and will normally increase with decreasing size. Therefore, larger nonlinearities are expected for glasses containing smaller particles and larger volume fractions of semiconductor particles.

Pereira et al. reported the complexity of the solution to theoretical treatment of the thermally induced bistability in semiconductor-doped glass due to the thermal lens effect.[23]The photothermal lens results from optical absorption and heating of the sample in regions localized to the extent of the excitation source. The lens is created because of the temperature dependence of the sample refractive index. The lens usually has a negative focal length since most materials expand upon heating and, as a first approximation; the refractive index is simply proportional to the density. This negative focal length lens causes beam divergence and the signal is detected as a time-dependent decrease in power at the center of the beam.[24] However, we find that the optical glasses have a positive temperature-dependent refractive index change coefficient.

Models are used to calculate temperature changes resulting from the absorption of excitation laser power. The combination of experiment and theory, then, allows one to determine the temperature-dependent refractive index change, dn/dT, for the transparent sample. Theoretical models of thermal lens effects in fluids are well established; a number of approximations are commonly used to obtain tractable analytical results.[25, 26] The ideal situation of a semi-infinite cylinder approximate model used to describe the photothermal lens experiment assumes the boundary condition wherein no heat is transferred from the sample to the surroundings along the dimension of the excitation laser beam propagation.

In most practical situations heat is transferred from the sample to the surroundings along the axial dimension. This is especially true when the heated sample is in contact with air or another coupling fluid, as in the case of the glass filters used herein. Therefore, some correction in the results from the experiment is required in order to obtain accurate predictions of parameters derived from the photothermal effect.

The aim of this paper is to use the thermal lens method to obtain accurate measurements of the thermo-optical properties of glasses, first by using pulsed laser excitation, which creates a temperature change on timescales short compared to heat transfer, and second by using finite element analysis (FEA) to model heat transfer to the surroundings. In pulsed laser excitation, the temperature change is produced almost instantly or at least in an amount of time during which little heat has diffused to the surroundings. In this regard, pulsed laser excitation can be advantageous for measuring absorbance.

Photothermal signals are modeled for heat transfer from glass to air after laser excitation and the FEA model results are subsequently compared to the experimental signals. FEA model results for colored glass filters with and without boundary conditions and the experimental investigations of thermal lensing in colored glass filters and liquid sample cells are presented.

THEORY

The thermal lens effect is caused by the deposition of heat via non-radiative decay processes after the laser beam with Gaussian profile has been absorbed by the sample.

The photothermal lens signal is dependent on the spatially dependent refractive index change produced due to the temperature change in the absorbing sample. The time- and space-dependent temperature change is described by the differential equation for thermal diffusion. In radial symmetry, using appropriate lasers for sample excitation, the equation describing heat diffusion is[24]

$$\frac{\partial}{\partial t}\delta T(r,z,t) - D_T \nabla^2 \delta T(r,z,t) = \frac{q_H(r,z,t)}{\rho C_p} \tag{1}$$

In this equation, $\delta T(r,z,t)$ (K) is the space and time-dependent temperature change, t (s) is time, r (m) and z (m) are radial and linear cylindrical coordinates, D_T (m^2 s^{-1}) is thermal diffusion constant, ρ (kg m^{-3}) and C_p (J kg^{-1}) are density and specific heat capacity, respectively, and q_H (W m^{-3}) is energy density.

For pulsed laser excitation on a time scale much shorter than that for thermal diffusion, optical absorption within the sample results in sample heating that mimics the excitation laser beam radial profile. The energy absorbed by the sample for a collimated, short-pulsed Gaussian profile laser propagating on the z-axis is[24]

$$q_H(r,z,t) = \alpha e^{-\alpha z} \frac{2QY_H}{\pi w^2} e^{-(2r^2/w^2)} \delta(t) \tag{2}$$

The z-axis origin is taken to be at the entrance interface of the sample. In this equation, α (m^{-1}) is sample exponential absorption coefficient. The first part of the energy

source equation is z-axis energy deposition due to sample absorption of the exponential attenuated laser light as it traverses the sample. The second part of Eq. 2 accounts for the radial distribution of energy produced by the Gaussian laser profile. Q (J) is laser energy, the Y_H, is a heat yield parameter accounting for energy loss dues to luminescence during sample excitation and w (m) is excitation laser beam electric field width. It is assumed that the laser beam waste does not change over the length of the sample. The last term in this equation is the time dependence, in this case a delta function, $\delta(t)$ which is zero unless $t = 0$.

Solutions to the thermal diffusion equation are well known for the 'infinite cylinder' approximation. The latter assumes that there is negligible attenuation along the z-axis that the laser beam radius does not change, and that heat diffuses only in the radial dimension. This approximation can be valid for thin samples that have thermally insulated windows or are in a vacuum. For excitation pulse duration much shorter than the thermal relaxation time, and assuming rapid excited state relaxation, Eq. 3 gives the analytical solution to the temperature change for $t \geq 0$.

$$\delta T(r,t) = \frac{2\alpha Q Y_H}{\pi \rho C_p} \frac{1}{w^2(1+2t/t_c)} e^{\left(\frac{-2r^2}{w^2(1+2t/t_c)}\right)} \tag{3}$$

The temperature evolution depends on the characteristic thermal diffusion time constant, t_c (s), defined by

$$t_c = \frac{w^2}{4D_T} \tag{4}$$

D_T is the thermal diffusion coefficient given by $D_T = k/\rho C_p$, and k (W $m^{-1}K^{-1}$) is the thermal conductivity of the sample.

The strength of the photothermal lens element is found from the second radial derivative, evaluated on-axis. Integration over path length results in the inverse lens strength[27]

$$\frac{1}{f(t)} = \left(\frac{dn}{dT}\right) \int_{path} \left| \frac{d^2}{dr^2} \delta T(r,z,t) \right|_{r=0} ds \tag{5}$$

The theoretical treatment of thermal lens effect used the "parabolic approximation" where the temporal evolution of the temperature profile $\delta T(r, z, t)$ and, consequently, the refractive index profile $\delta n(r, z, t)$ are approximated by a parabola. Thus the second derivative with respect to radius is inversely proportional to the focal length of the parabolic lens. dn/dT (K^{-1}) is the temperature-dependent refractive index change, also known as the thermal-optical coefficient. In liquids, dn/dT is usually negative, so the photothermal lens is equivalent to a negative lens.

The change of divergence of a laser beam passing through the sample, due to the thermal lens effect, can be measured simply by placing a pinhole over the optical detector in the far field in the center of the diverged beam. The relative change at the detector signal is proportional to inverse of focal length. The photothermal lens signal is related to

the inverse focal length. For pulsed laser excitation, the experimental photothermal signal, $S(t)$, is defined by[24]

$$S(t) = \frac{\Phi(\infty) - \Phi(t)}{\Phi(t)} \tag{6}$$

In Eq. 6, Φ (W) is the irradiance of the probe laser passing through a pinhole aperture placed far away from the sample and the probe laser is focused a distance z' (m) in front of the sample. The signal is proportional to the inverse focal length of the lens produced in the sample due to laser heating; $S(t) \approx -2z'/f(t)$. This is an approximation and better signal predictions may be made with diffraction theory. Marcano *et al*. described the mode-mismatched thermal lens experiment in the pulse regime.[24, 28]

Eqs. 3 and 5 yield a time-dependent inverse focal length under the infinite cylinder approximation of

$$\frac{1}{f(t)} = \left(\frac{dn}{dT}\right)\frac{8\alpha l Y_H Q}{\pi w^4 \rho C_p}\frac{1}{(1 + 2t/t_c)^2} \tag{7}$$

l (m) is pathlength through the sample. The magnitude of the inverse focal length directly after excitation and assuming instantaneous temperature and refractive index change is thus

$$\frac{1}{f(0)} = \left(\frac{dn}{dT}\right)\frac{8\alpha l Y_H Q}{\pi w^4 \rho C_p} \tag{8}$$

The *dn/dT* term, which can be positive or negative since it is affected by counteracting factors. Thermal expansion decreases density and thus the refractive index due to the greater inter-molecular spacing. Secondly, an increase in the electronic polarizability causes the refractive index to gradually increase. In glasses, this effect is associated with the shift for longer wavelength of the UV absorption edge. Prod'homme showed that[29]

$$\frac{dn}{dT} = \frac{(n_0^2 - 1)(n_0^2 + 2)}{6n_0^2}\left[\frac{1}{\gamma}\frac{d\gamma}{dT} - 3\beta\right] \tag{9}$$

Here $\beta = 1/V\,(dV/dT)_P$ (K^{-1}) is the volume expansion coefficient and γ is the optical frequency polarizability coefficient. In liquids, *dn/dT* is usually negative as the thermal expansion is the dominant term in Eq. (9). For glasses, *dn/dT* can be either positive or negative, depending on the glass structure.[30, 31] A highly expansive and loosely bound networks as opposed to strongly bound networks presents negative and positive *dn/dT*, respectively. With few exceptions, in particular, near-phase-change temperatures, most materials expand with increased temperature. However, there are mechanisms for increasing refractive index with temperature. Solid phase changes, expansion induced stress, semiconductor conduction band population changes, and production of new states may result in a positive temperature-dependent refractive index change.

EXPERIMENTAL

Thermal Lensing Apparatus. The diagram in Figure 2-1 illustrates the apparatus setup for the thermal lens experiment. A Lambda Physik XeCl excimer laser pumped dye laser operating at 490 nm was used as the excitation source. This laser delivers maximum pulse energies of 0.44 mJ over the 20 ns pulse duration. The laser was operated with a repetition frequency of 3.75Hz. A 632.6 nm HeNe laser (Uniphase, Model 1107P) is used to probe the resulting photothermal lens. Collinear excitation-probe geometry was utilized in this thermal lens set up. The distance between the sample and the photodiode detector is optimized to satisfy the far-field paraxial approximation. Two lenses (10 cm and 25 cm focal length) are used to focus the excitation beam in the sample after the HeNe beam focus. The excitation source power is measured with a laser power meter.

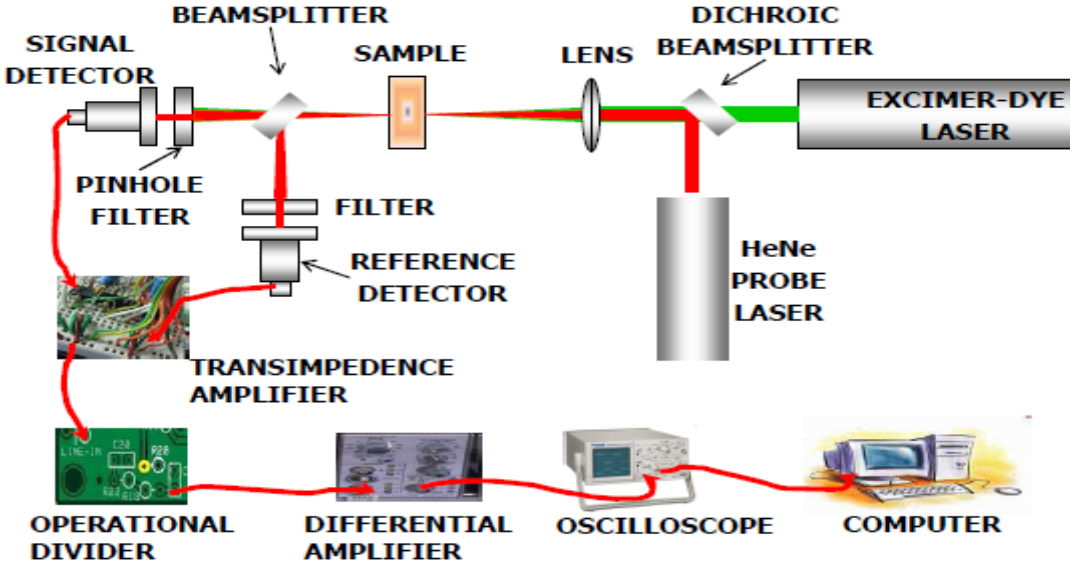

Figure 2-1. A schematic drawing of a photothermal lens experimental setup.

The photothermal lens caused focusing and defocusing of the probe laser. This is measured as a change in the power at the center of the beam. The center HeNe beam power is measured using a pinhole and a United Detector Technology (UDT) Model PIN-10DP photovoltaic photodiode detector. A 632.8 nm laser line bandpass filter is used to prevent the transmitted dye laser beam and ambient light from being detected by the photodiode detector. A small fraction of the probe beam is split off prior to the pinhole aperture and a second bandpass filter/photodiode is used to monitor the probe laser power past the sample. The photodiodes used transimpedance amplifiers. Changes in the detected probe laser power is compensated for by using an operational amplifier divider, the circuit of which divides the thermal lens signal by the signal proportional to the HeNe laser power. This probe laser power compensated thermal lens signal is amplified and electronically filtered with a Tektronix model AM-502 differential amplifier. The analog signal is subsequently digitized with a 16-bit analog-to-digital converter board and processed by multichannel analysis software. The latter averages several signal transients. Multichannel averaging was performed to improve the raw photothermal lens signal estimation precision. The photothermal lens signal was calculated from this raw data using a simple spreadsheet program.

Samples. Standard Corning colored glass optical filters doped with cadmium sulfoselenide microcrystals of about 10 nm are investigated as an absorbing solid material. 5 cm x 5 cm Corning 3389 (CS3-73, 1.45, and 3.05 mm thickness) optical filters were used for glass samples. Solutions of iron (II) dicylopentadiene (FeCp2) in ethanol were used as the liquid standards. Linear dilution is used to obtain lower absorbance from stock solutions of high enough absorbance to measure using a spectrophotometer in a

conventional 1 cm path length liquid cuvette. The sample is positioned at the focus of the excitation beam for maximum temperature gradient, and the solid versus liquid experiment is carried out separately at room temperature under the same conditions. Sample absorbance was recorded with a Cary 3E UV-Visible spectrophotometer.

Finite Element Analysis. Finite Element Analysis (FEA) software provides numerical solutions to the heat transfer equations with the realistic boundary conditions imposed by the experimental geometry. To better understand the transient temperature profile in the samples, FEA is used to model temperature changes. Results from the FEA calculations are then compared to conventional analytical solutions to gage the error. The experimental setup and the apparatus constraints are guided by the error analysis. Comsol Multiphysics 3.4 analysis is carried out on a Compaq Presario SR1330X, AMD Athlon XP 3200 processor using MS Windows XP.

The Comsol Multiphysics software in conduction and convection mode solves the heat diffusion equation given as

$$\rho C_p \frac{\partial}{\partial t}\delta T(r,z,t) - k\nabla^2 \delta T(r,z,t) = q_H(r,z,t) - \rho C_p u \cdot \nabla \delta T(r,z,t) \tag{10}$$

here u (m s^{-1}) is the flow velocity. All other symbols are the same as those introduced above. Note that Eq. 1 and 10 differ only by the second term on the right side of the equation. This term can account for convection or mass flow heat transfer. Convection is not important in glass but could be important in gases and liquids.

Finite element analysis modeling consists of drawing the sample geometry and specifying material boundary conditions, heat sources, and sinks. The problems are then solved with rough finite element definition and further refinement of elements and domain are made. Finally, *dT* can be obtained either at a single time, over a time series, or at steady state. The relative photothermal lens signal strength is found from Eq. 5 with *dn/dT* set to unity. The path integral of the second radial derivative was found by using the Comsol integration-coupling variable to integrate the second derivative function of the temperature change.

The model solid absorbing media were small square plates, 5 cm x 5 cm x 0.305 cm, or 5 cm x 5 cm x 0.145 cm, and had the same dimensions of the glass samples used in the experiments. Optical excitation was along the small dimension. For convenience, glass heating was modeled with 2D axial symmetry with the origin at the center of the z-axis runs along the path length of the excitation and probe beams. We have tested this and found that the results are equivalent to those obtained in the three dimensional Cartesian model. However, the cylindrical model is smaller and quicker to solve. The temperature profile of the glass was obtained by having the FEA software solve the heat equation with and without the glass surfaces set at 0 K (assuming no convectional heat transfer at the surfaces) and heat input along the z-axis defined by Eq. 4. In this fashion, the temperature solution represents *dT*. On the other hand, room temperature is used for temperature-dependent thermodynamic parameters of well-known library materials (air). Our model did not consider convection because the sample is solid. The values of α, Q, and w used were 3.8 m^{-1}, 0.44 mJ, and 170 μm, respectively.

RESULTS AND DISCUSSION

Figure 2-2 shows the experimental thermal lens signals for commercial colored glasses and a FeCp2 solution using a 490 nm pulsed excitation laser. Figure 2-2b shows that the thin glass produces a smaller magnitude signal. The magnitude of the signal for glass is clearly less than that for the FeCp2 solution. The conventional thermal lens signal is expected to arise from negative focal length because most materials have a negative dn/dT. The thermal lens signal (unitless) for a FeCp2 solution with a measured absorbance of 0.0212 AU for 1 cm path length (Figure 2-2a) indicates a decrease in refractive index of the sample. Figure 2-3 shows a FEA modeling and experimental signal of the FeCp2 solution in ethanol.

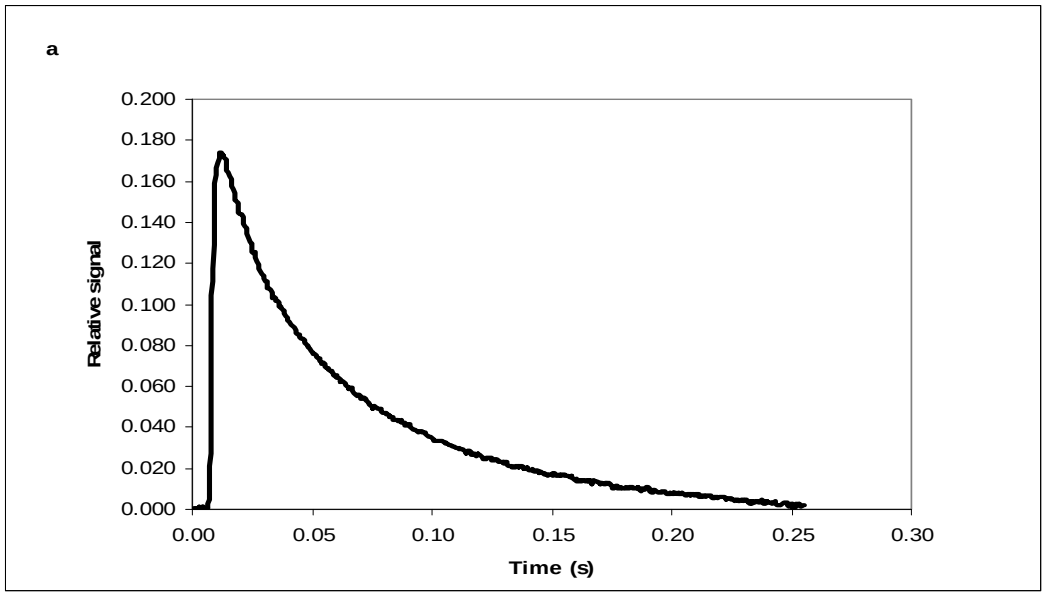

Figure 2-2a. Experimental thermal lens signals for 2 mm quartz cuvette with $FeCp_2$ solution.

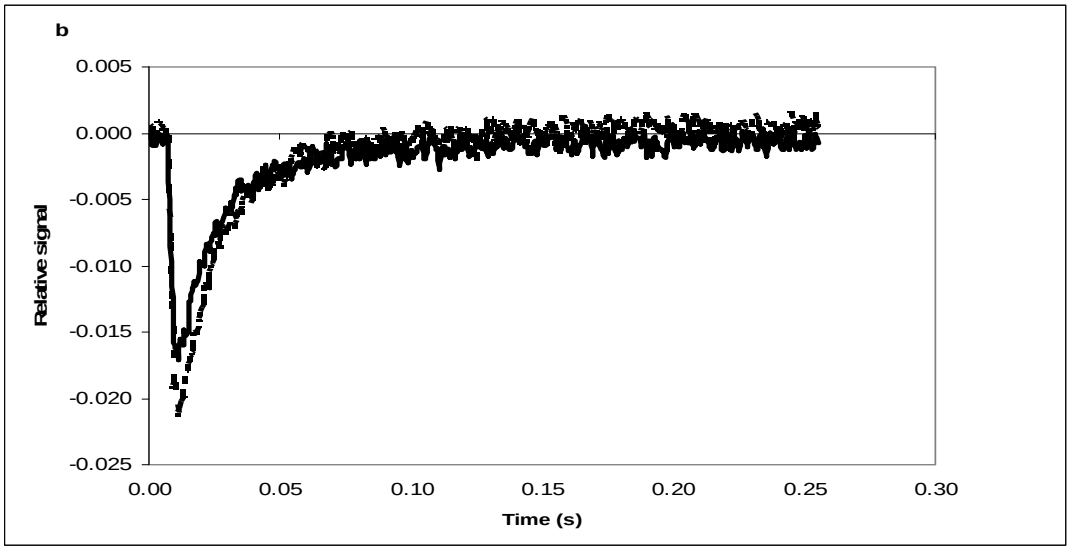

Figure 2-2b. Experimental thermal lens signals for 3.05 mm thick CdS_xSe_{1-x} doped Corning glass filter (dotted curve) and 1.45 mm thick CdS_xSe_{1-x} doped Corning glass filter (solid curve).

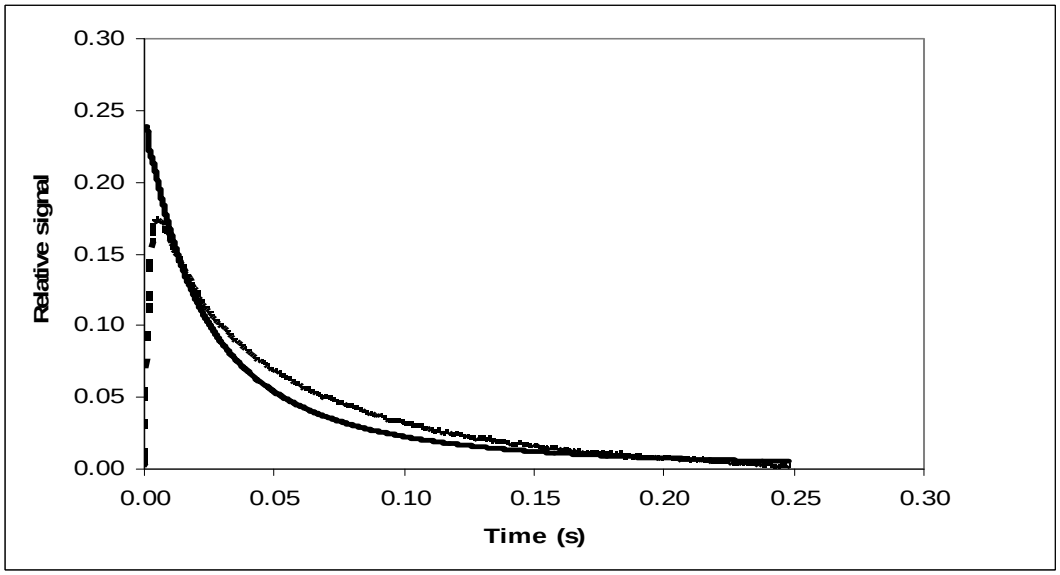

Figure 2-3. FEA modeling (solid line curve) and experimental signal (dotted curve) of the $FeCp_2$ solution.

The thermal lens signals of Corning commercial glass filters of 3.05 mm and 1.45 mm with absorbencies 0.0117 and 0.0025 AU (Figure 2-2b) are inverted relative to that of the FeCp2 solution, indicating a positive dn/dT. The time constant for the glass signal is shorter than that of the FeCp2 solution due to a large D_T and perhaps thermal coupling with the surrounding fluid.

The time-dependent FEA thermal lens signals in Figure 2-4 were calculated assuming $dn/dT = 1.0$ for both liquid and glasses. The FEA models of the photothermal heating of the glass samples showed significant heat transfer between the glass and air. Boundary conditions normally assumed in thermal lenses are that this heat transfer is negligible.

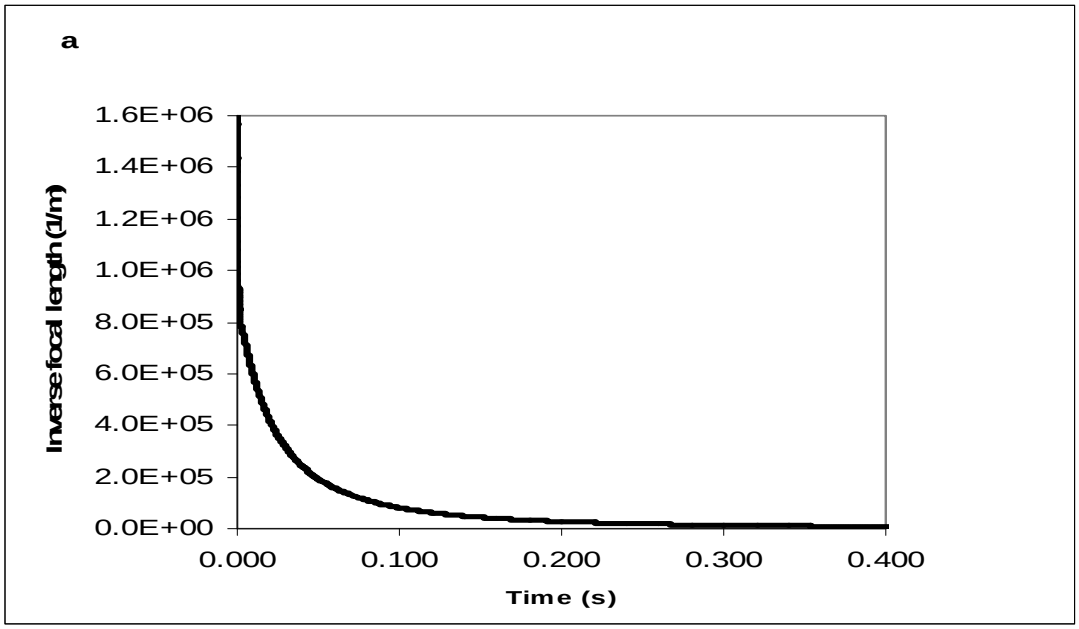

Figure 2-4a. FEA modeling of photothermal lens of $FeCp_2$ solution.

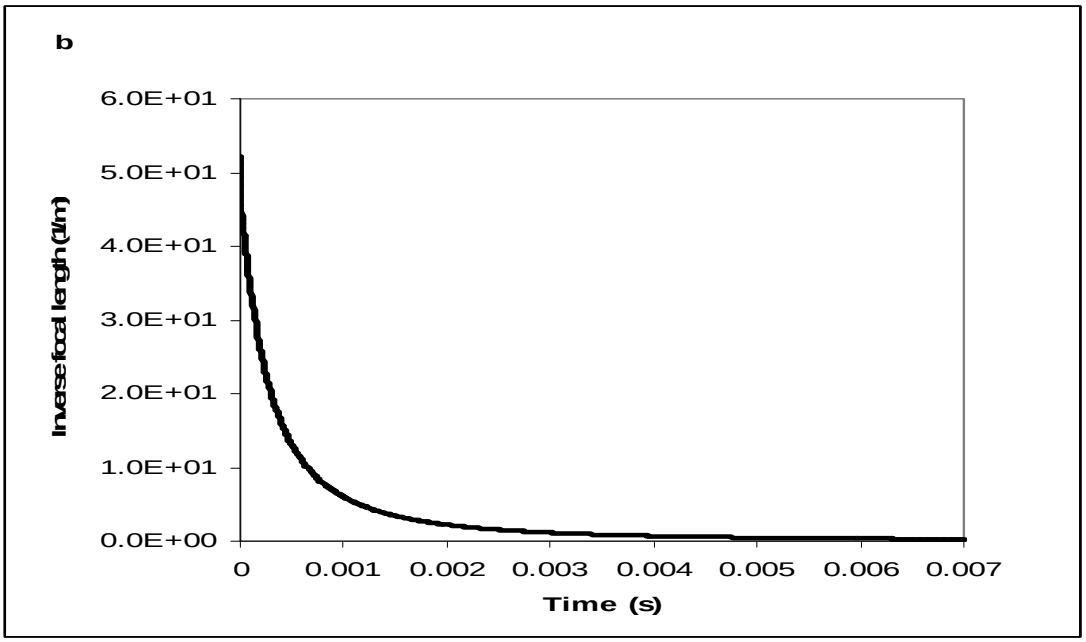

Figure 2-4b. FEA modeling of photothermal lens of 3.05 mm thick glass filter.

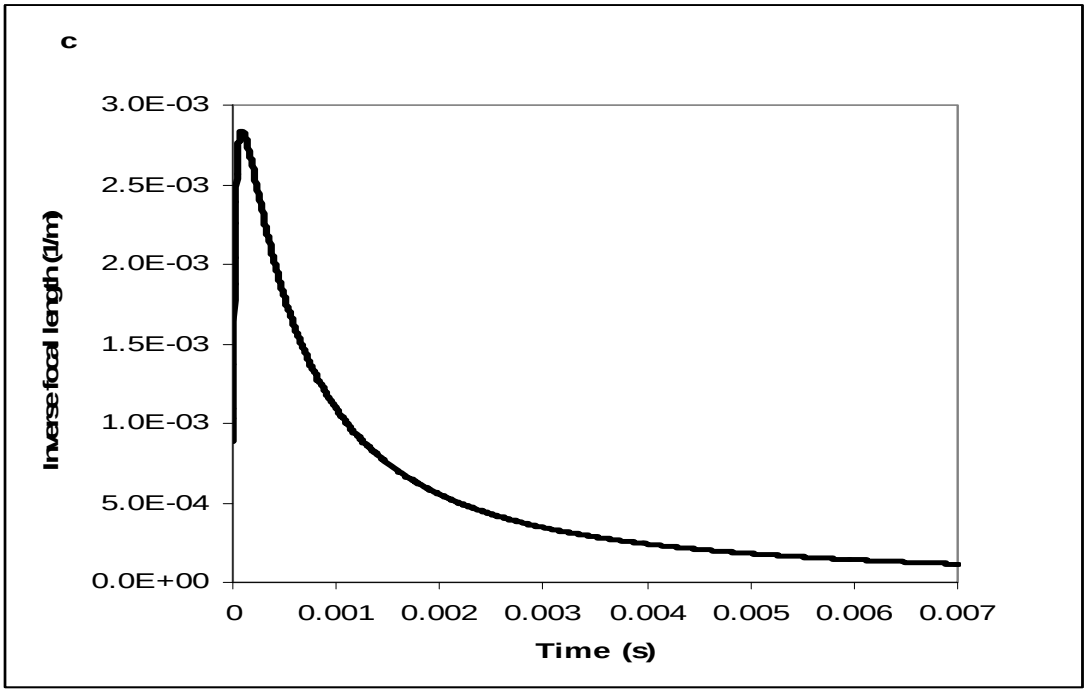

Figure 2-4c. FEA modeling of photothermal lens of air around the glass filter.

Figures 2-4b and 2-4c show that the magnitude of the signal of glass is far greater than that of the signal of the air (thermal coupling fluid). The photothermal signal in air is due

to the diffused heat from the glass. If we compare the magnitude of the photothermal signal in glass (Figure 4b) and in the surrounding air (Figure 2-4c), the signal in glass is about four orders greater than that in air. This is because the temperature change with pulsed laser excitation is much faster than the heat diffusion to the surroundings.

Figures 2-4b and 2-4c show that the signal reaches maximum in glass very quickly but in air it takes some time to reach the highest value. This is due to the fact that the diffusion of heat from glass to air is a relatively slow process in comparison to the excitation process.

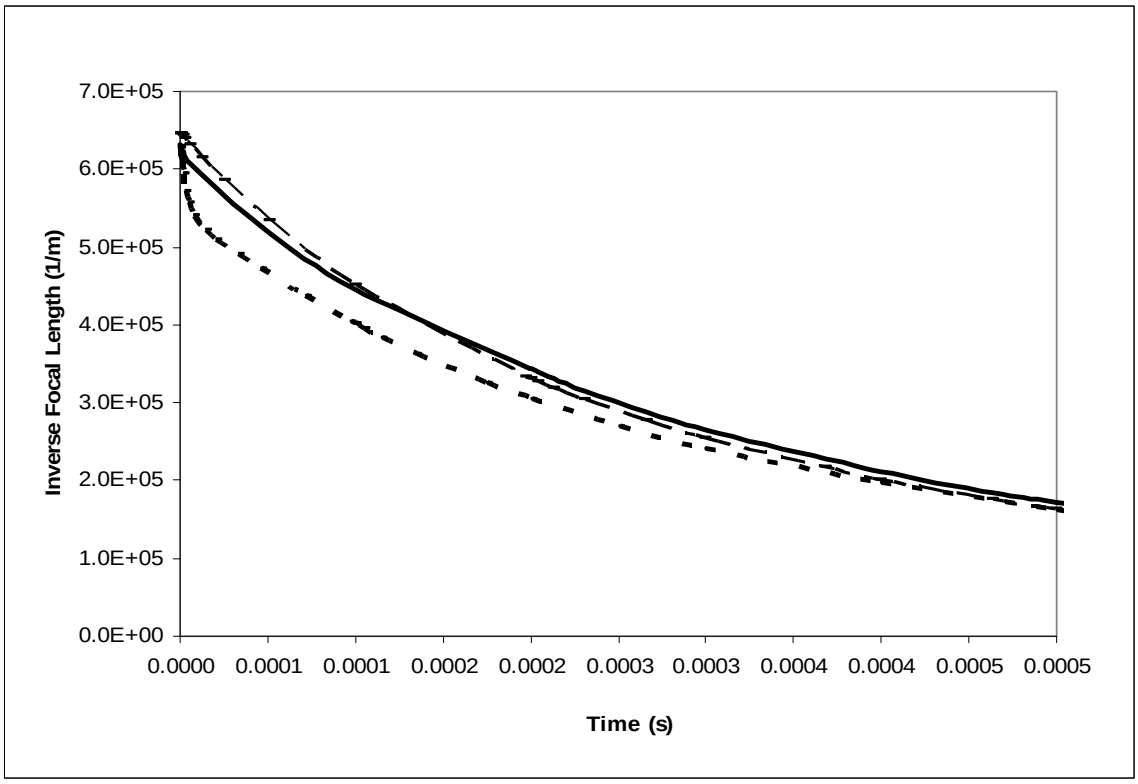

Figure 2-5. Plot of semi-infinite cylinder (dashed line) and FEA modeling of glass with (solid line) and without (dotted line) air boundary.

Figure 2-5, the FEA modeling of glass with (no transfer of heat from glass to air) and without (transfer of heat from glass to air) boundary conditions clearly shows that there is no heat transfer from glass to the air. Of interest here is, first, as expected, that there is very little difference between the semi-infinite cylinder approximation and the FEA model for the case where no heat transfer occurs between glass and air. Second, including glass-air heat coupling results in an initial rapid decrease in inverse focal length followed by decay closely resembling the semi-infinite cylinder case. The rapid decay is due to heat loss to the air at the surfaces, which decreases the length of the photothermal lens.

The signal magnitudes ($1/f$) at zero time, by FEA modeling and the analytical equation of the photothermal lens, are within two percent of each other. This is quite natural because FEA modeling depends on the mesh number, size of elements, and the types of solver used for the process.

We propose a simple method for comparing and correcting the measured photothermal lens signals in order to compare the different types of samples. FEA analysis is thought to be more accurate than the approximate solutions. In particular, the infinite cylinder approximation is clearly wrong for the glass samples. The photothermal signal is modeled for the glass by FEA modeling with the boundary condition (no transfer of heat from glass to air) and without the boundary condition (transfer of heat from glass to air). The ratio of the modeled signals should be equal to the ratio of the experimental signals without transfer of heat to transfer of heat. Similar measurements can be done for

the time constants to use the semi-infinite cylinder approximate model confidently for photothermal lens experiments.

$$\frac{S_{bm}}{S_{wm}} = \frac{S_{be}}{S_{we}} \tag{11}$$

Here, S_{bm} and S_{wm} are the photothermal signals of FEA modeling with and without heat coupling and S_{be} and S_{we} are experimental signals with and without heat coupling with the surroundings. A similar relation is true for time constants below

$$\frac{t_{c,(bm)}}{t_{c,(wm)}} = \frac{t_{c,(be)}}{t_{c,(we)}} \tag{12}$$

The values of *dn/dT* for the glasses were estimated by comparing data obtained from the thermal lens signals for the glasses and the well-established photothermal properties of ethanol. At steady-state conditions, Eq. 5 indicates that the thermal lens signal is proportional to the integral of the second derivative of the radial temperature profile. The integration term from Eq. 5 is obtained directly from the finite element analysis modeling solution.

Comparing Eq. 8 for the glass and the standard we have the following equation

$$\left(\frac{dn}{dT}\right)_g = \left(\frac{dn}{dT}\right)_s \frac{S_g \rho_g \alpha_s C_{p,g}}{S_s \rho_s \alpha_g C_{p,s}} \tag{13}$$

The subscripts ‘‘*g*’’ and ‘‘*s*’’ refer to glass and standard, respectively. The *dn/dT* for the glasses was estimated by using Eq. 13. Corrected values for material were obtained by using Eqs.11, 12, and 13. The experimental thermal diffusion constant calculated for glass using the proposed equation gives excellent agreement with the theoretical value obtained from the given values of density, specific heat capacity, and the corrected time constant obtained from experiment and modeling.

Table I, shows the calculated *dn/dT* and the temperature coefficient of electronic polarizability, σ (K^{-1}), and is given by

$$\sigma = \frac{1}{\gamma}\frac{d\gamma}{dT} \tag{14}$$

for the glasses. Given β and *n*, from Eq. 10, the σ was calculated using estimated *dn/dT*. The accuracy of the result was due to the calibration with the liquid samples and the fact that the transmission of the liquid sample was measured with a conventional spectrophotometer. The values of the polarization coefficient are in agreement with Prod’homme’s report on silica glasses with low thermal expansion. This accounts for the fact that electronic polarization is the dominant factor contributing to refractive index variation. An increase in electronic polarization causes the refractive index to increase in silica glasses.

Table 2-1. Thermo-optical constants of optical glasses.

Properties	Ethanol	Corning CS3-73 (3.05 mm)	Corning 3389 (1.45 mm)
dn/dT ($\times 10^5$ K^{-1})	-40	1.53	5.72
β ($\times 10^5$ K^{-1})	99	2.67	2.67
n	1.361	1.506	1.506
σ ($\times 10^5$ K^{-1})		5.2	12.2
α (m^{-1})	2.1	3.8	1.7
κ (W m^{-1} K^{-1})	0.167	1.38	1.38

The thermo-optical coefficient, *dn/dT*, is negative for liquid samples, and for solids and glasses it may be positive or negative due to many counteracting effects.[30,31] Some researchers have explained the factors contributing positive refractive index gradient in solids.[18,32] The nonlinear absorption coefficient and the index of refraction change in semiconductor-doped glass are due to the photo-darkening effect,[19,20] and it is attributed to a photochemical process in the semiconductor microcrystallite.[33] Trends in the nonlinear properties of semiconductor-doped glass may depend on the band-gap wavelength and doped particle sizes.[34–37] The nonlinear refractive index change is expected to be positive in the semiconductor-doped glass at excitation wavelengths below the band-gap wavelength and negative at wavelengths above the band-gap wavelength. The signal for glass filters that are doped with other materials rather than the semiconductor microcrystals has been shown to have positive *dn/dT* and shows that the positive *dn/dT* cannot only be a result of the semiconductor microcrystals.[18, 38] The excitation beam wavelength falls below the CdS_xSe_{1-x} band-gap wavelength, which produces a positive refractive index change due to increased carrier density.

Thermal lens experiments and FEA modeling are presented to investigate the temperature profile, change in refractive index of CdS_xSe_{1-x} doped glass, and to determine the thermo-optical coefficient, *dn/dT*.

We previously reported the photothermal lens signal for similar glasses using continuous laser-excited photothermal spectrometry.[38] One of the problems realized at that time was that the heat transfer from a glass plate excited with a laser is far from the ideal situation described by the semi-infinite cylinder approximate models that are most often used to describe photothermal lens experiments. Here we have resolved the problem using: (1) pulsed laser excitation where the signal decays is faster than the heat diffusion to the surroundings, and (2) FEA modeling to take account of the likely deviation from the semi-infinite cylinder approximate models. The measured *dn/dT* and the temperature coefficient of electronic polarizability values of glasses are very reasonable compared to our previous labs reports[38] and are much nearer to the report by Prod'homme on silica glass.

The anomalous behavior of the temperature-dependant refractive index changes in glasses has previously been explained in terms of optical nonlinearities and stress birefringence. However, this is still is not a well-known phenomenon. Finite elemental analysis modeling may help in understanding the dynamics of the temperature distribution with other experimental parameters. Research has been done on surface-deformation phenomena due to the excitation source in glasses.[39, 40] FEA modeling and the study of the transmission profile of the probe beam along with the surface-deformation phenomenon due to excitation may help to better explain the secret of anomalous behavior of the doped glasses.

CONCLUSION

Finite element analysis modeling can be used to better understand the pulsed laser excited photothermal spectroscopy signals by correctly accounting for the heat transfer of the sample to the surroundings. FEA modeling is particularly useful to account for surface heat transfer that will occur in glasses and other samples where the absorbing material is in direct contact with the coupling fluid surroundings. The cylindrical approximation is not valid in these cases. Anomalous *dn/dT* behavior of these glass filters is thought to be due to counteracting effects: optical nonlinearity, stress induced birefringence, and the structural network in the glass structure. Further investigation, using FEA modeling to take into account physical effects such as surface deformation due to thermal expansion, will be required to understand the thermo-optical phenomenon.

REFERENCES

1. J. Shen, and R. D. Snook, Anal. Proc. **26**, 403 (1989).
2. M. L. Baesso, J. Shen, and R. D. Snook, J. Appl. Phys. **75**, 3733 (1994).
3. M. L. Baesso, J. Shen, and R. D. Snook, Chem. Phys. Lett. **197**, 255 (1992).
4. S. M. Lima, T. Catunda, R. Lebullenger, A. C. Hernandes, M. L. Baesso, A. C. Bento, and L. C. M. Miranda, Phys. Rev. B **60**, 15173 (1999).
5. M. L. Baesso, A. C. Bento, A. R. Duarte, A. M. Neto, L.C. Miranda, J. A. Sampaio, T. Catunda, S. Gama, and F. C. G. Gandra, J. Appl. Phys. **85**, 8112 (1999).

6. S. A. Payne, C. D. Marshall, A. Bayramian, G. D. Wilke, and J. S. Hayden, Appl. Phys. B **61**, 257 (1995).

7. N. Neuroth, Opt. Eng. **26**, 96(1987).

8. P. Greason, J. Detrio, B. Bendow, and D. J. Martin, Mater. Sci., Forum **6,** 607 (1985).

9. M. Sparks, J. Appl. Phys. **42**, 5029(1970).

10. T. Izumitani, and H. Toratani, J. Non-Cryst. Solids **40**, 611 (1980).

11. J. M. Jewell, and I. D. Aggarwal, J. Non-Cryst. Solids **142**, 260 (1992).

12. J. M. Jewell, C. Apkins, and I. D. Aggarwal, Appl. Opt. **30**, 3656 (1991).

13. C. A. Klein, Opt. Eng. **29**, 343 (1990).

14. P. O. McLaughlin, and D. T. Moore, Appl. Opt. **24**, 4342 (1985).

15. W. D. S. John, B. Taheri, J. P. Wicksted, R. C. Powell, D. H. Blackburn, and D. C. Cranmer, J. Opt. Soc. Am. B **9**, 610 (1992).

16. C. J. Parker, and W. A. Popov, Appl. Opt. **10**, 2137 (1971).

17. B. A. M. Taheri, F. W. D. St. John, J. P. Wicksted, R. C. Powell, D. H. Blackburn, and D. C. Cranmer, J. Appl. Phys. **71**, 3693 (1992).

18. S. M. Lima, J. A. Sampaio, T. Catunda, A. C. Bento, L. C. M. Miranda, and M. L. Baesso, J. Non-Cryst. Solids **273**, 215 (2000).

19. P. Maly', F. Troja'nek, and A. Svoboda, J. Opt. Soc. Am. B **10**, 1890 (1993).

20. P. Horan, and W. Blau, J. Opt. Soc. Am. B **3**, 304 (1990).

21. T. Moyo, K. Maruyama, and H. Endo, J. Phys. Condens. Matter **4**, 5653 (1992.)

22. C. J. Murphy, and J. L. Coffer, Appl. Spectrosc. **56**, 16A (2002).

23. F. Pereira, J. R. Salcedo, and M. Belsley, J. Opt. Soc. Am. B **16**, 228 (1999).

24. S. E. Bialkowski, *Photothermal Spectroscopy Methods for Chemical Analysis* (John Wiley and Sons, New York 1996).

25. A. Chartier, and S. E. Bialkowski, Opt. Eng. **36**,303 (1997).

26. J. R. Whinnery, Acc. Chem. Res. **7**, 225 (1974).

27. W. B. Jackson, N. M. Amer, and A. C. Boccara, and D. Fournier, Appl. Opt. **20**, 1334 (1981)

28. A. Marcano O. L. Rodriguez, and Y. Alvarado, J. Opt. A: Pure Appl. Opt. **5**, S256- S261 (2003)

29. L. Prod'homme, Phys. Chem. Glasses **1**, 119 (1960).

30. F. Gan, *Laser Materials* (World Scientific, Singapore, 1994).

31. T. S. Izumitani, *Optical Glass* (American Institute of Physics, New York, 1986).

32. C. Jacinto, D. N. Messias, A. A. Andrade, S. M. Lima, M. L. Baesso, and T. Catunda, J. Non-Cryst. Solids **352**, 3582 (2006).

33. J. L. Coutaz, and M. Kull, J. Opt. Soc. Am. B **8**, 95 (1991).

34. N. Finlayson, W. C. Banyai, C. T. Seaton, G. I. Stegeman, M. O'Neill, T. J. Cullen, and C. N. Ironside, J. Opt. Soc. Am. B **6**, 675 (1989).

35. W. D. St. John, B. Taheri, J. P. Wicksted, R. C. Powell, D. H. Blackburn, and D. C. Cranmer, J. Opt. Soc. Am. B **9**, 610 (1992).

36. T. Toyoda, and Q. Shen, Analytical Sciences (Japan) **17**, s259 (2001).

37. H. Shinojima, IEICE Trans, Electron, **E90-C**, 127 (2007).

38. O. O. Dada, M. R. Jorgensen, and S. E. Bialkowski, Appl. Spectrosc. **61**, 1373 (2007).

39. N. G. C. Astrath, L. C. Malacarne, P. R. B. Pedreira, A. C. Bento, and M. L. Baesso J. Shen, Appl. Phys. Lett. **91**, 191908 (2007).

40. L. C. Malacarne, F. Sato, P. R. B. Pedreira, A. C. Bento, R. S. Mendes, M. L. Baesso, N. G. C. Astrath, and J. Shen, Appl. Phys. Lett. **92**, 131903 (2008).

CHAPTER 3

DETECTION OF FAST AND SLOW SIGNAL DECAY COMPONENT IN GLASS BY PHOTOTHERMAL EXPERIMENT USING FAST RESPONSE DETECTOR

ABSTRACT

Finite element analysis modeling of the photothermal lens signal produced with Gaussian pulsed laser excitation of colored silica glass plates surrounded by air is presented. Models show fast and slow time-dependent signal decay components present in photothermal lens produced within the glass. Experiments are carried out to verify the model prediction. Transmission and reflection photothermal lens experiments are carried out to detect the event using fast response detector. The fast and slow decay signal components are experimentally verified and interpreted as being due to the fast transfer of heat in axial direction and slow transfer of heat in radial direction relative to the excitation laser beam. The time constant of slow and fast components is evaluated to present the correct prediction of material properties with the help of the finite element analysis model.

INTRODUCTION

Thermal lens spectrometry (TLS) is a photothermal technique, which has been widely used for the determination of very low optical absorption coefficients of different materials with high sensitivity and versatility. [1–4] Since its discovery by Gorden *et al*.[5] in 1964 the method has been used for the intracavity measurements of absorption of nearly transparent materials. [1, 2] Knowledge of the thermo-optical properties is essential for

evaluating the figures of merit of optical glasses which can readily be used to determine the working glass conditions[6,7] such as thermal shock, thermal stress resistance,[8] and thermal lens effect.[6-9]

CdS_xSe_{1-x}-doped glass was used as a sample in this work. In the past few years, semiconductor doped glasses and other analogous materials with semiconductor quantum dots have been investigated intensively and many physical phenomenon have been found.[10-16] In particular CdS_xSe_{1-x}-doped glasses have received considerable attention as a promising nonlinear material with a large optical nonlinearity[17]and fast optical response.[18] Theoretical models of TLS effects in fluids are well established. But accurate theoretical descriptions of thermal diffusion in solids excited by laser beams is still an active area of research although a number of approximations are commonly used to obtain tractable analytical results.[19,20] The use of thermal lens techniques for analysis glasses has been reported by some authors with the help of finite element analysis. [21, 22]

The limit of detection for thermal lens methods are related to how realistically the experimental description can be theoretically modeled.[19, 20] Generally, simple and applicable theoretical model are obtained by introducing modeling approximations that lead to analytical solutions. In some cases, these approximations can be accounted for by using appropriate experimental setups. However, it is not always feasible. In most practical situations, for example, heat is transferred from sample to the surroundings along to the axial dimension. This is especially true when the heated sample is direct in contact with air or another coupling fluid. Recently, it has been shown that sample/air heat coupling in the thermal lens experiment could significantly contribute to the thermal lens signal.[21, 23] In fact; the fluid thermal coupling is always treated as a perturbation to

the thermal lens signal. This perturbation could become stronger as the sample thickness is reduced and /or depending on the thermo-optical properties of the sample/ fluid system.

Conventional TLS models treat the sample as an infinite medium, [5,24] both in radial and axial directions (in cylindrical coordinates), which has the weakness that the temperature rise in the sample never reaches steady state.[5] Wu and Dovichi[25] derived a cw laser-induced single-beam TLS model for their steady-state thin-film measurement which takes the axial heat loss into account. Accordingly, when the sample is thin the axial heat flow cannot be neglected and the axial-infinite treatment is no longer valid. In their work the sample in the radial direction is still assumed to be infinite. However there are two ways to remove the heat energy from the illuminated sample: axial and radial heat flows into the surrounding air which depends on the sample boundary conditions.

The theoretical model for the thermal lens signal is difficult to deduce analytically when heat coupling with the surrounding in taken into account using more realistic boundary conditions. Such models can be obtained with approximations but the lack of a more complete theory makes validation difficult. FEA methods provide numerical solutions to the heat transfer equations with the realistic boundary conditions imposed by the experimental geometry. FEA software has been recently applied to describe complex heat coupling conditions on photothermal techniques. [21, 23] Numerical and approximated solutions have been compared to FEA modeling. FEA has been shown to be a powerful tool to model continuous and pulsed-laser photothermal methods.

This work presents FEA methods for modeling of the pulsed laser excited photothermal lens signal of glass samples surrounded by air. The model accounts for the

coupling of heat both within the sample and out to the surroundings. While studying the FEA model of pulsed-laser excited thermal lens signal of colored glass filters surrounded by air, a kind of irregular decay of signal was predicted. On a close scrutiny it was realized that it could be due to fast and slow heat transfer components. Transmission and reflection photothermal lens experiments using fast response detector were carried out to verify and detect these events. These fast and slow decay signals can be explained in terms of axial and transverse heat diffusion from the sample.

THEORY

Thermal lens spectrometric method is based on the periodic formation of a lens-like element in a medium that absorbs laser radiation with the TEM_{00} mode. The focal distance of the resulting thermal lens depends on the absorbance of the sample. The thermal lens signal depends on the temperature gradient of the refractive index and the thermal conductivity coefficient of the medium. The energy absorbed by the sample for a collimated, short-pulsed Gaussian profile laser propagating on the z-axis is[26]

$$q_H(r,z,t) = \alpha e^{-\alpha z} \frac{2Q}{\pi w^2} e^{-(2r^2/w^2)} \delta(t) \tag{1}$$

The z-axis origin is taken to be at the entrance interface of the sample. In this equation, α is the sample exponential absorption coefficient. The first part of the energy source equation is *z*-axis energy deposition due to sample absorption of the exponential attenuated laser light as it traverses the sample. The second part of Eq. 1 accounts for the radial distribution of energy produced by the Gaussian laser profile. Q (J) is laser energy,

Y_H is a heat yield parameter accounting for energy loss dues to luminescence during sample excitation, and w (m) is the excitation laser beam electric field width. It is assumed that the laser beam waist does not change over the length of the sample. The last term in this equation is the time dependence, in this case a delta function, $\delta(t)$, which is zero unless $t = 0$.

The spatial heat distribution in the sample in the absence of radiation losses is defined by the three-dimensional differential equation of thermal diffusion.[26]

$$\frac{\partial}{\partial t}\delta T(r,z,t) - D_T \nabla^2 \delta T(r,z,t) = \frac{q_H(r,z,t)}{\rho C_p} \tag{2}$$

Here r and z are the radial and linear cylindrical coordinates, C_P is the heat capacity, ρ is the density of the medium, δT (r, z, t) is the change in the sample temperature with respect to the initial level, z is the coordinate along the axis coinciding with the beam propagation direction, t is the time, and D_T is the thermal diffusion constant.

The infinite cylinder approximation for excitation pulse duration much shorter than the thermal relaxation time, and assuming rapid excited-state relaxation, the analytical solution to the temperature change is given by Eq. 3 for $t \geq 0$:

$$\delta T(r,z,t) \approx \delta T(z,t).\delta T(r,t)$$

$$\delta T(r,z,t) \approx \delta T(z,t)\frac{2\alpha Y_H Q}{\pi\rho C_p}\frac{1}{w^2(1+2t/t_c)}e^{\left(\frac{-2r^2}{w^2(1+2t/t_c)}\right)} \tag{3}$$

t_c (s) is the characteristic thermal diffusion time constant defined by

$$t_c = \frac{w^2}{4D_T} \tag{4}$$

The strength of the photothermal lens element is found from the second radial derivative, evaluated on-axis. Integration over path length results in the inverse lens strength.

$$\frac{1}{f(t)} \approx \left(\frac{ds}{dT}\right)\int_{path}\delta T(z,t)\left|\frac{d^2}{dr^2}\delta T(r,t)\right|_{r=0} ds \tag{5}$$

where $f(t)$ is focal length and ds/dT is the thermo-optical coefficient allowing for pathlength expansion also known as the thermal-optical coefficient.

If the sample is thick and surface is insulated than there is no diffusion of heat through the surface and there no is axial temperature change. In most practical situations heat is transferred from the sample to the surroundings along the axial dimension. This is especially true when the heated thin sample is in contact with the air or another coupling fluid. In that case $\delta T(z, t)$ also contribute to the total signal. This surface diffusion along axial direction is responsible for initial fast decay of signal.

The change of divergence of a laser beam passing through the sample, due to the thermal lens effect, can be measured simply by placing a pinhole over the optical detector in the far field in the center of the diverged beam. The relative change at the detector signal is proportional to the inverse of the focal length. The photothermal lens signal is related to the inverse focal length. For pulsed laser excitation, the experimental photothermal signal, $S(t)$, is defined by[26]

$$S(t) = \frac{\Phi(\infty) - \Phi(t)}{\Phi(t)} \tag{6}$$

In Eq. 6, Φ is the irradiance of the probe laser passing through a pinhole aperture placed far away from the sample and the probe laser is focused a distance z' in front of the sample. The signal is proportional to the inverse focal length of the lens produced in the sample due to laser heating; $S(t) = 2z'/f(t)$. This is an approximation and better signal predictions may be made with diffraction theory.

MATERIALS AND METHODS

Experimental apparatus. A conventional two-color photothermal lens apparatus, with probe laser 632.6 nm HeNe, and excitation source XeCl excimer dye pulsed laser operating at 490 nm was used. A detailed description of experiment and apparatus used can be found elsewhere.[21] However; we have used fast response photodiode as a detector. The Figure 3-1 illustrates the apparatus set up for photothermal lens experiment.

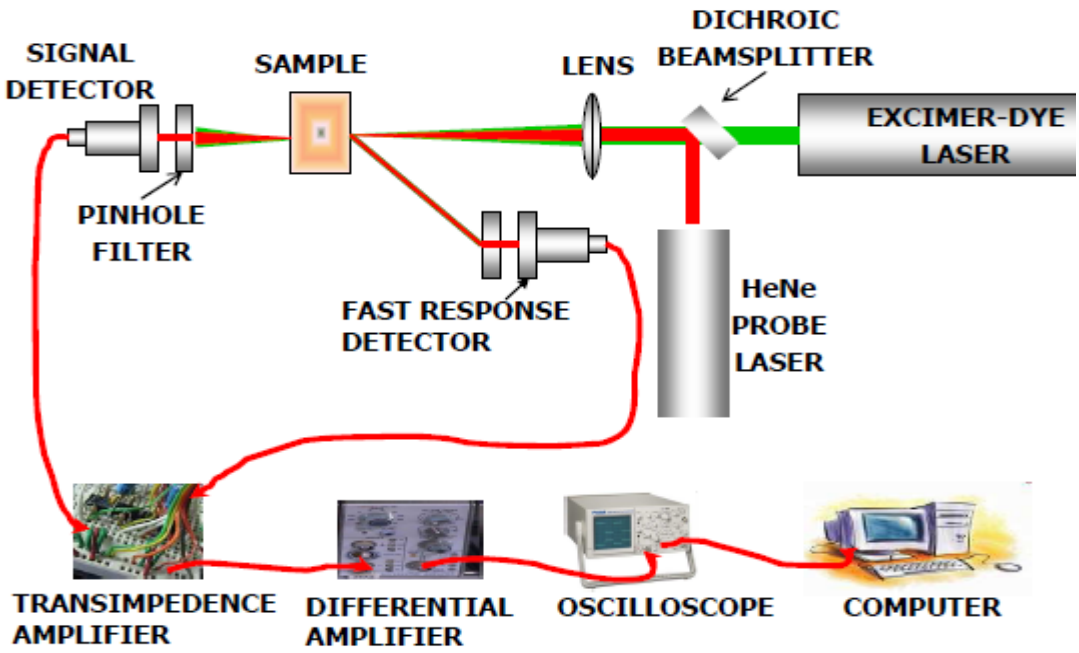

Figure 3-1. A schematic drawing of a photothermal lens experimental setup.

Sample. Standard Corning colored glass optical filters doped with cadmium sulfoselenide microcrystals of about 10 nm are investigated as an absorbing solid material. 5 cm x 5 cm Corning 3389 (CS3-73, 3.05 mm thickness) optical filters was used for glass samples. The sample is positioned at the focus of the excitation beam for maximum temperature gradient

Modeling. Photothermal signals are modeled for heat transfer from glass to air after laser excitation and the FEA model results are subsequently compared to the experimental signals. FEA is a tool for numerical solutions to complex differential equations. Comsol Multiphysics 3.5a analysis is carried out on a Compaq Presario SR1330X, AMD Athlon XP 3200 processor using MS Windows XP.

The Comsol Multiphysics software (v.3.5a) in conduction and convection mode solves the heat diffusion equation given as

$$\rho C_p \frac{\partial}{\partial t}\delta T(r,z,t) - k\nabla^2 \delta T(r,z,t) = q_H(r,z,t) - \rho C_p u \cdot \nabla \delta T(r,z,t) \tag{7}$$

where u is the flow velocity. Note that Eqs. (2) and (7) differ only by the second term on the right side of the equation. This term can account for convection or mass flow heat transfer, which is not important for the solid sample investigated in this work.

A detailed description of FEA modeling has been described elsewhere.[21] Briefly; it consists of drawing the sample geometry and specifying material boundary conditions, heat sources, and sinks. The problems are then solved with rough finite element definition and further refinement of elements and domain are made. The element mesh is refined until model results become independent of mesh size. Finally, the temperature profile can be obtained either at a single time, over a time series, or at steady state, for the sample and air domain. The path integral of the second radial derivative was found by using the Comsol integration-coupling variable to integrate the second derivative function of the temperature change.

For convenience, glass heating was modeled with 2D axial symmetry with the origin at the center that the *z*-axis runs along the pathlength of the excitation and probe beams. We have tested this and found that the results are equivalent to those obtained in the three dimensional Cartesian model. However, the cylindrical model is smaller and

quicker to solve. The model solid-absorbing media taken were cylindrical plate of 5 mm diameter and 0.5 to 3.05 mm of different thickness.

RESULTS AND DISCUSSION

Figure 3-2 is temperature profile along the *z* direction (air-glass-air) using the FEA modeling, and clearly shows that there is heat transfer from glass to air.

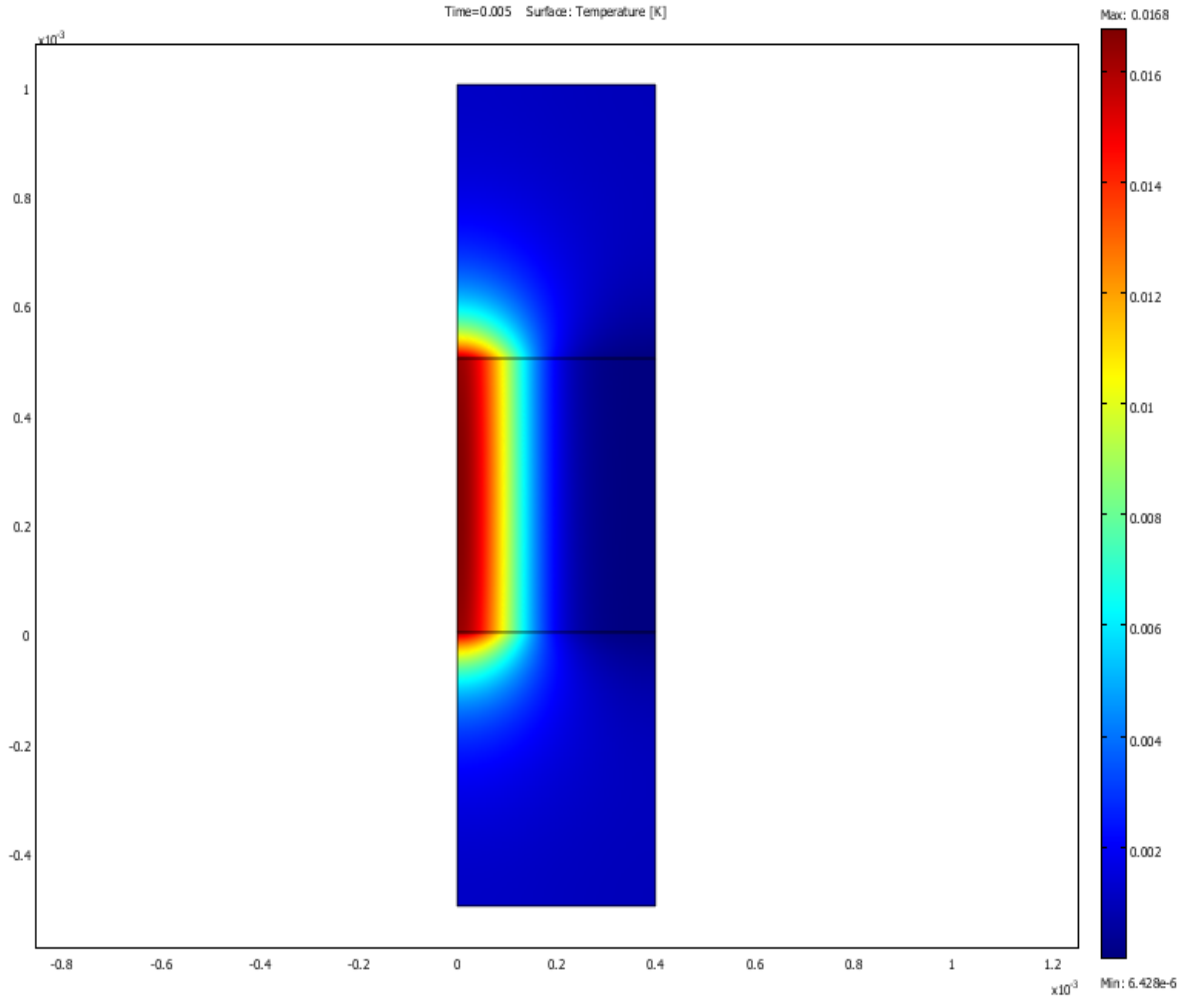

Figure 3-2. FEA modeling of glass surrounded by air (2D axial symmetry).

Figure 3-3 shows the FEA modeling of photothermal signal of 3.05 mm thick glass surrounded by air. The plot is inverse focal length versus time for 40-100 μm beam width pulse-laser excitation. Clearly, Figure 3-3 illustrates that the signal increases with decreasing beam size. The interesting thing here is that the glass-air heat coupling is probably responsible for the faster initial decay of the time-resolved photothermal signal. The slower decay is due to radial heat diffusion. The faster signal decay becomes prominent when the beam size decreases. The faster signal decay is apparently due to the axial heat transfer. There is no fast signal decay for the thick samples indicating less contribution from axial heat transfer to the total cooling.

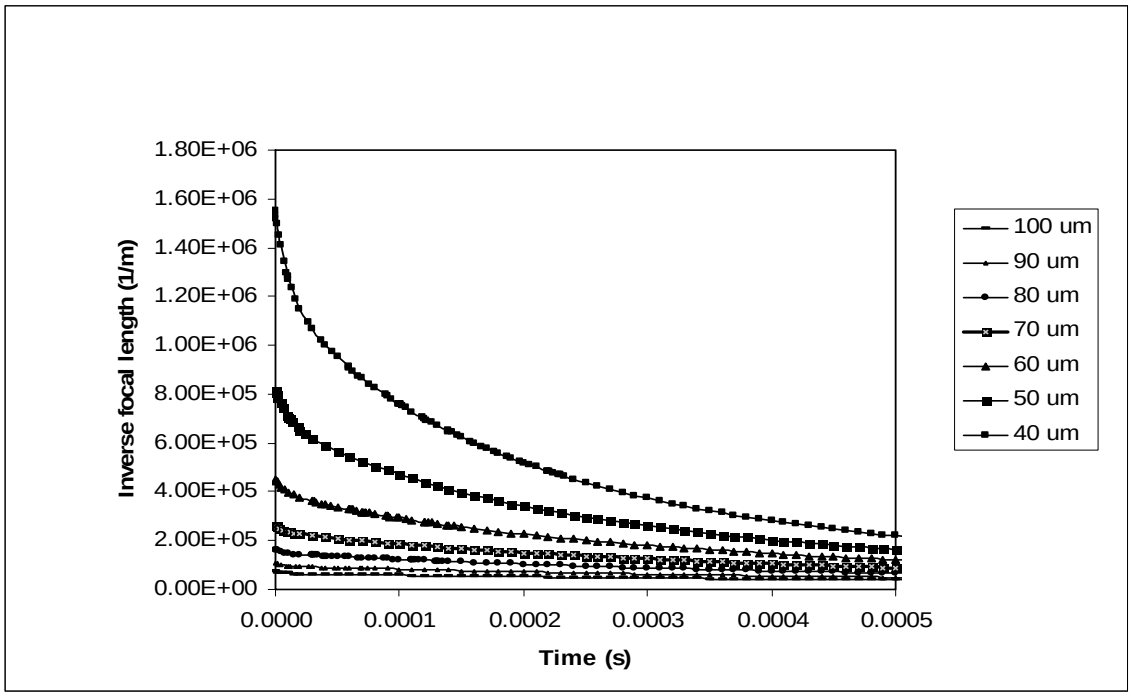

Figure 3-3. FEA modeling of 3.05 mm glass surrounded by air using 40-100 μm diameter pulsed-laser excitation.

The theoretical time-resolved photothermal lens signals can be used to evaluate the t_c and thus the thermal diffusion constant using $D_T = w^2 / t_c$. The slower component of the time-resolved photothermal signal is extrapolated and t_c is calculated based on the time to ½ maximum signal ($t_{1/2}$). The glass D_T obtained from this extrapolation method gives a more realistic value than the one calculated from the Figure 3-4 which is the plot of w^2 versus t_c.

Figure 3-5 indicates that the signal intensity goes down with thickness of glass and the axial heat transfer is more severe. This is because of rapid diffusion of heat at the surface.

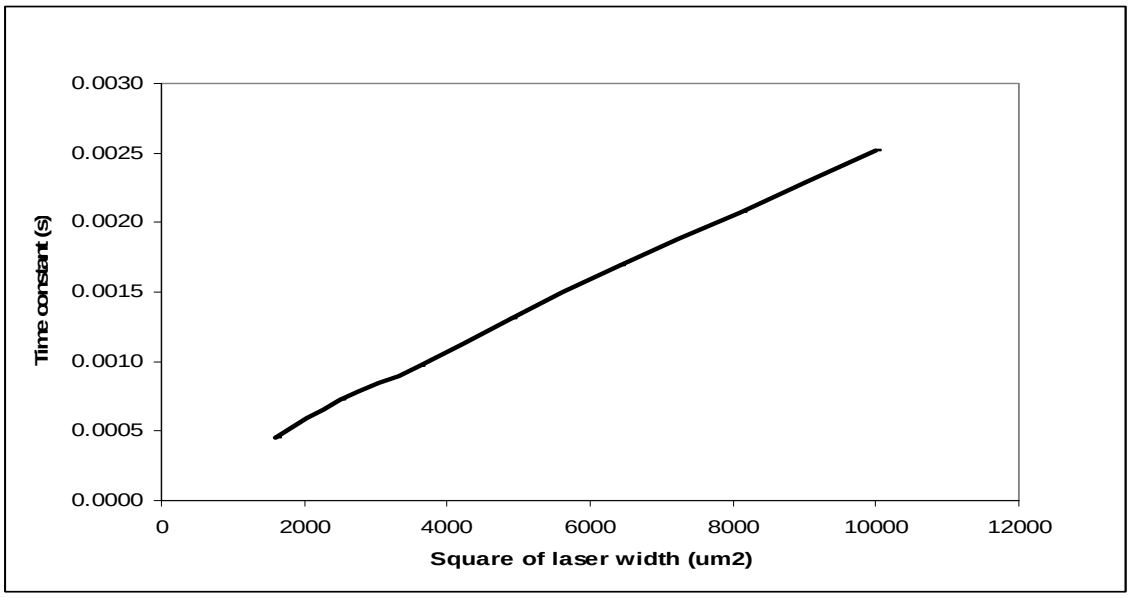

Figure 3-4. Variation of time constant (t_c) with square of laser width (w^2).

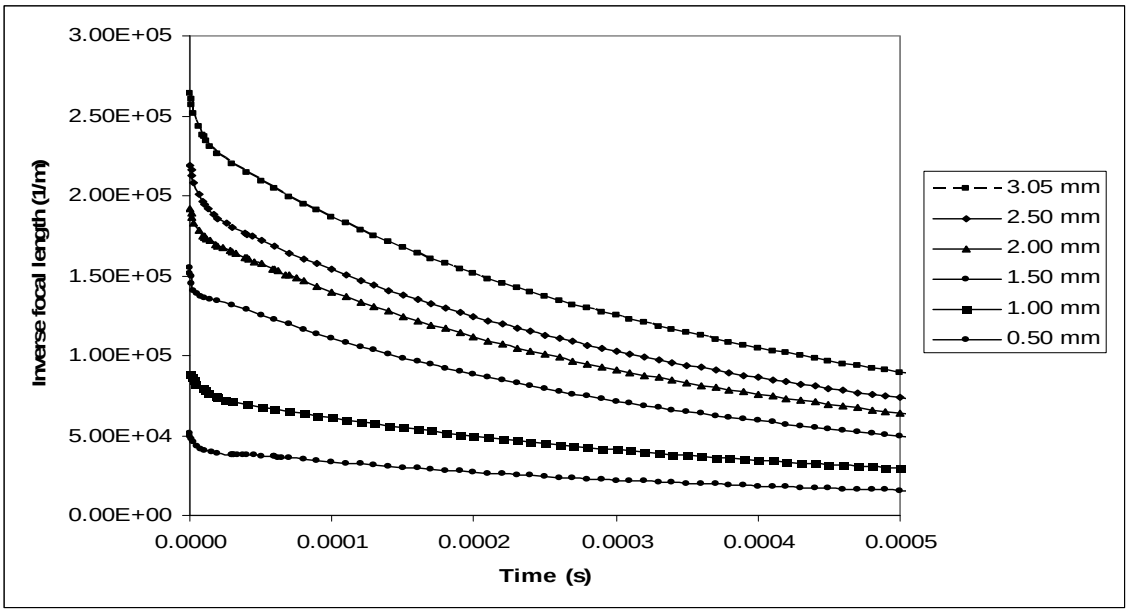

Figure 3-5. FEA modeling of glasses of 0.50-3.05 millimeter thickness.

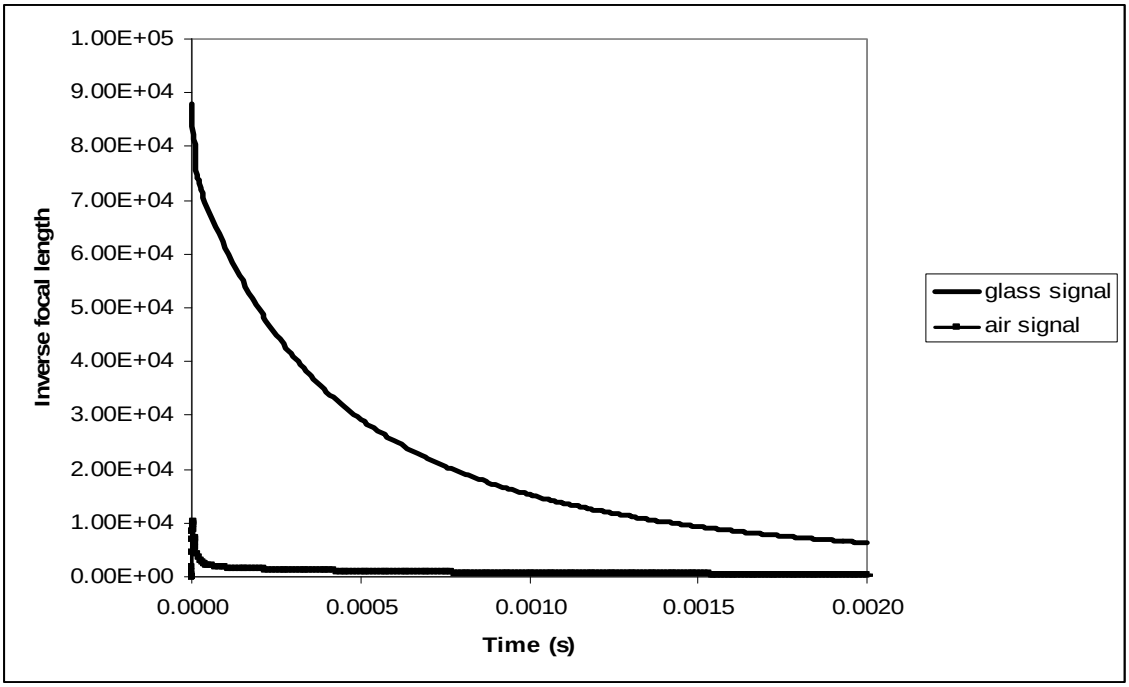

Figure 3-6. FEA modeling of photothermal signal in 1 mm glass and air.

The heat transfer dynamics of glass surrounded by air is modeled and the photothermal signal of glass and air are subsequently evaluated separately. The results show that the air signal contribution to the total photothermal lens signal is significant. This is shown in Figure 3-6. The signal in air, which is due to the transfer of heat from the glass surface, presented in Figure 3-7, does not change with the size of glass.

Transmission and reflection photothermal lens experiments were carried out by using fast response photodiode detector on 3.05 mm glass. The experimental schematic is shown in Figure 3-8. The fast response signal has been detected. Transmission and reflection signal look similar which indicates that they are due to the axial heat transfer.

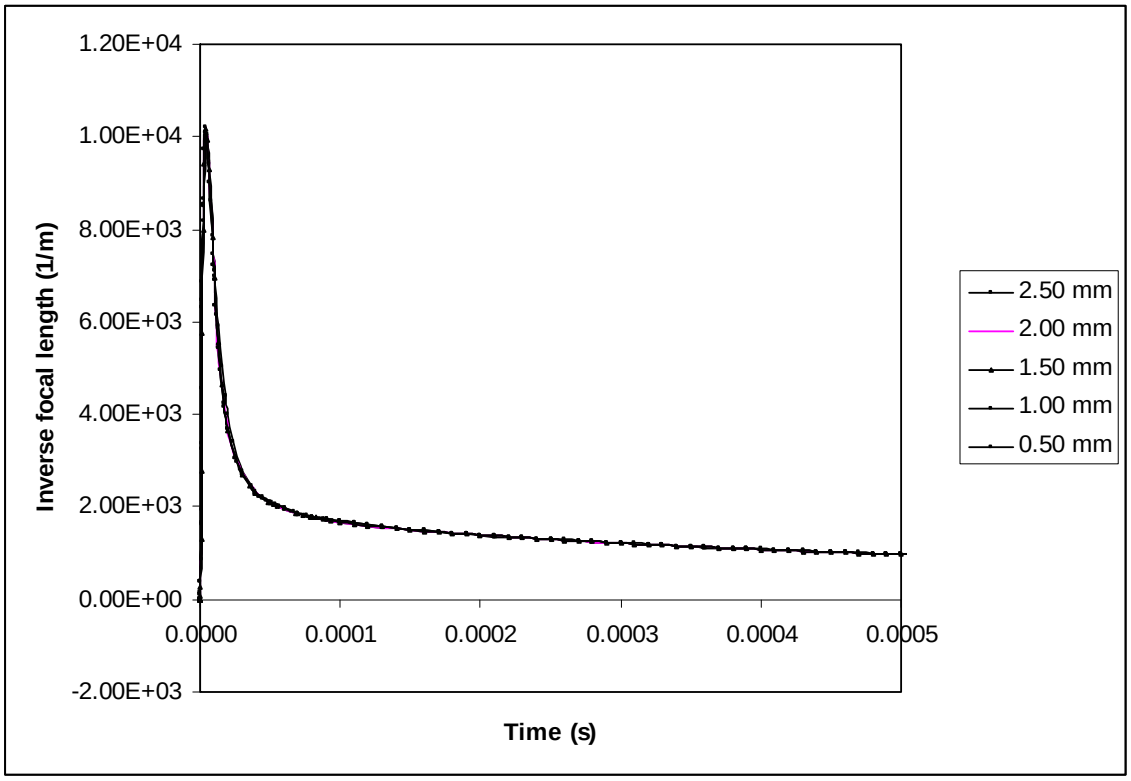

Figure 3-7. FEA modeling of photothermal signal in air.

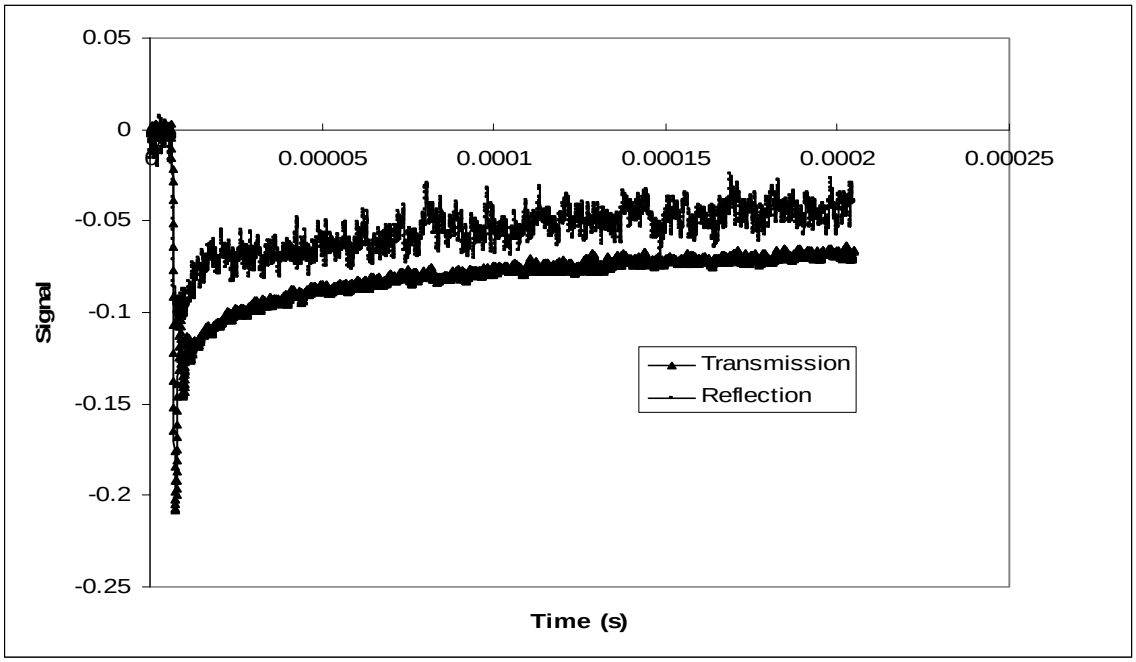

Figure 3-8. Experimental photothermal signals (transmission and reflection).

CONCLUSION

Finite element analysis modeling has been used to describe the pulsed laser excited photothermal lens signal by considering both the heat transfer from sample to air and the thermal lens generated in the air surroundings.

The results show that the air signal contribution to the total photothermal lens signal is significant. It also shows that there are slow and fast signal decay component in glass. Transmission and Reflection Photothermal lens experiments have been carried out using fast response detector and the fast signal decay is detected. The fast decay of signal is interpreted to be due to the fast transfer of heat in axial direction, the direction of the excitation laser beam.

When the heated sample is direct in contact with air or another coupling fluid, heat is transferred from sample to the surroundings along to the axial dimension. The fluid thermal coupling is treated as a perturbation to the thermal lens signal. Here this perturbation appeared in the form of initial faster signal decay. It has been shown that FEA modeling could be used to correct the perturbation to the thermal lens signal for material parameter determination.

These studies open up the possibility of application of FEA modeling and the pulsed excited thermal lens method for accurate prediction of the heat transfer to the coupling fluid and subsequently to study the gas surrounding the samples by using a known material solid sample.

REFERENCES

1. Leite R.C.C., Moore R.S., and Whinnery J.R., Appl. Phys. Lett, **5**, 141 (1964).
2. Solominini D., J. Appl. Phys., **37**, 3314 (1965).
3. Marcano A.O., Loper C., and Melikechi N., Appl. Phys. Lett., **78**, 3415 (2001).
4. Marcano A.O., Loper C., and Melikechi N., J. Opt. Soc. Am. B, **19**, 119 (2002).
5. J. P. Gordon, R. C. C. Leite, R. S. Morre, S. p. S. Porto, and J. R. Whinnery, J. Appl. Phys. **36**, 3 (1965).
6. S. A. Payne, C. D. Marshall, A. Bayramian, G. D. Wilke, and J. S. Hayden, Appl. Phys. B **61**, 257 (1995).
7. N. Neuroth, Opt. Eng. **26**, 96 (1987).
8. P. Greason, J. Detrio, B. Bendow, and D. J. Martin, Mater. Sci. Forum **6**, 607 (1985).

9. M. Sparks, J. Appl. Phys. **42**, 5029 (1970).

10. N.F.Borrelli, D.W. Hall, H.J. Holland, and D.W. Smith, J. Appl. Phys. **61**, 5399 (1987).

11. M.G. Bawendi, P. J. Carroll, W. L. Wilson, and L. E. Brus, J. Chem. Phys. **96**, 946 (1992)

12. T. Miyoshi, Jpn. J. Appl. Phys. **31**, 375 (1992).

13. P. Roussignol, D. Richard, C. Flytzanis, and N. Neuroth, Phys. Rav. Lett. **62**, 312 (1989).

14. M. C. Klein, F. Hache, D. Richard, and C. Flytzanis, Phys, Rev. B **42**, 11 123 (1990).

15. J. J. Shiang. S. H. Risbud, and A. P. Alivisatos, J. Chem. Phys. **98**, 8432 (1993).

16. L. E. Brus, J. Chem. Phys. **80**, 4403 (1984).

17. R. K. Jain and R. C. Lind, J. Opt. Soc. Am. **73**, 647 (1983).

18. J. Yumoto, S. Fukushima, and K. Kubodera, Opt. Lett. **12**, 832 (1987).

19. A. B. Chartier and S. E. Bialkowski, Opt. Eng. **36**, 303 (1997).

20. J. R. Whinnery, Acc. Chem. Res. **7**, 225 (1974).

21. P. R. Joshi, O. O. Dada, and S. E. Bialkowski, Appl. Spectrosc., **63** 815 (2009).

22. O. O. Dada, M. R. Jorgensen, and S. E. Bialkowski, Appl. Spectrosc. **61**, 1373 (2007).

23. O. O. Dada, and S. E. Bialkowski, Appl. Spectrosc. **62**, 1326 (2008).

24. J. Shen, R. D. Lowe, and R, D. Snook, Chem. Phys. **165**, 385 (1992).

25. S. Wu and N. J. Dovichi, J. Appl. Phys. **67**, 1170 (1990).

26. S. E. Bialkowski, *Photothermal Spectroscopy Methods for Chemical Analysis* (John Wiley and Sons, New York, 1996).

CHAPTER 4

MEASUREMENT OF SURFACE DEFORMATION OF GLASS BY PULSED-LASER EXCITED PHOTOTHERMAL REFLECTION LENS EFFECT

ABSTRACT

A time resolved reflection photothermal lens method for the measurement of thermo-mechanical properties of glasses is presented. Finite elemental analysis software with a thermal-structural module is used to model the thermal lens effect by simulating the coupling of heat both within the sample and out to the surroundings. It is shown that the thermal lens produced in the coupling fluid can have significant influence on the total lens strength in air but can be greater for the coupling fluid with larger thermo-optical coefficient. An experimentally monitored thermoelastic surface displacement result is found to be in agreement with the predictions of the finite element analysis model.

INTRODUCTION

Photothermal methods have been used to determine thermal and optical properties of materials since 1981 when photothermal beam deflection or "mirage effect" was first described.[1] There has since steady improvements to both theory and experiment. Several pulsed laser excited methods for measuring optical absorptance and thermal expansion properties of transparent and opaque solids have been described.[2-4] Applications include semiconductors and nanomaterials.[5]

In order to measure optical and thermo-physical properties of solid in microscopic scale, photothermal spectroscopy is considered to be the one of the most widely applicable techniques because of its noninvasive in nature. Noncontact optical methods are preferred over traditional methods because of the simplicity of sample preparation and the absence of thermal contact problems.[6] A microscopic capability also provides the advantage of using a small sample and the potential for scanning or mapping of the properties on a surface.

A tightly focused pulsed laser beam is most often used to excite the solid sample in photothermal spectroscopy. In addition to photothermal effect, one of the most ordinary observed effects is the surface displacement or deformation due to optical excitation. Absorbed energy converts to heat; resulting in thermoelastic expansion (or contraction) of the heated sample thereby producing a curved mirror-like change in the sample structure. This structure acts as a lens altering the divergence of the probe laser. The deformation behaves as a concave or convex mirror[4,7-10] depending on the optical and thermomechanical properties of the sample, such as thermal expansion and/or electronic polarizability coefficients. The displacement is measured by the divergence of the surface-reflected probe laser beam.

The term photothermal reflection lens was first used by Bialkowski at the Gordon Research Conference on Photoacoustic and Photothermal Phenomena (Trieste, IT 2005) for thermoelastic surface displacement produced optical component.[11] But it is now called photothermal mirror by some researcher.[12-15]

There are several ways to monitor the effect of sample heating. Among them are photothermal radiometry, photothermal deflection or “mirage effect,” and measuring

divergence of surface-reflected laser beam. The latter may be having advantages relative to the measurement of beam angle changes used in the photothermal displacement apparatus. The most important advantage is the relative insensitivity to the position of excitation and probe laser beams on the surface.

Modulated irradiation produces a frequency-domain signal. Changing the modulation frequency results in signal magnitude and phase angle changes relative to the excitation. Thermo-elastic properties of the sample are derived by the frequency-dependent amplitude and phase angle changes. On the other hand continuous and pulsed irradiation heating results in time-domain signals. The thermoelastic properties are extracted though analysis of the time-dependent signals. Analysis of the signal, either frequency- or time-dependent, yields the thermal diffusivity and expansion coefficient. Analysis of the transient time-dependent surface displacement and/or temperature change signals allows the measurement of thermal diffusion coefficient.

Bennis et al. and Li solved for the thermoelastic displacement following pulsed irradiation for the case where no heat is conducted to the fluid at the surface and for the case where there is a large surface absorption.[4-5] The excitation beam is incident along the *z* direction and is absorbed at the surface of the sample. The back-reflected photothermal mirror observes the resulting deformation. Photothermal displacement will produce a lens-like mirror with a time-dependent inverse focal length. And solving the Navier-Stokes equation with Duhamel's approximation leads to the term required calculating the inverse focal length.

Although the physical basis is given in Bennis et al. and Li's approximations, better analysis can be done with more realistic models. Two shortcomings of models

described above are 1) that heat transfer to the coupling fluid (the gas or liquid at the sample surface) has negligible effect on the time-dependent temperature and displacement and 2) that refractive index changes in the coupling fluid does not affect the photothermal measurements. To our knowledge, solutions to the time-dependent thermal and thermoelastic where heat is coupled to the surroundings are not known for pulsed laser irradiation.

The cylindrical-symmetric finite element analysis FEA simulation for Corning glass in air shows that there is significant amount of heat coupling to air.[16] The surface temperature is less than that at the interior of the glass. In the absence of the coupling fluid the surface temperature would be at the maximum. Thus models that do not account for heat transfer to the surroundings are in error and the time-dependent surface temperature measurements would not give an accurate estimate for thermal diffusivity because the surface cools faster than these models predict. Another point is that heat does not diffuse to the back surface of a thick glass on the short small timescales of the transient surface displacement.

The aim of this work is to improve measurements of optical and thermal properties of solids by using a pulsed excitation and utilizing photothermal reflection lens effect to monitor thermoelastic surface displacement and by using more accurate physical models that account for surface heat transfer to the surrounding gas or fluid.

THEORY

In pulsed-laser excited photothermal measurements, a short pulse of light excites the surface of the sample. Energy absorbed and not subsequently emitted as luminescence

results in surface heating. The initial temperature change is $\delta T = H\alpha Y_H/\rho C_P$. Here H is radiant exposure, α is the optical absorption coefficient, which for surface absorption is 1-R where R is reflectivity and Y_H is the heat yield or absorptance. Heat subsequently dissipates through both the sample and the gas or fluid in contact with the sample surface changing both the surface temperature and that of the contact fluid.

Bennis *et al.* and Li solved for the thermoelastic displacement following pulsed irradiation.[4-5] The excitation beam is incident along the z direction and is absorbed at the surface of the sample. The back-reflected photothermal mirror is used to observe the resulting deformation. Photothermal displacement will produce a lens-like mirror with a time-dependent inverse focal length given by

$$\frac{1}{f(t)} = 2\left.\frac{\partial^2 u_z(t)}{\partial r^2}\right|_{r=0} \tag{1}$$

where $u_z(t)$ is the z-component of the thermoelastic displacement vector $\mathbf{u}(r,z,t)$. The thermoelastic deformation vector is found from the solution of

$$(\lambda+\mu)\nabla(\nabla\cdot\mathbf{u}(r,z,t)+\mu\nabla^2\mathbf{u}(r,z,t)=\rho_0\frac{\partial^2\mathbf{u}(r,z,t)}{\partial t^2}+\alpha_t(3\alpha+2\mu)\nabla T(r,z,t) \tag{2}$$

Here, $T(r, z, t)$ is the temperature change, λ and μ are Lamé coefficients describing the time-dependent elastic deformation, ρ_0 is density, and α_t is the coefficient of thermal

expansion. For times longer than the acoustic relaxation time, Duhamel's approximation leads to static equation

$$\nabla(\nabla \cdot \mathbf{u}(r,z,t) + (1+2\upsilon)\nabla^2 \mathbf{u}(r,z,t) = \alpha_t(1+\upsilon)\nabla T(r,z,t) \tag{3}$$

v is Poisson's ratio.

The temperature follows the thermal diffusion equation solved with appropriate boundary conditions

$$\frac{\partial T}{\partial t}(r,z,t) - D_T \nabla^2 T(r,z,t) = \frac{U(r,z,t)}{\rho_0 C_p} \tag{4}$$

$U(r,z,t)$ is the energy density, and $D_T = k_T/\rho_0 C_P$ is the thermal diffusivity where k_T is thermal conductivity

Initial surface heating. For a Gaussian excitation laser with a radiant exposure, the distribution is

$$H(r,t) = \frac{2Q}{\pi w^2} e^{-(2r^2/w^2)} \delta T \tag{5}$$

The energy density for a short-pulsed excitation laser is

$$U(r,z,t) = \frac{2Q\alpha Y_H}{\pi w^2} e^{-(2r^2/w^2)} e^{(-\alpha z)} \delta(t) \tag{6}$$

α is the optical absorption coefficient, Q is the pulsed laser energy, w is the electric field beam waist radius, and Y_H is the heat yield. The heat yield may be related to reflectivity through $Y_H = 1 - R$ where R is reflectivity.

Time-dependent temperature and thermoelastic displacement. The thermal diffusion and thermoelastic displacement equations have been solved for the case where no heat is conducted to the fluid at the surface and for the case where there is a large surface absorption.[4-5] The temperature change can be expressed by

$$T(r,z,t) = C_1 \int_0^{\infty} J_0(\lambda r) e^{\left(-\frac{\lambda^2 w}{8}\right)} \times \left[\sum_{k=0}^{\infty} N_k(\lambda, \eta_k) \cos(\eta_k z) e^{\{-D_T(\lambda^2+\eta_k^2)(t-\tau)\}} \right] \lambda d\lambda \qquad (7)$$

where $N_k(\alpha, \eta_k) = [1 - e^{\{-D_T(\lambda^2+\eta_k^2)\tau\}}] M_k(\lambda, \eta_k)$

and $$M_k(\lambda, \eta_k) = \frac{2\alpha^2 [1 - (-1)^k e^{(-\alpha L)}]}{(\alpha^2 + \eta_k^2)(\lambda^2 + \eta_k^2)}$$

$\eta_k = \pi k/L$ where L is the sample thickness, $C_1 = (QY_H/2\pi kTL\,\tau)$ and τ is the laser pulse duration. Similarly, solving the Navier-Stokes equation with Duhamel's approximation leads to the term required to calculate the inverse focal length

$$\frac{\partial^2 u_z(t)}{\partial r^2}\Big|_{r=0} = 2C_1\alpha_t(1+\upsilon) \int_0^{\infty} e^{\left(-\frac{\lambda^2 w^2}{8}\right)} X \left[\sum_0^{\infty} A_k(\lambda, \eta_k) e^{\{-D_T(\lambda^2+\eta_k^2)(t-\tau)\}} \right] d\lambda \qquad (8)$$

where $$A_k(\lambda,\eta_k) = 2\left[1 - e^{\{-D_T(\lambda^2+\eta_k^2)\tau\}}\right]B_k(\lambda,\eta_k)$$

and $$B_k(\lambda,\eta_k) = \frac{\lambda^4}{(\lambda^2+\eta_k^2)^2}\left[\frac{\cosh(\lambda L)-(-1)^k}{\sinh(\lambda L)+(-1)^k\,\lambda L}\right]$$

This model shows that the magnitude of the reflection lens signal will be proportional to $\alpha_t(1+\nu)$ while the time-dependent behavior is related to D_T. There are facile forms of the above results for high absorption coefficient, short pulse duration, and for samples with large L.

Heat transfer with coupling fluid. Solutions to the time-dependent thermal and thermoelastic where heat is coupled to the surroundings are not known for pulsed laser irradiation. The simplest is for one-dimensional thermal diffusion along the z-direction

$$T(z,t) = \frac{Q\alpha Y_H}{\rho_s C_{p,s} D_{T,s}^{1/2} + \rho_f C_{p,f} D_{T,f}^{1/2}} (\pi t)^{-1/2} e^{(-z^2/4D_{T,f}t)} \tag{9}$$

Subscripts s and f refer to solid and fluid respectively. Measurements of the time-dependent surface temperature (z=0) are used to determine the thermal relaxation time, which in turn is related to the thermal diffusion and heat capacity of the solid and fluid. When these properties are known for the contact fluid and the parameter $\rho_S C_{P,S} D_{T,S}^{1/2} = (\rho_S C_{P,S} k_{T,S})^{1/2}$ is derived from the time-dependent temperature decay. Duhamel's Navier-Stokes approximation is used to determine displacement if the temperature distribution is known.

The temperature change and thermoelastic displacement can be calculated using finite element analysis (FEA). FEA modeling using Comsol Multiphysics software in conduction and convection mode solves the heat diffusion equation given above. The thermoelastic equation is coupled to the temperature change. Hook's law models the time-dependent expansion with parameters approximating the Lamé coefficients describing the time-dependent elastic deformation.

Photothermal reflection lens. In photothermal reflection lens or mirror apparatus, the excitation and probe laser beams strike the sample in collinear arrangement. There is no displacement between the two beams at the sample. Practically speaking, beam alignment is easier because the signal is optimized when the two beams are collinear. Thermoelastic surface displacement acts as an optical element modeled as a defocusing mirror. Thus the spot size of the reflected probe laser changes with surface deformation. The spot size can be calculated using ray transfer matrix methods based on the inverse focal length of the mirror.[6]

The photothermal lens element is analyzed by directing the probe laser beam at the sample. The reflected beam is detected past a pinhole aperture through a beam splitter set to direct the reflected beam to the pinhole and detector. Treating the displacement as a lens, the power of the probe laser beam passing through an aperture place in far field is the photothermal lens signal. The signal is defined as $S(t) = -2z'/f(t)$ where z' is the sample-detector distance.

Effects of coupling fluid refractive index change. In general, the inverse focal length consists of two terms: $1/f(t) = 1/f_f(t) + 1/f_s(t)$ where f and s refer to fluid and sample reflection, respectively. The two terms are

$$\frac{1}{f_f(t)} = 2\left(\frac{dn}{dT}\right)\int_{path}\frac{\partial^2 T(r,z,t)}{\partial r^2}\Big|_{r=0} ds \tag{10}$$

$$\frac{1}{f_s(t)} = 2\frac{\partial^2 u_z(t)}{\partial r^2}\Big|_{r=0} \tag{11}$$

Recent calculation have shown that the photothermal lens produced in the coupling fluid can have significant (5%) influence on the total lens strength in air but can be greater for the coupling fluid with larger thermo-optical coefficient*, dn/dT*.

MATERIALS AND METHODS

Experimental apparatus. A conventional two-color photothermal lens apparatus with a probe laser 632.6 nm HeNe probe laser and a XeCl laser pumped dye laser excitation source operating at 490 nm was used. Directing the collinear excitation and the probe laser beam onto the sample surface performed the photothermal reflection lens measurement. The beams were made collinear using a polarizing or dichroic beamsplitter. In this way, one laser was transmitted and the other was reflected off the front surface of the beamsplitter. Other mirrors were used to direct the beams onto the beamsplitter and then onto the sample. A beamsplitter was placed along the beam propagation axis. The back reflected probe laser was redirected toward a thermal lens detection setup. The latter consists of an optical bandpass filter used to block the excitation laser radiation, a pinhole aperture placed at the center of the probe laser beam.

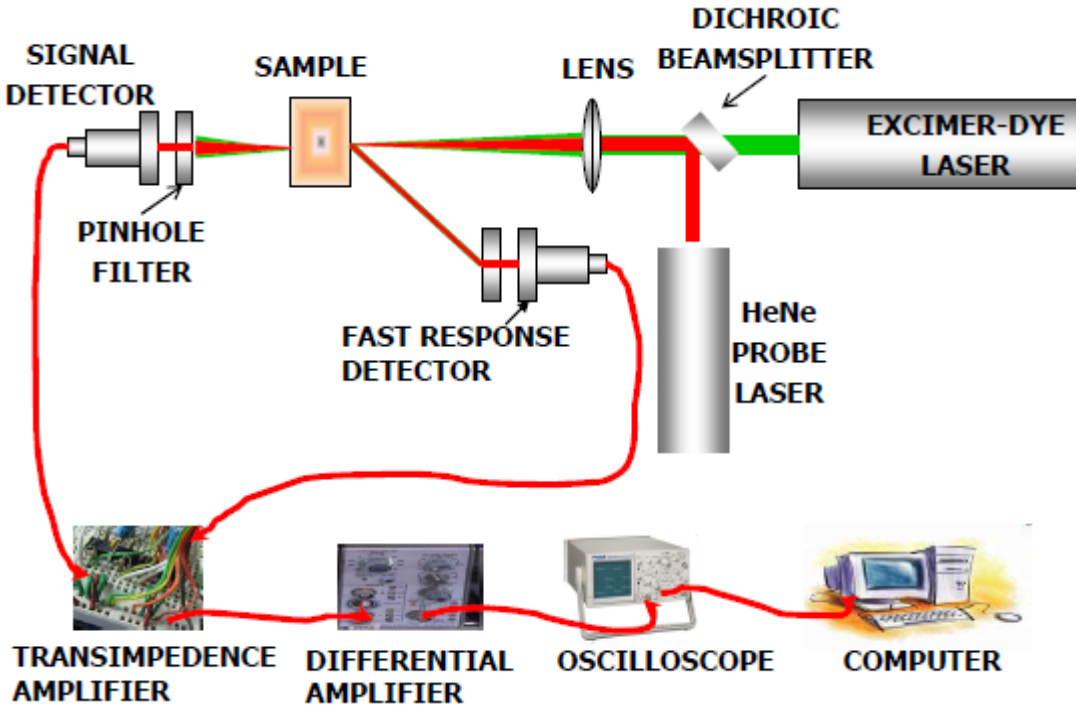

Figure 4-1. A schematic drawing of a photothermal lens experimental setup.

The fast response photodiode signal was buffered with a transimpedence circuit, amplified with a variable gain voltage amplifier and averaged over several repetitions of the pulsed laser with a digital oscilloscope. The transient data were subsequently transferred to a computer for data analysis. Figure 4-1 illustrates the schematic drawing of a photothermal lens experimental set up.

Sample. Standard Corning, 5 cm x 5 cm, 3389 colored glass optical filters (CS3-73, 3.05 mm thickness) of absorption coefficient $3.8m^{-1}$ were investigated as an absorbing solid sample. The sample is positioned at the focus of the excitation beam for maximum temperature gradient. Sample absorbance was recorded with a Cary 3E UV-Visible spectrophotometer.

Modeling. Finite element analysis (FEA) software provides numerical solutions to the heat transfer equations with the realistic boundary conditions imposed by the experimental geometry. The model solid absorbing media was small square plates, 5 cm x 5 cm x 0.305 cm, or 5 cm x 5 cm x 3.05 mm, and had the same dimensions of the glass samples used in the experiments. Optical excitation was along the small dimension. For convenience, glass heating was modeled with 2D axial symmetry with the origin at the center that the z-axis runs along the path length of the excitation and probe beams.

Comsol Multiphysics in thermal structural interaction module (v 3.5a) analysis was carried out on a Compaq Presario SR1330X, AMD Athlon XP 3200 processor using MS Windows XP. The software in conduction and convection mode solves the heat diffusion equation given as

$$\rho C_p \frac{\partial}{\partial t}\delta T(r,z,t) - k\nabla^2 \delta T(r,z,t) = q_H(r,z,t) - \rho C_p u \cdot \nabla \delta T(r,z,t)$$

While the stress-strain analysis for axial symmetry uses Newton's 2nd Law with Rayleigh viscous damping.

$$\rho \frac{\partial^2 \mathrm{u}}{\partial t^2} - \nabla \cdot c\nabla \mathrm{u} = \mathrm{F}$$

$$m\frac{\partial^2 \mathrm{u}}{\partial t^2} + \xi \frac{\partial \mathrm{u}}{\partial t} + k\mathrm{u} = f(t)$$

$$\frac{\partial \sigma_r}{\partial r} + \frac{\partial \tau_{rz}}{\partial z} + \frac{\sigma_r - \sigma_\theta}{r} + K_r = 0$$

$$\frac{\partial \tau_{rz}}{\partial r} + \frac{\partial \sigma_z}{\partial z} + \frac{\tau_{rz}}{r} + K_z = 0$$

Finite element analysis modeling consists of drawing the sample geometry and specifying material boundary conditions, heat sources, and sinks. The problems are then solved with rough finite element definition and further refinement of elements and domain are made. Finally, *dT* can be obtained either at a single time, over a time series, or at steady state. The path integral of the second radial derivative was found by using the Comsol integration-coupling variable to integrate the second derivative function of the temperature change.

RESULTS AND DISCUSSION

Figures 4-2 and 4-3 are FEA modeling of thermal expansion of 3.05 millimeter silica glass without and with air surrounding. Pulsed laser ($4.4x10^{-4}$J) of 60 μm size was used for modeling. The time is 0.01second after pulse irradiation. The extent of temperature goes up from blue to red in figures. Two things are apparent from these figures. First is the glass- air heat coupling resulting in heat loss from the sample to the surroundings. Second, glass expansion is affected by coupling fluid because of the heat transfer.

Figures 4-4 and 4-5 compares the temperature change in the glass with and without the coupling fluids around it. Temperature change is slightly lower when the sample is surrounded by air than insulated glass case. This is due to the heat diffusion to the air. Similarly Figure 4-6 and 4-7 surface displacements along z direction, which is also a direction of excitation laser, of glass without and with air environment. Again these figures show that the thermal displacement of glass is affected by surrounding of glass sample.

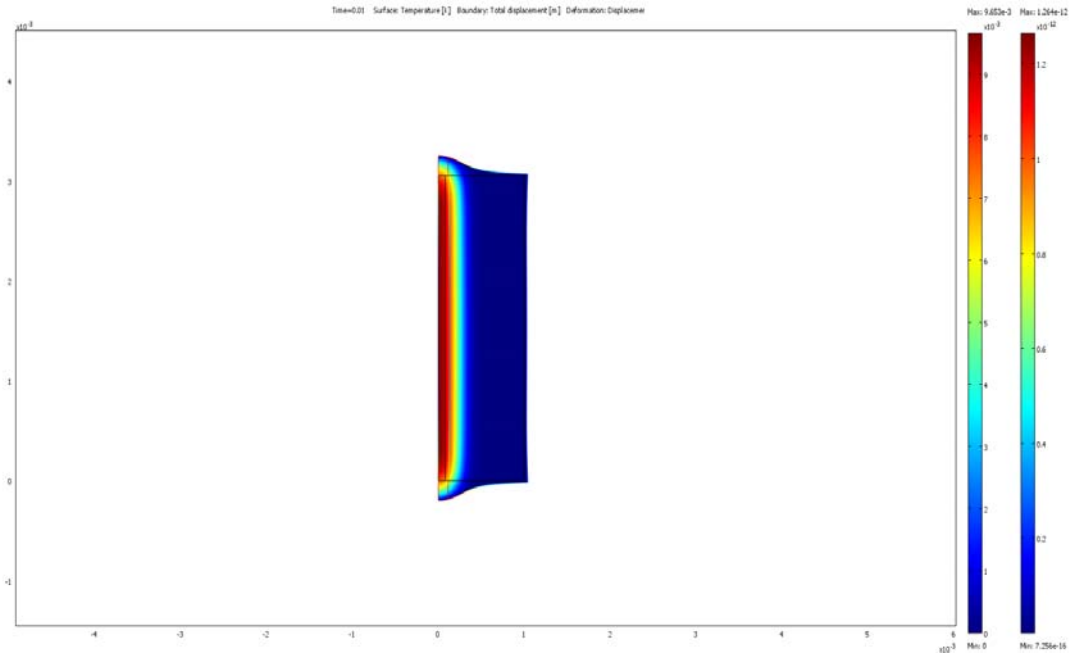

Figure 4-2. FEA model of thermal expansion of 3.05mm silica glass.

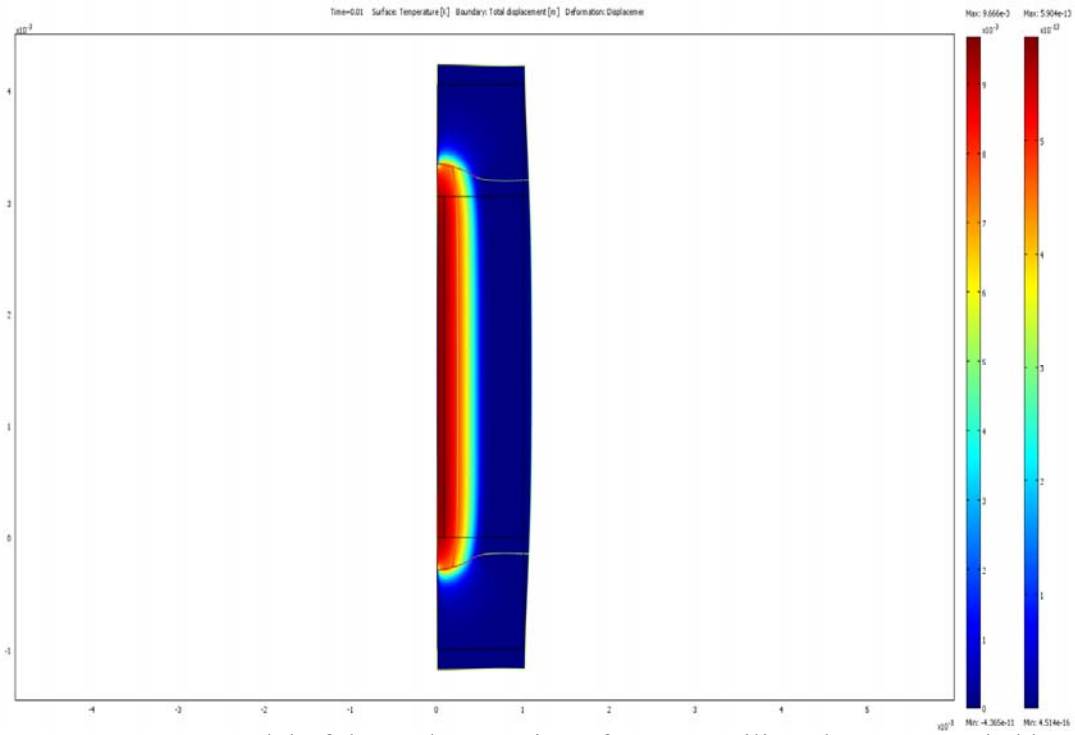

Figure 4-3. FEA model of thermal expansion of 3.05mm silica glass surrounded by air.

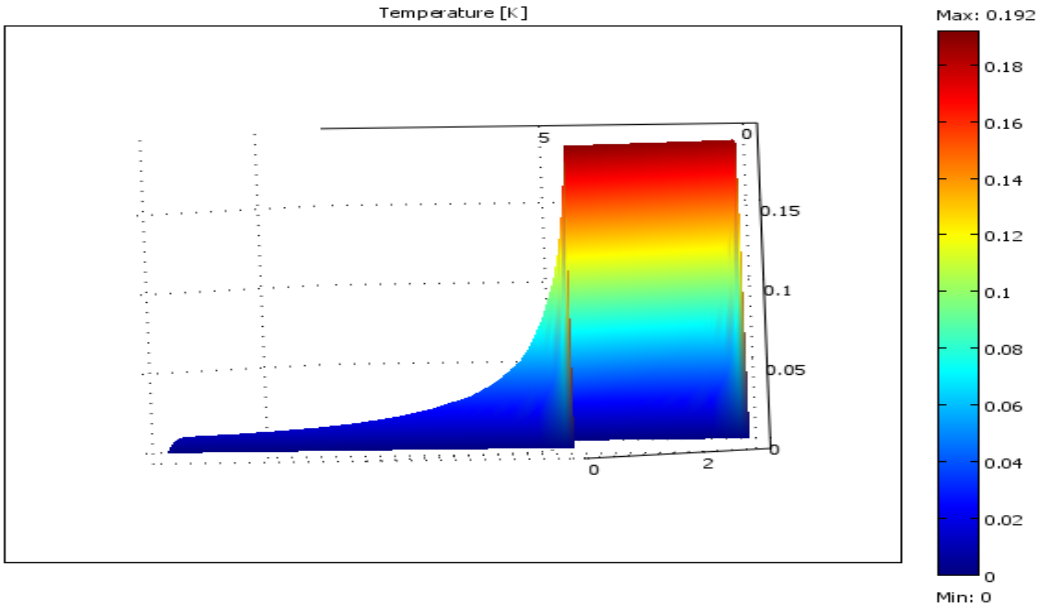

Figure 4-4. FEA model (plot of temperature change) of thermal expansion of 3.05mm silica glass.

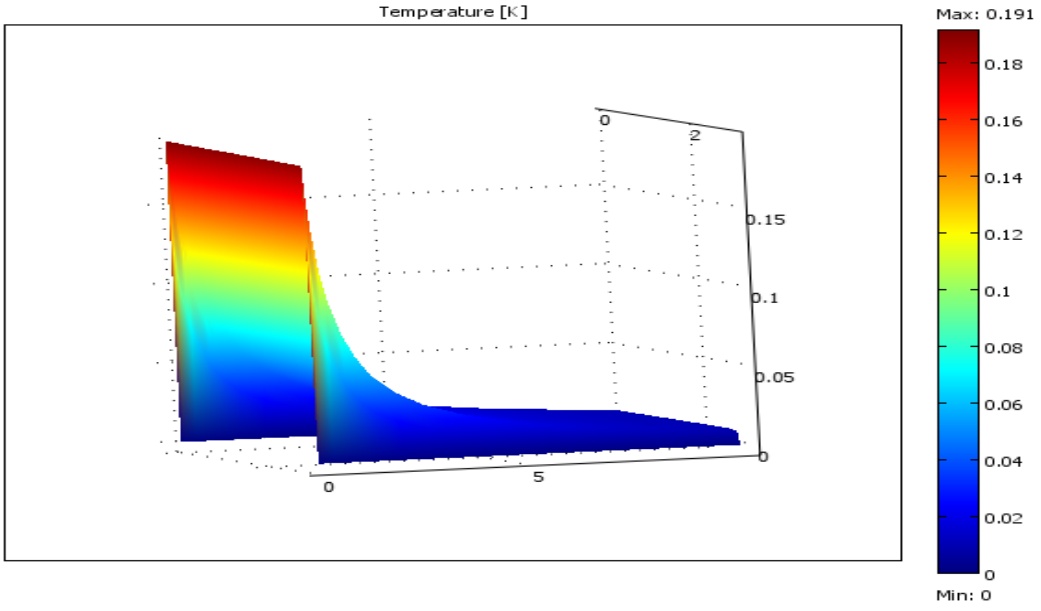

Figure 4-5. FEA model (plot of temperature change) of thermal expansion of 3.05mm silica glass surrounded by air.

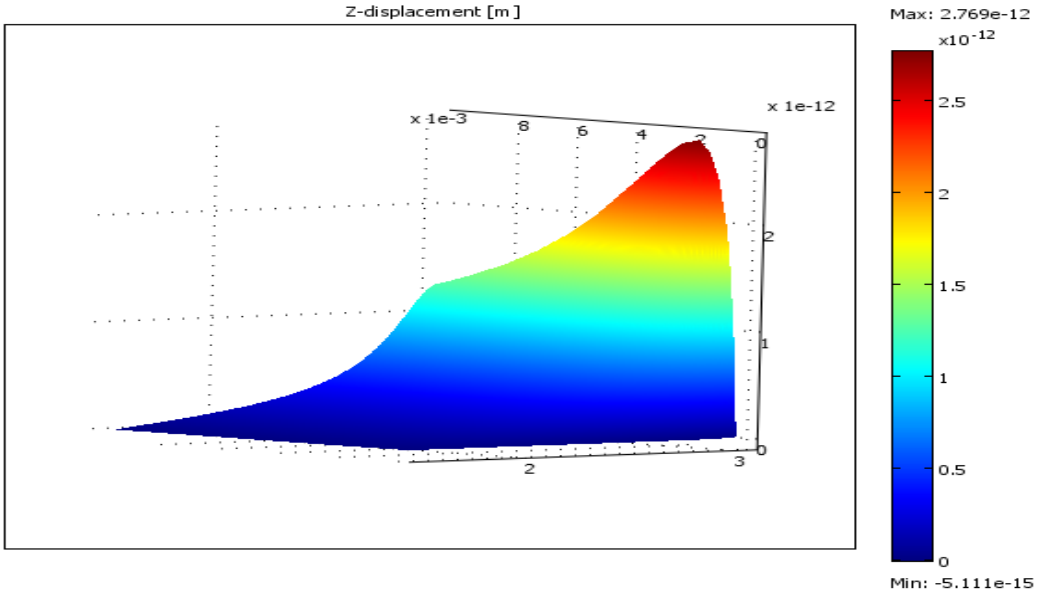

Figure 4-6. FEA modeling of (surface displacement along the z direction) silica glass.

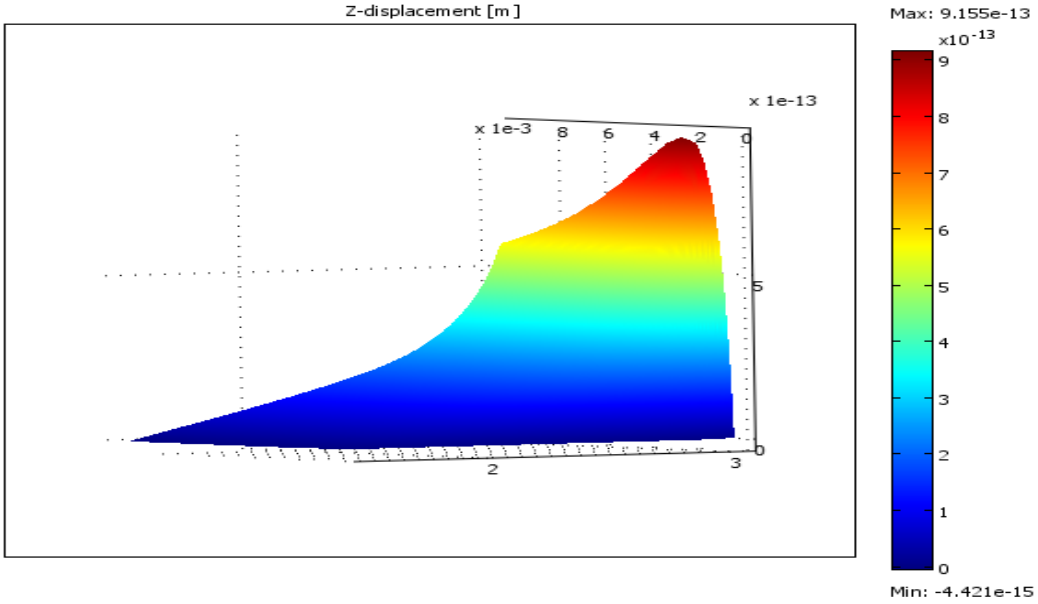

Figure 4-7. FEA modeling of (surface displacement along the z direction) silica glass surrounded by air.

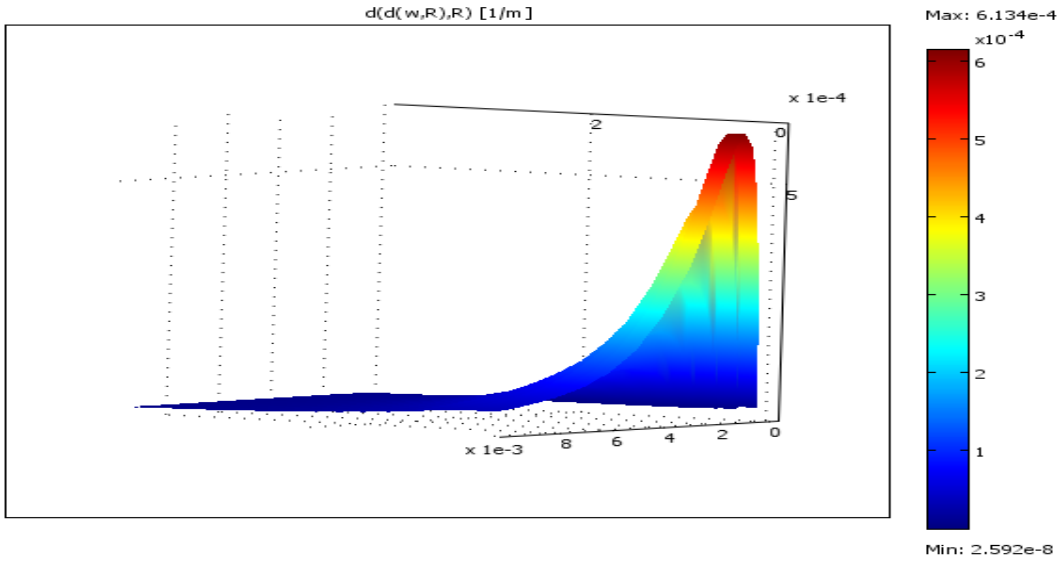

Figure 4-8. FEA modeling of (second derivative of *z* displacement with respect to *r* vs axial distance) silica glass.

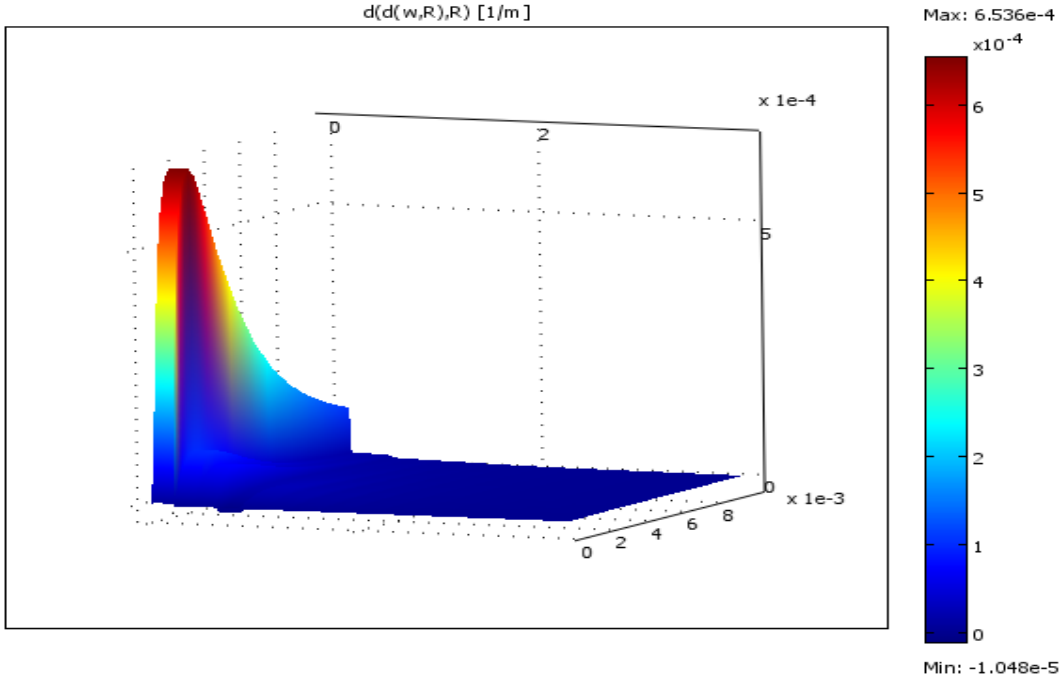

Figure 4-9. FEA modeling of (second derivative of *z* displacement with respect to *r* vs axial distance) silica glass surrounded by air.

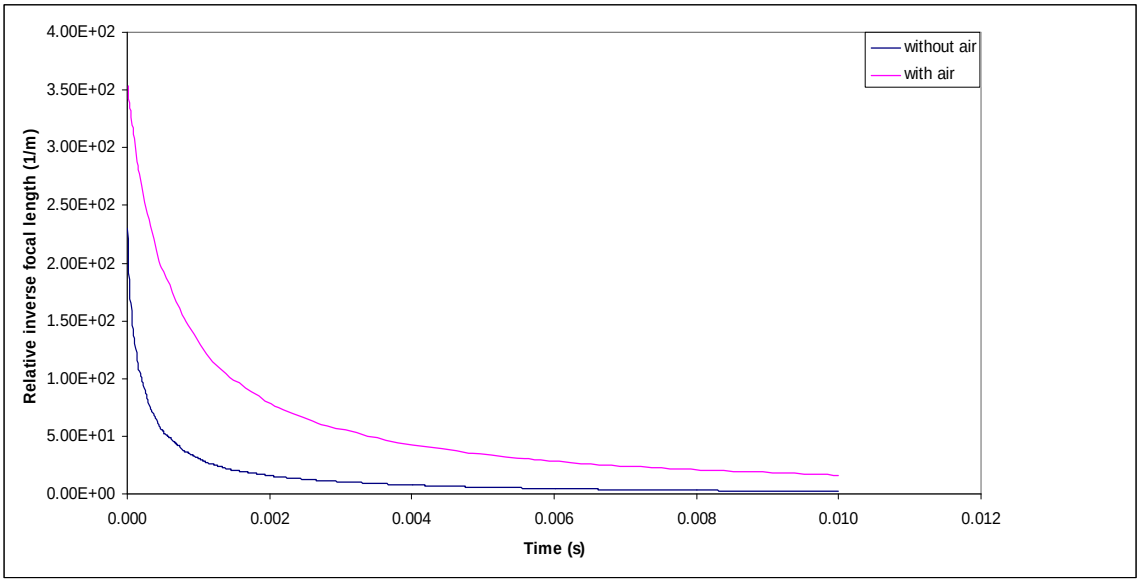

Figure 4-10. FEA modeling of normalized relative inverse focal length versus time of silica glass with and without air environment.

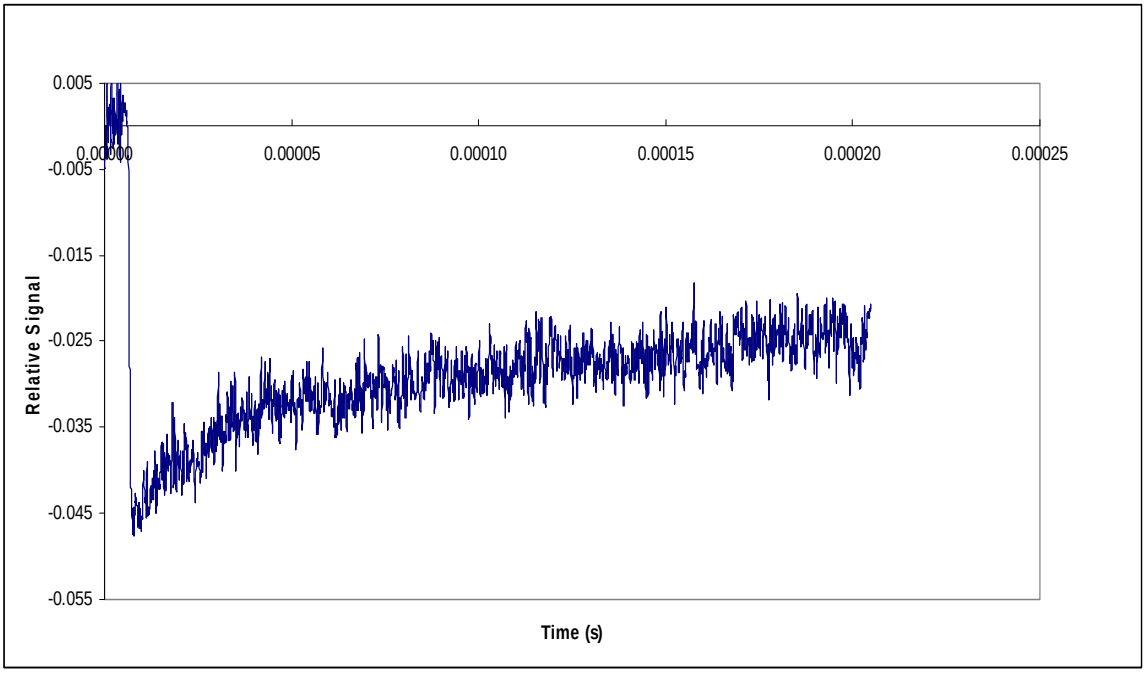

Figure 4-11. Reflection photothermal lens signal.

Surface deformation is larger in insulating system of glass than in air environment. With the help of FEA modeling second derivative of displacement with respect to radial distance can be evaluated.

The second derivative of displacement with respect to radial distance of glass with and without heat coupling surrounding can be compared from Figure 4-8 and 4-9.These values are also different. FEA modeling of normalized relative inverse focal length versus time of silica glass with and without air environment is presented in Figure 4-10. And it shows that the magnitude of signal in glass with coupling fluid is larger than that of without coupling fluid.

Figure 4-11 is an experimental reflection photothermal lens signal of Corning glass filter 3389. It has positive optical-thermal coefficient and gives negative signal. The inverse focal length measured from it is comparable that of the FEA modeling to estimate the thermal physical properties of solid samples.

The models that do not account for heat transfer to the surroundings are apparently in error. Using these models to determine optical and thermophysical properties of solids by photothermal spectroscopic methods will result in inaccurate results. Taking account of the contributing effect of coupling fluids should enhance the accuracy of the optical-thermo-physical properties of the solid sample in heat coupling environments when analyzing experimental results obtained using photothermal reflection lens methods. The inverse focal length of the system, consists of two terms, is sum of inverse focal length of sample and coupling fluid. If we know the *dn/dT* of coupling fluid, inverse focal length of it can be evaluated which can be used to correct the values. FEA modeling is helpful to evaluate the inverse focal length.

CONCLUSION

The existing models ignore the effects of immediate surroundings of solid sample to measure the thermal physical properties by photothermal spectroscopy. But our studies show that there is significant effect of contact surroundings of solid sample to the thermal expansion, surface temperature change, and the photothermal signal of sample. Therefore, models that do not account for heat transfer to the surroundings are in error to measure optical and thermophysical properties of solids by photothermal spectroscopic methods. An improved approach to measure correct thermo- physical and optical parameter of solid sample by thermal lens spectrometry has been presented.

Time resolved reflection photothermal lens experiment is carried out on Corning colored glass filters and thermoelastic surface displacement is measured. FEA simulation of thermal lens effect on glass coupling of heat both within the sample and out to the surroundings for pulsed laser excitation is done. An experimental thermoelastic surface displacement result is compared with that of modeling and are found to be very close. The effect of the coupling fluid is incorporated into this model in order to minimize the error in measuring physical constants.

REFERENCES

1. W. B. Jackson, N. M. Amer, A. C. Boccara, and D. Fournier, Appl. Opt. **20**, 333(1981).
2. Olmstead, M. A, N.M. Amer, S.Kohn, D. Fournier, and A. C. Boccara., Appl. Phys. A: Solid Surf. **32**, 141 (1983).

3. Opsal, J, A. Rosencwaig, and D. L. Willenborg, Appl. Opt. **22**, 3169 (1983).

4. Li, B. C.; J. Appl. Phys. **68**, 482 (1990).

5. G. L. Bennis, R. Vyas, R. Gupta, S. Ang, and W. D. Brown, J. Appl. Phys. **84**, 2602 (1998).

6. Bialkowski, S. E., *Photothermal Spectroscopy Methohod of chemical analysis* (Wiley, New York, 1996).

7. J. C. Cheng, and S. Y. Zhang, J. Appl. Phys. **70**, 7007 (1991).

8. P. K. Kuo, and M. Munidasa, Appl. Opt. **29**, 5326 (1990).

9. J. W. Fang, and S. Y. Zhang, Appl. Phys. B: Lasers Opt. **67**, 633 (1998).

10. B. Li, H. Blaschke, and D. Ristau, Appl. Opt. **45**, 5827 (2006).

11. O. O. Dada,., M. R. Jorgensen, and S. E. Bialkowski, Appl. Spectrosc. **61,** 1373 (2007).

12. N.G.C. Astrath, , L.C. Malacarne, P.R.B. Pedreira, A.C. Bento, and M.L.Baesso, Appl. Phys. Lett. **91**, 191908 (2007).

13. Francine B. G. Astrath, Nelson G. C. Astrath, Jun Shen, Jianqin Zhou, Luis C. Malacarne, P. R. B. Pedreira, and Mauro L. Baesso, Optics Express **16**, 12214 (2008).

14. N. G. C. Astrath, , F.B.G. Astrath, , J. Shen, C. E. Gu, L,. C. Malacarne, P.R.B. Pedreira, A. C. Bento, and M. L. Baesso, Appl. Phys. B **94**, 473 (2009).

15. F.Sato, L.C. Malacarne, P.R.B. Pedreira, M.P. Belancon, R.S. Mendas, M.L. Baesso, N. G.C. Astrath, and J.Shen., J.Appl. Phys. **104**, 053520 (2008).

16. P. R. Joshi, O. O. Dada, and S. E. Bialkowski, Appl. Spectrosc. **63**, 815 (2009).

CHAPTER 5

PHOTOTHERMAL LENS SPECTROMETRY IN NANOLITER CYLINDRICAL SAMPLE CELLS

ABSTRACT

A novel apparatus for performing photothermal lens (PTL) spectroscopy is described which uses a low-volume cylindrical sample cell with pulsed excitation laser and a continuous probe laser. The whole sample cell volume is irradiated with constant irradiance beam produced by an excitation laser. The photothermal lens element is formed by thermal diffusion from the irradiated sample volume through the sample cell walls. The apparatus has been found to work with cells designed to contain sample volumes to 361 nL. Larger and smaller volume cells are practical. However, the response time increases with increasing sample cell radius. The theoretical thermal lens signal increases with decreasing sample cell radius for a source with constant integrated irradiance. Finite Element Analysis (FEA) modeling is used to examine the temperature profile and the photothermal signal. The result of FEA is compared with the experimental result.

INTRODUCTION

The technique of photothermal spectrometry has been used for low absorbance measurements for several decades. It is an ultra-sensitive spectroscopy technique useful for analytes that do not fluoresce. It has not, however, found widespread use in chemical

analysis owing, in part, to anomalous behavior arising from sample temperature changes, changes in thermodynamic properties of the matrix, and nonlinear optical effects.[1]

There are several physical effects that limit sensitivity and influence the accuracy of measurements obtained using photothermal lens spectrometry.[2-4] First, the photothermal lens signal is related to the lens formed the sample as a consequence of light absorption and subsequent energy transfer to the matrix. The optical element produced when laser beams are focused into a homogeneous sample is not a simple lens. The aberrant natures of the photothermal lens results in signal magnitudes that are somewhat smaller than expected and also more difficult relate to sample absorbance. [5,6] Second, sample irradiation can produce large temperature changes. In theory, the on-axis temperature change approaches infinity at long times for any excitation power when using continuous laser excitation sources. In practice, large temperature changes distort the thermal lens perturbation due to density differences and convection heat transfer or even boiling may occur. [7-9] The later distorts the signal and ruins the analytical utility.

This paper described a novel apparatus that apparently circumvents many of problems associated with photothermal spectrometry of homogeneous samples. The apparatus uses a low-volume cylindrical sample cell, a chopped or pulsed excitation laser, and a continuous probe laser. The full volume of the sample is irradiated with constant, e.g., non-Gaussian, irradiance beam produced by the excitation laser. Constant irradiance excitation source does not directly produce the photothermal lens element in the sample. The lens element is formed by thermal diffusion from the irradiated sample volume,

through the sample cell walls. Under continuous irradiation, thermal diffusion results in a parabolic temperature change profile.

The most important aspect of this experiment arrangement is that artifacts due to excited state refractive index changes, volume changes, etc. do not affect the signal. Although the refractive index change may depend on the partial refractive index and partial molar volume of transient species, these changes do not result in a photothermal lens element. By monitoring both the central portion and the full probe laser beam, the apparatus can compensate for transmission changes due to bulk density, refractive index, or absorbance changes.

This paper outlines the model used to relate the heat transfer and the photothermal effect to experimental observation. Experiments to verify the operation of the apparatus are performed with iron (II) dicyclopentadine ($FeCp_2$) in ethanol. Photothermal lens signals processed in the usual fashion are found to be relatively linear, reproducible, and consistent with the model based on heat conduction through the sample cell walls. The experimental photothermal lens enhancement is found to be that predicted from theory within experimental error. FEA modeling has been also used for the better understanding of temperature profile and for the comparison of the experimental results.

THEORY

In photothermal lens spectrometry, the measured signal is related to the focal length of the lens formed when the sample absorbs optical radiation. Absorbed energy it converted to heat. Sample heating changes the temperature and subsequently the refractive index of the sample, producing the lens-like refractive index change. A probe

laser is used to detect the refractive index change. The theoretical signal is found by first solving the thermal diffusion equation to determine the time-dependent temperatures, second finding the thermal lens this temperature change produces, and finally, calculating the signal that will be produced in the experimental apparatus.

Temperature change. The temperature change is found using the thermal diffusion equation with the appropriate boundary conditions. For weakly absorbing sample without significant attenuation along the *z*-axis, the radius, *r* (m), and time, *t* (s), dependent thermal diffusion equation is

$$\frac{\partial}{\partial t}\delta T(r,t) - D_T \nabla_r^2 \delta T(r,t) = \frac{q_H(r,t)}{\rho C_P}$$
$$\nabla_r^2 = \frac{1}{r}\frac{\partial}{\partial r}\left(r\frac{\partial}{\partial r}\right) \qquad (1)$$

In this equation, δT (r, t) is the temperature change, D_T (m^2 s^{-1}) is the thermal diffusion coefficient, q_H (r, t) (W) is the heat source term given as a rate of heat production, ρ is density (kg m^{-3}), and C_P (J kg^{-1} K^{-1}) is heat capacity.

This equation may be used to find an analytical solution when thermal diffusion along the z-axis is negligible compared to that in the radial direction. This implies that the sample is optically thin, i.e., low absorbance and that the cell windows are thermally insulating relative to the cell walls. The later approximation is probably reasonable for metal sample cells with glass windows, as is used here.

For illumination of the full sample cell volume, and when pulsed excitation and excited state relaxation occurs much faster than thermal diffusion, the instantaneous heat source term is independent of radius and the initial temperature change is

$$\delta T_0 = \frac{Q\alpha Y_H}{\pi a^2 \rho C_P} \tag{2}$$

Q (J) is the pulsed laser energy passing through the sample cell, α (m^{-1}) is the exponential absorption coefficient, and a (m) is the radius of the sample cell. The term Y_H is a unit less heat yield term included to account for any radiative energy loss. It is the fraction of energy absorbed and not lost by reemission of radiation. This term is unity for non-luminescent samples. The heat source term is thus

$$q_H(r,t) = \frac{\partial}{\partial t}\frac{Q\alpha Y_H}{\pi a^2}\delta(t) \tag{3}$$

$\delta(t)$ is a delta function. Since the thermal conductivity and heat capacity of the metal are large relative to that of the sample, it is assumed that temperature change is zero at the sample-cell wall interface. The time-dependent impulse-response for the temperature change produced in a cylindrical cell with an internal radius, a (m), and zero cell wall temperature is [10-11]

$$\delta T(r,t) = 2\delta T_0 \sum_{n=1}^{\infty} \exp\left(-\chi_n^2 D_T t / a^2\right)\frac{J_0\left(r\chi_n / a\right)}{\chi_n J_1\left(\chi_n\right)} \tag{4}$$

where δT_0 is the instantaneous initial temperature change of the cylindrical region, J_0 and J_1 are the zero and first order Bessel's functions, and χ_n is the n'th root of the Bessel's function equation, $J_0(\chi_n)=0$.

Photothermal lens signal. The photothermal lens strength is found from [1,12]

$$\frac{1}{f(t)} = -\frac{1}{2}\left(\frac{dn}{dT}\right)\int_{path}\left|\frac{d^2}{dr^2}\delta T(r,t)\right|_{r=0} ds \tag{5}$$

The term (dn/dT) is the thermal-optical coefficient. It relates the change in refractive index to temperature change. Using the relationship $|d^2J_0(ar)/dr^2|_{r=0}=-a^2$, and substituting the integral by the path length, l (m), product, the time-dependent inverse focal length is

$$\frac{1}{f(t)} = \left(\frac{dn}{dT}\right)\frac{l}{a^2}\delta T_0 \sum_{n=1}^{\infty}\exp\left(-\chi_n^2 D_T t/a^2\right)\frac{\chi_n}{J_1(\chi_n)} \tag{6}$$

Using the initial temperature change results in the photothermal lens strength of

$$\frac{1}{f_{cyl}(t)} = \left(\frac{dn}{dT}\right)\frac{\alpha l Q Y_H}{\pi a^4 \rho C_P}\sum_{n=1}^{\infty}\frac{\chi_n \exp\left(-\chi_n^2 t/4t_c\right)}{J_1(\chi_n)} \tag{7}$$

The characteristic thermal time constant is defined as $t_c=a^2/4D_T$.

The photothermal lens signal for the cylindrical sample cell is defined in the same fashion as in the large-volume sample cell. [1] The time-dependent signal is found from

$$S(t) = \frac{\Phi_p(\infty) - \Phi_p(t)}{\Phi_p(t)} \tag{8}$$

Φ_p(t) is the time-dependent probe laser power passing through a pinhole placed beyond the sample cell. The reference at infinite time is used to indicate power of the unperturbed probe laser, i.e., with no thermal lens. For a pinhole aperture placed far from the sample cell, the signal is $S(t) \approx 2z'/f(t)$, where z' (m) is the distance from the probe laser beam focus position to the sample cell.

Model calculations exhibit an exponential response after a relatively short induction period. The model behavior indicates that a single Bessel's root dominates the time-dependent behavior. Examination of the model data shows that the first root, χ_1=2.405, dominates after an initial induction period. The inverse focal length is approximated by

$$\frac{1}{f_{cyl}(t)} \approx \left(\frac{dn}{dT}\right)\frac{\alpha l E Y_H}{2\pi a^2 \kappa}\left[1 - 2\frac{e^{-\chi_1^2 t/4t_c}}{\chi_1 J_1(\chi_1)}\right] \tag{9}$$

The characteristic time constant may be obtained from $t_c = 2.632\Delta t_{10\%\text{-}90\%}$, where $\Delta t_{10\%-90\%}$ is the time required for the signal to change from 10% to 90% of the maximum.

Thermal lens signal. The photothermal lens element is detected using a probe laser. The thermal lens signal is defined as the relative change in optical power of a probe laser beam passing first through the sample, and then through a small pinhole

aperture set to monitor the beam center and positioned far from the sample. The photothermal lens strength is initially zero and increases with time. The maximum signal is found from the relationship, S (∞) = [$\Phi_p(0)$-$\Phi_p(\infty)$]/$\Phi_p(\infty)$, where $\Phi_p(0)$ and $\Phi_p(\infty)$ are the probe laser powers at zero and infinite times, respectively. Paraxial refraction theory is used to determine the effect of the thermal lens on the probe laser propagation characteristics. [13] When the pinhole aperture is placed far from the sample cell, the signal is $S_{cyl}(t)=2z'/f(t)$, where $S_{cyl}(t)$ is used to signify the signal produced in the cylindrical cell and z' (m) is the distance between the probe beam focus position and the sample cell. The maximum thermal lens signal is thus

$$S_{cyl}(\infty)=\left(\frac{dn}{dT}\right)\frac{q_{H,\,path}\;z'}{\kappa_f} \tag{10}$$

The practical probe laser focus distance, z', will be limited by the diverging probe laser beam. Although this result was obtained using paraxial refraction, equivalent results should be obtained using the diffraction optics approach since the limiting photothermal lens element is parabolic in form. Note that the photothermal lens signal does not depend on the spatial properties of the excitation beam, except through the constant irradiance condition implied in the derivation. An exact signal equation for long pathlength sample cells or high absorbance samples can be derived using the ray transfer matrix for a quadratic profile medium.[1]

EXPERIMENTAL

A pulsed dye laser (Lambda Physik) operating at 490 nm is used as the excitation source and a 632.6 nm HeNe laser (Uniphase, Model 1107P) is used to probe the resulting photothermal signal. Collinear dual-beam geometry for the thermal lens experiments is set up. The distance between the sample and the photodiode detector is optimized to satisfy the far-field paraxial approximation. Two lenses (5 cm and 25 cm focal length) are used to focus the excitation beam in the sample after the HeNe beam focus.

The excitation source power is measured with a laser power meter. The photothermal lens caused focusing and defocusing of the probe laser. This is measured as a change in the power at the center of the beam. The center HeNe beam power is measured using a pinhole and a United Detector Technology (UDT) Model PIN-10DP photovoltaic photodiode detector. A 632.8 nm laser line bandpass filter is used to prevent the transmitted dye laser beam from being detected by the photodiode detector. A small fraction of the probe beam is split off prior to the pinhole aperture and a second bandpass filter/photodiode is used to monitor the probe laser power past the sample. Changes in the probe laser power are compensated for using an operational amplifier divider, the circuit of which divides the thermal lens signal by the signal proportional to the HeNe laser power. This probe laser power compensated thermal lens signal is amplified and electronically filtered with a Tektronix model AM-502 differential amplifier. The analog signal is subsequently digitized with a 16-bit analog-to-digital converter board and processed by multichannel analysis software.

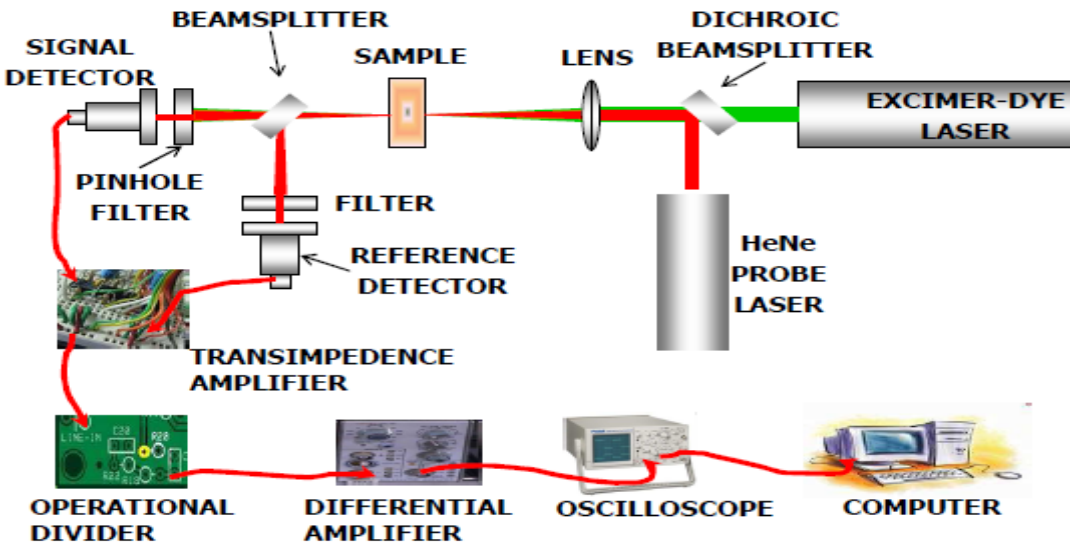

Figure 5-1. A schematic drawing of a photothermal lens experimental setup.

The latter averages several signal transients. Multichannel averaging was performed to improve the raw photothermal lens signal estimation precision. The photothermal lens signal was calculated from this raw data using a simple spreadsheet program. The diagram in Figure 5-1 illustrates the apparatus setup for the thermal lens experiment.

Sample cells and sample. A cylindrical sample cell made of fused silica glass having an internal diameter 240 µm and external diameter 1000 µm and fitted in 1 cm^3 steel block was used for the study. Cylindrical sample cell results were compared to those obtained using a conventional 1 cm pathlength spectrophotometry cell (cuvette). Ethanol $FeCp_2$ solutions were used as liquid samples for the study. Linear dilution was used to obtain lower absorbance from stock solutions of high enough absorbance to measure using a spectrophotometer with a 1 cm cuvette. The sample was positioned at the focus of the excitation beam for maximum temperature gradient and the cylindrical sample cell

versus conventional cell experiment was carried out separately at room temperature under the same conditions. Sample absorbances were recorded with a Cary 3E UV-Visible Spectrophotometer.

Finite element analysis. Finite element analysis software provides numerical solutions to the heat transfer equations with the realistic boundary conditions imposed by the complicated experimental geometries. To better understand the transient temperature profile in the samples, finite element analysis is used to model stationary temperature changes. The result of the finite element analysis is then compared to conventional analytical solutions to gauge the error. The experimental setup and the apparatus constraints are guided by the error analysis. Analysis based on Comsol Femlab v3.3 is carried out on a personal computer (Compaq Presario SR1330x, AMD Athlon XP 3200 processor).

The analysis consists of the drawing the sample geometry; specify material boundary conditions, heat sources, and sinks. And then the problems are solved with rough finite element definition and further refinement of elements and domain are made. Finally, dT can be obtained either at single time, a time series or at steady state. The relative photothermal lens signal strength is found from Eq. 5.The dn/dT for ethanol is taken as -4×10^{-4} K^{-1}. The path integral of the second radial derivative was found by using the Comsol Integration coupling variable to integrate the 2nd-derivative function of the temperature change. The relation $S(t) = 2z'/f(t)$ is used to generate the theoretical signal.

A cylindrical sample cell made of silica glass having an internal diameter 240 and external diameter 1000 μm of 8 mm height, fitted in 1 cm^3 steel blocks filled with ethanol was modeled using Comsol Multiphysics to represent the actual sample cell used in the

experiment. For convenience, the cell was modeled with 2D axial symmetry the origin at the center that the *z*-axis runs along the path length of the excitation and probe beams. The temperature profile of the ethanol (containing $FeCp_2$) in cylindrical cell was obtained by having the FEA software solve the heat equation with the boundaries of glass and steel set at zero degrees and heat input along the z-axis defined by Eq. 4. This way, the temperature solution represents dT. The model was solved using steady-state conditions. The values of α, Q, and w used were 2.1 (m^{-1}), 0.167 (mW), and 45 (μm), respectively.

RESULTS AND DISCUSSION

Figure 5-2 shows 100 averaged signals obtained using 2.1 AU m^{-1} $FeCp_2$ ethanol solutions in cylindrical and standard cells. The time-dependent response and signal magnitude differences are expected due to the thermal diffusion boundary conditions. Maximum signals for cylindrical and standard cell experiments are 0.31 and 2.65. The different signal magnitudes are expected from the theoretical signal ratio

$$S_{cylindrical} / S_{standard} = w^2 / 2a^2$$

w (m) is the laser beam waist radius and a(m) is cylinder radius. The experimental signal response time for cylindrical and standard sample cell is 0.011 s and 0.0057 s respectively. This slower response time is expected for cylindrical sample cell.

The time constants of cylindrical and standard sample cell PTS are 0.079 and 0.128 second respectively ($t_{10\%}$-$t_{90\%}$-method). Using the thermal diffusion coefficient of 8.9×10^{-8} m^2s^{-1} for ethanol, cylindrical cell radius of 167 μm is obtained from the characteristic time constant for cylindrical cell photothermal signal.

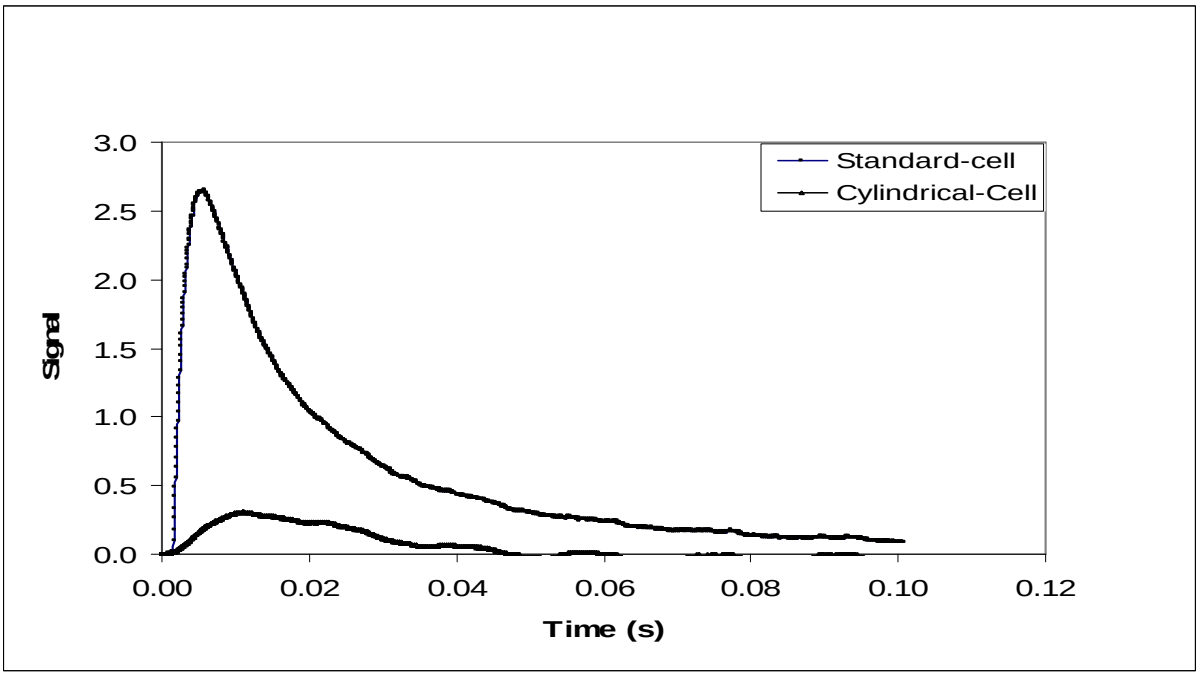

Figure 5-2. Photothermal lens signal of standard and cylindrical sample cell of $FeCp_2$ in ethanol.

This is in reasonable agreement with the 120 μm measured radius of the sample cell.

FEA modeled signals for 60-200 μm radii are presented in figure 5-3. There is variation of signal magnitude as well as the time constants for the signals of theses sizes. The Comsol multiphysics modeling signal versus cylindrical sample cell radius plot in the Figure 5-4 supports the theory that the signal magnitude increase with decreasing radii of cells. Signal produced from the FEA modeling of 120-micron size cell and that of the experimental signal of the same size in the figure 5-5 shows that they have reasonably close in magnitude (0.62 & 0.31). From modeling it is sown that (Figure 5-6, 5-7) the signal response time and time constant are directly related with the radii of cells.

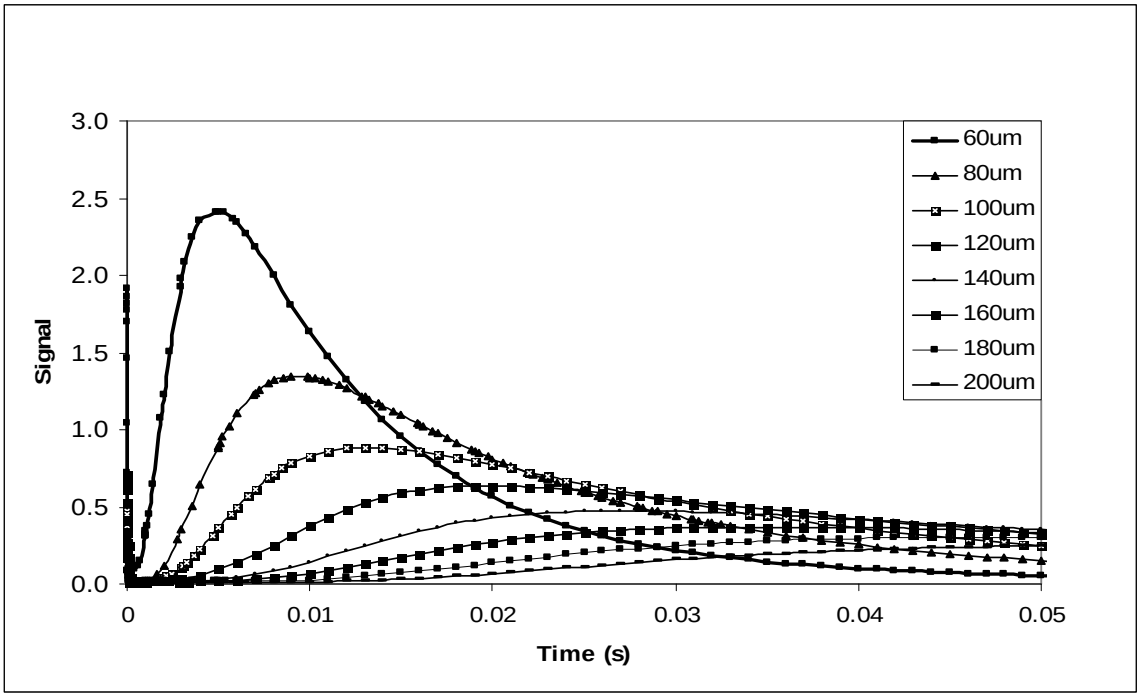

Figure 5-3. FEA modeling PTL signals of cylindrical sample cells of 60 to 200 μm sizes.

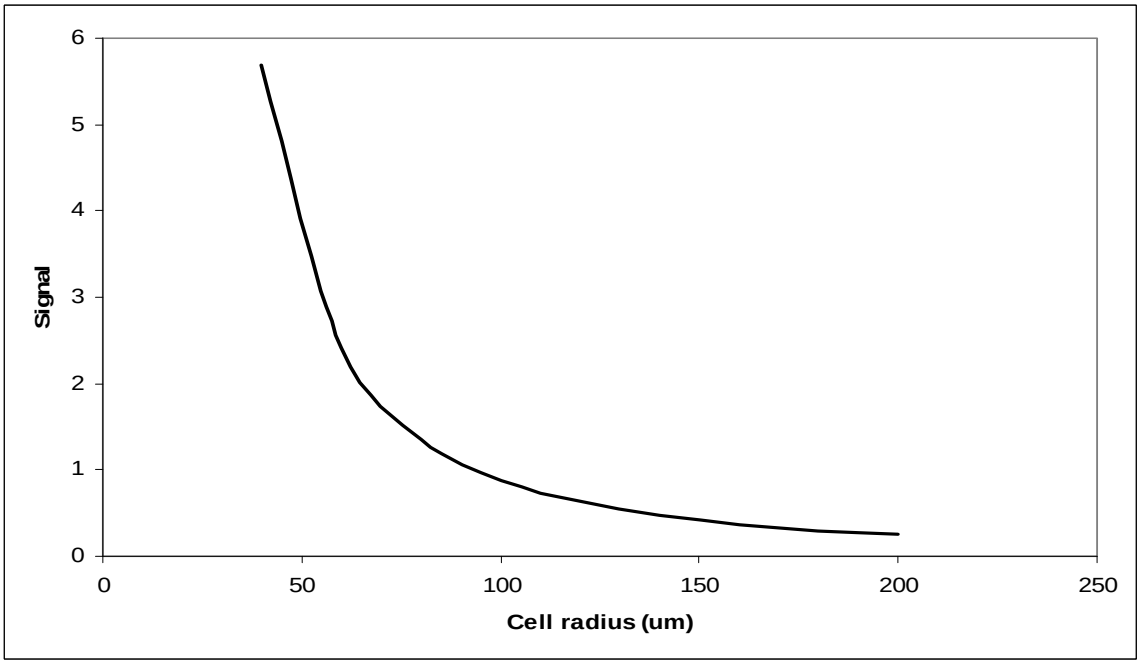

Figure 5-4. Variation of signal magnitude with sample cell radius.

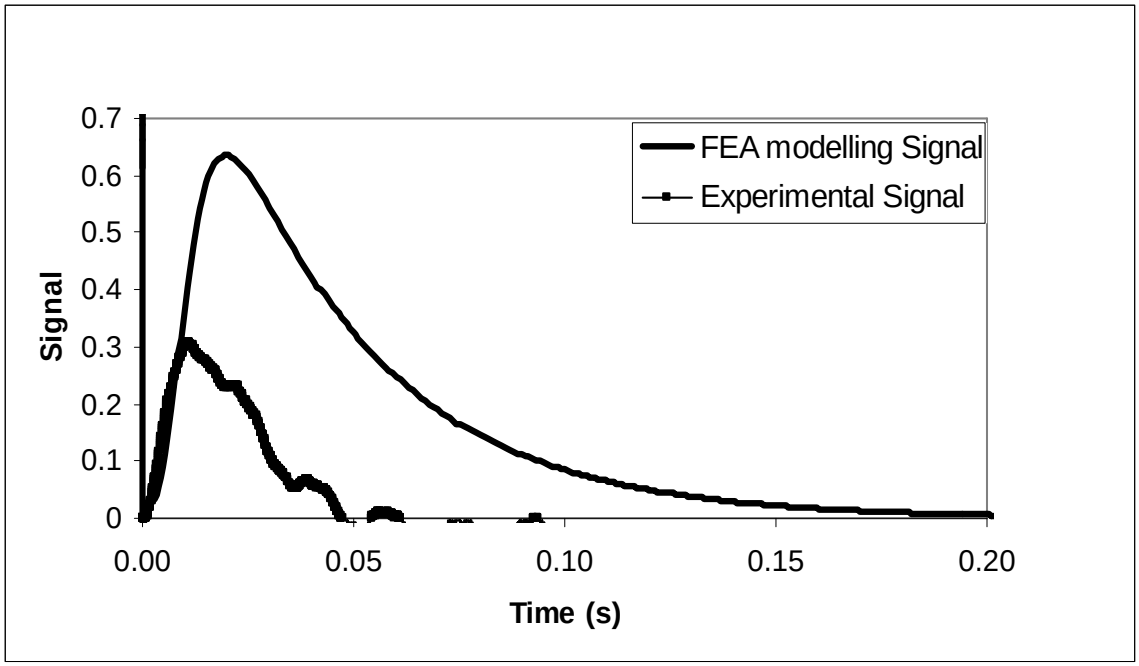

Figure 5-5. FEA modeling and experimental PTL signal in 120-μm radius sample cell of FeCp2 in ethanol solution.

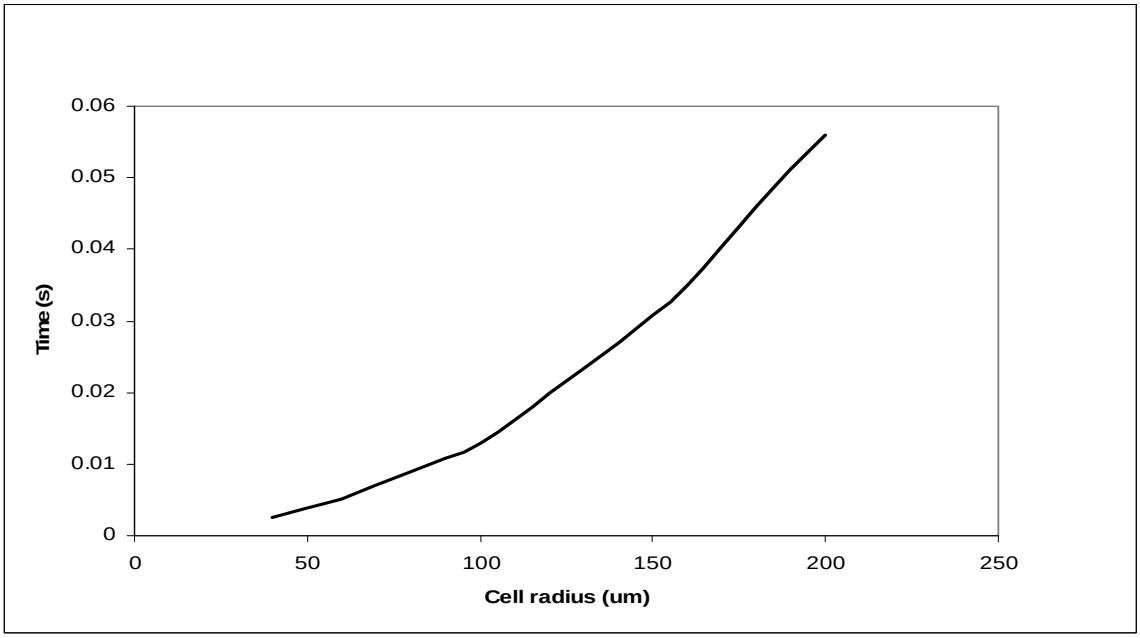

Figure 5-6. Variation of signal rises time with sample cell radius.

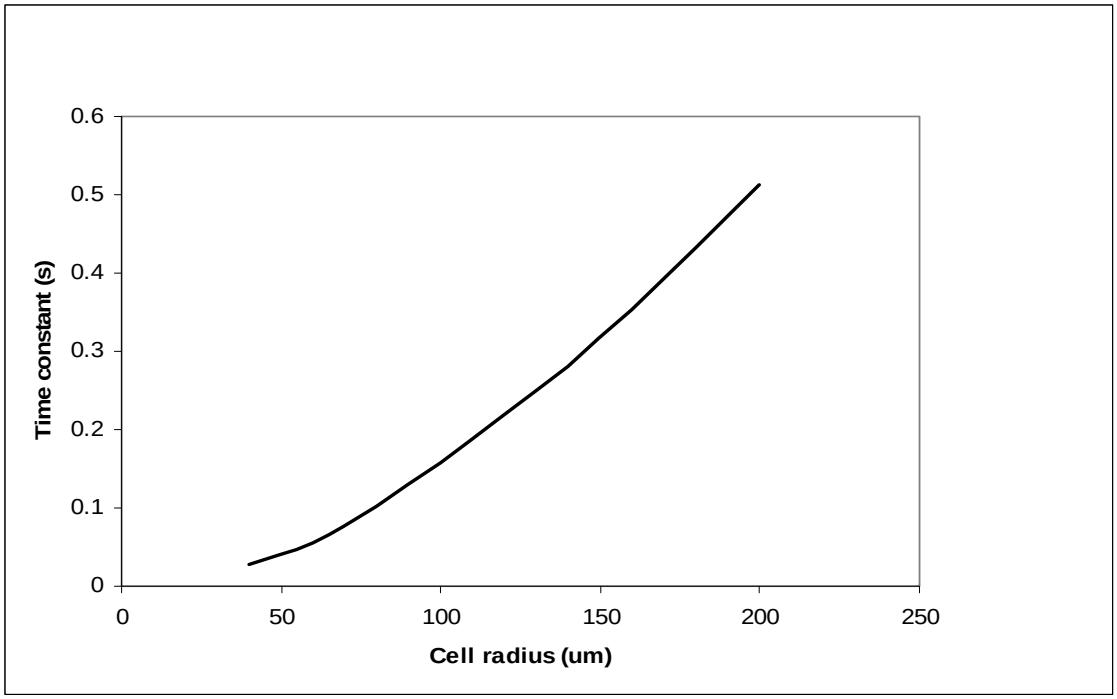

Figure 5-7. Variation of time constant with cell radius.

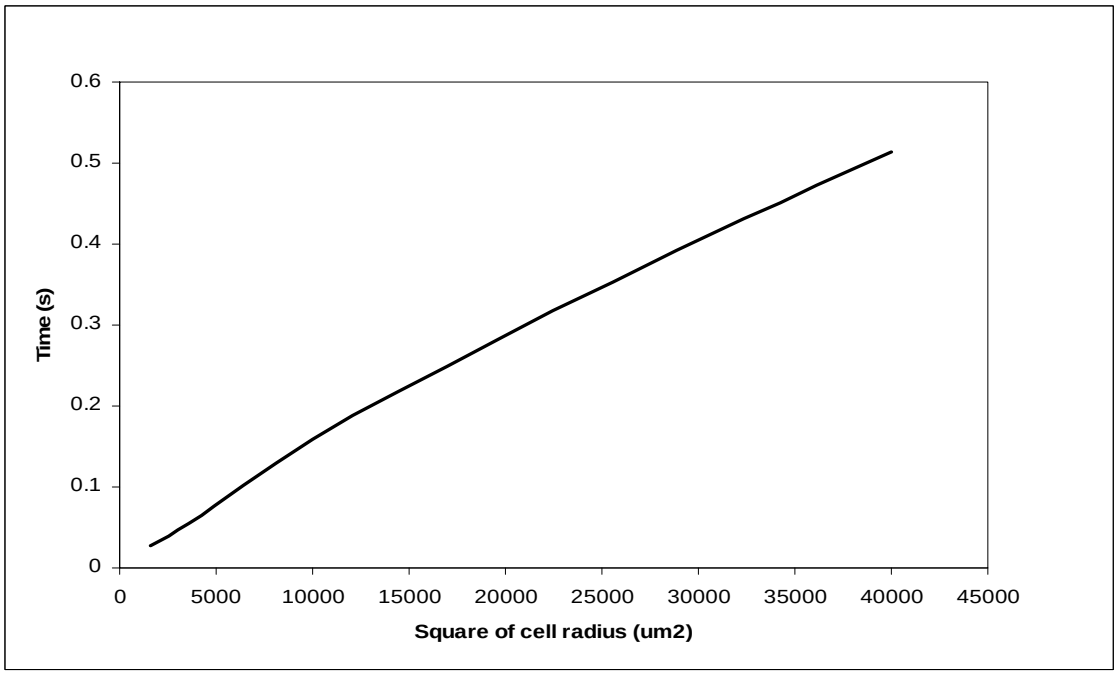

Figure 5-8. Variation of time constant with square of the cell radius.

Figure 5-8 is variation of time constant with square of the cell radius defined by the equation $t_c=a^2/4D_T$.

A signal magnitude of 0.31 is obtained for a sample with an absorbance of 0.021 this corresponds to a signal enhancement of 14.76. [1] The theoretical enhancement for the 4.4e-4J energy used is 123 this discrepancy is not surprising. The maximum theoretical enhancement is rarely realized due to the dependence on optical design parameters such as the probe laser focus position and distance to the pinhole detector.

CONCLUSION

A novel apparatus for performing photothermal lens (PTL) spectroscopy has been described which uses a low-volume (361nL) cylindrical sample cell with pulsed excitation laser. And FEA modeling is used to examine the temperature profile and the photothermal signal.

The advantages of apparatus over conventional cell are that it requires a little sample, and signals produced by thermal diffusion through the sample wall are less susceptible to the bulk heat transfer effects due to convection. The finite on axis temperature change, when low energy pulsed laser is used, prevents the solvent from boiling and prevent signal instabilities due to turbulent convection heat transfer. The cylindrical sample cell circumvents the large temperature changes by heat transport to the surrounding. The parabolic-form photothermal lens produced by thermal diffusion is aberration free. Subsequently, the beam propagation theory that only approximately describes the effect of the photothermal lens produced from laser excitation exactly

describes the effect of the cylindrical cell lens. Although the refractive index change may depend on the partial refractive index and partial molar volume of transient species, these changes do not result in a photothermal lens element. By monitoring both the central portion and the full probe laser beam, the apparatus can compensate for transmission changes due to bulk density, refractive index, or absorbance changes.

The experimental photothermal lens enhancement has been found to be that predicted from theory within experimental error. Further study to optimize the apparatus and the experiment is required for the best performance.

REFERENCES

1. S. E. Bialkowski, *Photothermal Spectroscopy Methods for Chemical Analysis* (Wiley, New York, 1996).
2. N. J. Dovichi, and J. M. Harris, Anal. Chem. **51**, 728 (1979).
3. K. Mori, T. Imasaka, and N. Ishibashi, Anal. Chem. **55**, 1075 (1983).
4. C. A. Carter, and J. M. Harris, Anal. Chem. **55**, 1256 (1983).
5. C. A. Carter, and J. M. Harris, Appl. Opt. **23**, 476 (1984).
6. J. Shen, R. D. Lowe, and R. D. Snook, Chem. Phys.**165**, 385 (1992).
7. N. J. Dovichi, and J. M. Harris, Anal. Chem. **53**, 106 (1981).
8. C. E. Buffett, and M. D. Morris, Appl. Spectrosc. **37**, 455 (1983).
9. E. F. Simo Alphonso, M. A. Rius Revert, M. C. Garcia Alvarez-Coque, and G. Ramis Ramos, Appl. Spectrosc. **44**, 1501 (1990).
10. A. Chartier, and S. E. Bialkowski, Opt. Eng. **36,** 303-311 (1997).

11. H. S. Carlaw, and J. C. Jaeger, *Conduction of Heat in Solids,* 2nd ed. (Clarendon Press, Oxford, 1959).

12. W. B. Jackson, N. M. Amer, A. C. Boccarra, and D. Fournier, Appl. Opt. **20**, 1333–1344 (1981)

13. A. Yariv, *Optical Electronics*, 3rd ed. (CBS College Publishing, New York, 1985).

CHAPTER 6

ANALYTICAL SOLUTION FOR MODE-MISMATCHED THERMAL LENS SPECTROSCOPY WITH SAMPLE-FLUID HEAT COUPLING [b]

ABSTRACT

This paper presents an improved theoretical description of the mode-mismatched thermal lens effect using models that account for heat transport both within the sample and out to the surrounding coupling medium. Analytical and numerical finite element analysis (FEA) solutions are compared and subsequently used to model the thermal lens effect that would be observed using continuous laser excitation. FEA model results were found to be in excellent agreement with the analytical solutions. The model results show that heat transfer to the air-coupling medium introduces only a minor effect when compared with the solution obtained without considering axial air-sample heat flux for practical examples. On the other hand, the thermal lens created in the air coupling fluid has a relatively more significant effect on the time-dependent photothermal lens signals.

INTRODUCTION

Thermal lens (TL) spectroscopy is a remote, nondestructive, fast, and highly sensitive photothermal technique for the measurement of optical absorption and thermo-optical properties of materials.[1-13] This technique has been applied to obtain optical and

[b]COAUTHORED BY PR JOSHI, LC MALACARNE, NGC ASTRATH, PRB PEDREIRA, RS MENDES, ML BAESSO AND SE. BIALKOWSKI. REPRODUCED WITH PERMISSION FROM THE *JOURNAL OF APPLIED PHYSICS*, 107, 053104 (2010) COPYRIGHT 2010 AMERICAN INSTITUTE OF PHYSICS (SEE APPENDIX C)

thermal-optical properties of a wide range of material, including glasses, oils, polymers, and liquid crystals.[7–13] TL technique has also been demonstrated as a powerful method for chemical analysis.[4,8]

Theoretical analytical solutions restricted the use of TL spectroscopy to low optical absorbing samples. Recently, a simple approximation was proposed by taking the high optical absorbing material case into account[14] and also the complementary thermal mirror method[15–18] was developed to use concurrently with TL leading to additional information about physical properties of high and low absorbing samples. Despite numerous applications and theoretical descriptions, TL model has no analytical solution that considers the axial heat coupling between sample and external medium into account. Recently,[19–21] by using finite element analysis (FEA), it has been demonstrated that the effect of surface heat transfer from sample to the surroundings could introduce some modification in the physical parameters measured by pulsed laser excited photothermal lens spectroscopy.

In this work, we present a semi-analytical theoretical description of the mode-mismatched TL effect by taking the coupling of heat both within the sample and out to the surroundings into account. Our analytical results are compared with FEA solutions. These two methods for calculating the time- and space-dependent heat transfer are in excellent agreement lending some degree of confidence in the predictions of these solutions. We show that the interface effect occurs in finite characteristic lengths. For samples with thickness larger than this characteristic length, a simplified solution can be used to obtain the TL phase shift within the sample and surrounding fluid.

THEORY

A typical configuration used in mode-mismatched TL spectrometry is illustrated in Fig. 6-a. A continuous Gaussian excitation laser beam irradiates a weakly absorbing sample of thickness *l*, causing a TL. A second, often-weaker Gaussian beam propagates through the sample collinear to the excitation laser and is affected by the TL. The characteristic electric field radii of the excitation and probe beams in the sample are ω_{0e} and ω_{1P}, respectively. The probe beam propagates in the +*z*-direction, and the sample is centered at *z*=0. The distance between the sample and the detector plane is Z_2 and the distance between the sample and the minimum probe beam waist of a radius w_{0P} is Z_1. In this configuration, it is assumed that (i) the sample dimensions are large compared to the excitation beam radius to avoid edge effects; (ii) the absorbed excitation laser energy by the sample is low so that the excitation laser can be considered to be uniform along the *z*-direction.

Temperature gradient. To model the sample-fluid heating coupling, let us consider two semi-infinity spaces with boundaries at *z*=0 with the sample in the $0<z<\infty$ region and the fluid (air in this work) in the $\infty<z<0$ region. The temperature rise distributions inside the sample, $T_s(r, z, t)$, and in the fluid, $T_f(r, z, t)$, are given by the solution of the heat conduction differential equations

$$\frac{\partial T_s(r,z,t)}{\partial t} - D\nabla^2 T_s(r,z,t) = Q(r,z) \tag{1}$$

$$\frac{\partial T_f(r,z,t)}{\partial t} - D_f\nabla^2 T_f(r,z,t) = 0 \tag{2}$$

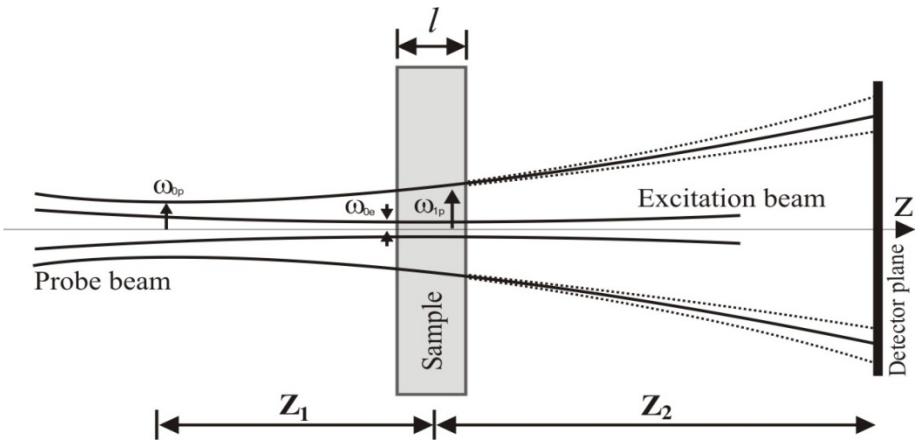

Figure 6-a. Scheme of the geometric positions of the beams in a mode-mismatched dual-beam TL experiment.

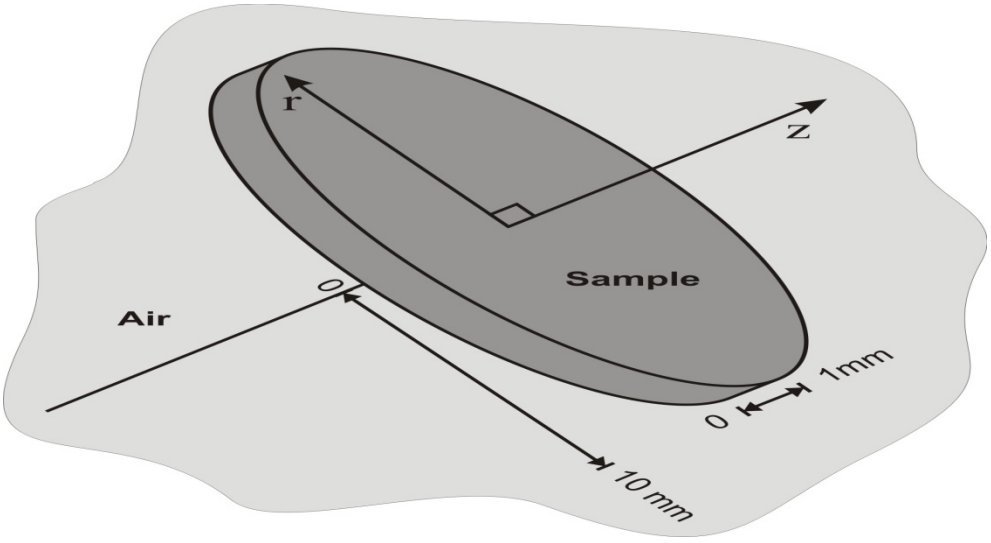

Figure 6-b. sample geometry used for the finite element analysis modeling.

The boundary and initial conditions are given by

$$
\begin{aligned}
& k\,\partial_z T_s(r,z,t)/\partial z\big|_{z=0} = k_f\,\partial_z T_f(r,z,t)/\partial z\big|_{z=0} \\
& T_s(\infty,z,t) = T_s(r,\infty,t) = 0 \\
& T_s(r,z,0) = T_f(r,z,0) = 0 \\
& T_s(r,0,t) = T_f(r,0,t) \\
& T_f(\infty,z,t) = T_f(r,-\infty,t) = 0
\end{aligned}
\tag{3}
$$

$D_i = k_i/\rho_i c_i$ is the thermal diffusivity of the material i (sample and fluid). c_i, ρ_i and k_i are the specific heat, mass density, and thermal conductivity of the material i, respectively. The Gaussian excitation laser profile is $Q(r,z) = Q_0\,Q(r)\,Q(z)$, where $Q(r) = \exp\left(-2r^2/\omega^2\right)$, $Q_0 = 2P_e A_e \phi/\pi c\rho\omega^2$, P_e is the excitation beam power, A_e is the optical absorption coefficient at the excitation beam wavelength λ_e, $\phi = 1-\eta\lambda_e/\langle\lambda_{em}\rangle$, where $\langle\lambda_{em}\rangle$ is the average wavelength of the fluorescence emission, and η is the fluorescence quantum efficiency, which competes for a share of absorbed excitation energy. $Q(z)=\exp(A_e z)$ is the sample absorptance. For the purposes here, the optical absorption coefficient is small and $Q(z)=1$ can be assumed.

Using Laplace and Hankel integral transform methods with the boundary conditions in Eq. (3), the solution of the heat conduction differential equations in the Laplace–Hankel space can be written as

$$
T_s(\alpha,z,s) = -\frac{Q(\alpha)\left(k_f\sqrt{D}\big/k\sqrt{D_f}\right)\sqrt{s+D_f\alpha^2}}{s\left(s+D\alpha^2\right)\left(1+\dfrac{k_f\sqrt{D}\sqrt{s+D_f\alpha^2}}{k\sqrt{D_f}\sqrt{s+D\alpha^2}}\right)}\frac{e^{-z\sqrt{\left(s+D\alpha^2\right)/D}}}{\sqrt{s+D\alpha^2}} + \frac{Q(\alpha)}{s\left(s+D\alpha^2\right)}
\tag{4}
$$

and

$$T_f(\alpha,z,s) = -\frac{Q(\alpha)\sqrt{s+D_f\alpha^2}}{s\left(s+D\alpha^2\right)\left(1+\dfrac{k_f\sqrt{D}\sqrt{s+D_f\alpha^2}}{k\sqrt{D_f}\sqrt{s+D\alpha^2}}\right)}\frac{e^{-z\sqrt{\left(s+D_f\alpha^2\right)/D_f}}}{\sqrt{s+D_f\alpha^2}} \tag{5}$$

Here $Q(\alpha) = Q_0 \exp\left(-\omega^2\alpha^2/8\right)\omega^2/4$ is the Hankel transform of the source term. If $k_f\sqrt{D}\sqrt{s+D_f\alpha^2} << k\sqrt{D_f}\sqrt{s+D\alpha^2}$, the term in the denominator of Eqs. (4) and (5) can be expanded in series as $(1+x)^{-1} = 1-x+x^2-O\left(x^3\right)$. This condition is fulfilled in the case of glass-air system. Thus, Eq. (4) can be written as

$$T_s(\alpha,z,s) = -Q(\alpha)\frac{k_f\sqrt{D}}{k\sqrt{D_f}}\frac{\sqrt{s+D_f\alpha^2}}{s\left(s+D\alpha^2\right)}\left(1-\frac{k_f\sqrt{D}\sqrt{s+D_f\alpha^2}}{k\sqrt{D_f}\sqrt{s+D\alpha^2}}+\cdots\right)\frac{e^{-z\sqrt{\left(s+D\alpha^2\right)/D}}}{\sqrt{s+D\alpha^2}}+\frac{Q(\alpha)}{s\left(s+D\alpha^2\right)} \tag{6}$$

and Eq. (5) becomes

$$T_f(\alpha,z,s) = -Q(\alpha)\frac{\sqrt{s+D_f\alpha^2}}{s\left(s+D\alpha^2\right)}\left(1-\frac{k_f\sqrt{D}\sqrt{s+D_f\alpha^2}}{k\sqrt{D_f}\sqrt{s+D\alpha^2}}+\cdots\right)\frac{e^{-z\sqrt{\left(s+D_f\alpha^2\right)/D_f}}}{\sqrt{s+D_f\alpha^2}} \tag{7}$$

The time-dependent temperatures are given by the inverse Laplace and Hankel transforms of Eqs. (6) and (7). Taking the expansion in Eqs (6) and (7) up to the first, the temperature gradient within the sample, $T_1(s)\ (r\ ,\ z\ ,\ t)$, is given by the integral equation

$$T_{1(s)}(r,z,t)=Q_0\int_0^t\int_0^\infty \frac{e^{-\omega^2\alpha^2/8}\omega^2}{4}\alpha \mathrm{J}_0(\alpha r)\Bigg[e^{-D\tau\alpha^2}- \\ -\frac{k_f\sqrt{D}}{k\sqrt{D_f}}e^{-D(t-\tau)\alpha^2}\frac{e^{\frac{-z^2}{4D(t-\tau)}}}{\sqrt{\pi(t-\tau)}}\left(\frac{\sqrt{\mathrm{D_f}}\,\mathrm{erf}\left(\sqrt{\tau}\alpha\sqrt{D_f-D}\right)-e^{-D\tau\alpha^2}\sqrt{\mathrm{D_f}-D}\,\mathrm{erf}\left(\sqrt{\tau}\alpha\sqrt{D_f-D}\right)}{\alpha D}\right)\Bigg]d\alpha\,d\tau \tag{8}$$

while that for the coupling fluid, $T_{1(f)}(r,z,t)$, is

$$T_{1(f)}(r,z,t)=\int_0^t\int_0^\infty \frac{e^{-\omega^2\alpha^2/8}\omega^2}{4}e^{-D_f(t-\tau)\alpha^2}\frac{e^{\frac{-z^2}{4D_f(t-\tau)}}}{\sqrt{\pi(t-\tau)}}\Bigg[\frac{\sqrt{D_f}\,\mathrm{erf}\left(\sqrt{\tau}\alpha\sqrt{D_f}\right)-e^{-D\tau\alpha^2}\sqrt{\mathrm{D_f}-D}\,\mathrm{erf}\left(\sqrt{\tau}\alpha\sqrt{D_f-D}\right)}{\alpha D}- \\ -\frac{k_f\sqrt{D}}{k\sqrt{D_f}}\left(\frac{2e^{-D\tau\alpha^2}\sqrt{\tau}\left(D-D_F\right)}{D\sqrt{\pi}}+\frac{\mathrm{erf}\left(\sqrt{\tau}\alpha\sqrt{D}\right)D_f}{D^{3/2}\alpha}\right)\Bigg]\alpha \mathrm{J}_0(\alpha r)d\alpha\,d\tau\ . \tag{9}$$

$\mathrm{J_n}(x)$ is the Bessel function of the first kind and $\mathrm{erf}(x)$ is the error function.

Considering the zero order expansion, which in fact correspond to the case where there is no heat flux from sample to air, or $\partial_z T(r,z,t)/\partial z\big|_{z=0}=0$, Eq. (8) becomes

$$T_{0(s)}(r,t)=\int_0^t\left(\frac{Q_0}{(1+2\tau/t_c)}\right)\exp\left(-\frac{2r^2/\omega_{0e}^2}{1+2\tau/t_c}\right)d\tau \tag{10}$$

Eq. (10) is the temperature gradient commonly used to describe the Thermal Lens and Thermal Mirror effects for low absorbing semitransparent solids.[9,15-17] In addition, the zero order approximation for the air temperature solution, which correspond to the

solution for a semi-space system with the temperature in $z = 0$ surface fixed by the sample's temperature, is given by

$$T_{0(f)}(r,z,t) = \int_0^t \int_0^\infty \frac{e^{-\omega^2\alpha^2/8}\omega^2}{4e^{D_f(t-\tau)\alpha^2}} \frac{e^{\frac{-z^2}{4D_f(t-\tau)}}}{\sqrt{\pi(t-\tau)}} \left[\frac{\sqrt{D_f}\,\mathrm{erf}\left(\sqrt{\tau}\alpha\sqrt{D_f}\right) - e^{-D\tau\alpha^2}\sqrt{\mathrm{D_f} - D}\,\mathrm{erf}\left(\sqrt{\tau}\alpha\sqrt{D_f - D}\right)}{\alpha D} \right] \alpha \mathrm{J}_0(\alpha r)\, d\alpha\, d\tau. \tag{11}$$

Finite element analysis. In order to ascertain the accuracy of our approximation the space and time dependences of the temperature equations for air and sample in Eqs. (8) to (11) are compared with the FEA modeling solutions for a system with glass sample of thickness *l* surrounded by air. FEA software provides numerical solutions to the heat transfer equations with the realistic boundary conditions imposed by the experimental geometry. To better understand the transient temperature profile in the samples, FEA is used to model temperature changes. Results from the FEA calculations are then compared with the semi-infinity analytical solutions to gauge the error. COMSOL MULTIPHYSICS 3.5 analysis is carried out on a Dell Studio XPS 435, i7 940 processor, using MS WINDOWS VISTA. The numerical integrations in Eqs (8)-(11) are performed using the standard functions in MATHEMATICA (version 7.0) software.

The COMSOL MULTIPHYSICS software in conduction and convection mode solves the heat diffusion equation given as

$$\rho C_p \frac{\partial}{\partial t}\delta T(r,z,t) - k\nabla^2 \delta T(r,z,t) = q_H(r,z,t) - \rho C_p u \cdot \nabla \delta T(r,z,t) \tag{12}$$

in which u is the flow velocity. All other symbols are the same as those introduced above. Note that Eqs. (1), (2), and (12) differ only by the second term on the right side of the equation. This term can account for convection or mass flow heat transfer, which is not important for glasses.

FEA modeling consists of drawing the sample geometry and specifying material boundary conditions, heat sources, and sinks. The problems are then solved with rough finite element definition and further refinement of elements and domain are made. The element mesh is refined until model results become independent of mesh size. Finally, $T(r, z, t)$ can be obtained either at a single time, over a time series, or at steady state. The model solid absorbing media was cylindrical plate of 10 mm in diameter and 1 mm thick. Optical excitation was along the z-axis. The values of the thermal, optical, and mechanical parameters used for the analytical and FEA modeling simulations are shown in Table 6-1.

Figure 6-2 shows the radial temperature profile within the glass sample at its center at z=0.5 mm. The results by the FEA model are compared with the temperature solution considering heat flux from glass to air, Eq. (8), at different exposure times. There is apparently little difference between the temperatures produced from the FEA model and the semi-infinite approximation with glass-air heat coupling.

Figure 6-3 shows the temperature profiles along the z-direction (air-glass-air) using the FEA modeling, the solution considering air surroundings, Eq. (8), and the solution with no transfer of heat from glass to air, Eq. (10), at different exposure times at r=0. It clearly shows an excellent agreement between the analytical solutions considering air-coupling Eqs. (8) and (9) and the FEA model. On the other hand, as expected, there is a

little difference for the predictions considering no heat transfer from glass to air, Eq. (10). This difference is more evident close to the boundary sample-air.

Table 6-1. Parameters used for the simulations. The thermal, optical and mechanical properties listed below are associated to characteristics values found in glasses [12,18] and for the surrounding medium we use the air properties. [22]

P_e	(mW)	161	ρ_f	(kg/m^3)	1.18
A_e	(m^{-1})	93	c_f	(J/kgK)	1005
D	(10^{-7} m^2/s)	5	ω	(μm)	50
k	(W/mK)	1.4	$t_c = \omega^2/4D$	(ms)	1.25
ρ	(kg/m^3)	933	ϕ		0.6
c	(J/kgK)	3000	α_T	(10^{-6} K^{-1})	7.5
D_f	(10^{-5} m^2/s)	2.2	ν		0.25
k_f	(W/mK)	0.026	Q_0	(WK s^{-1})	818. 80356
ds/dT	(10^{-6} K^{-1})	10	$(dn/dT)_f$	(10^{-6} K^{-1})	-1
m		60	V		5

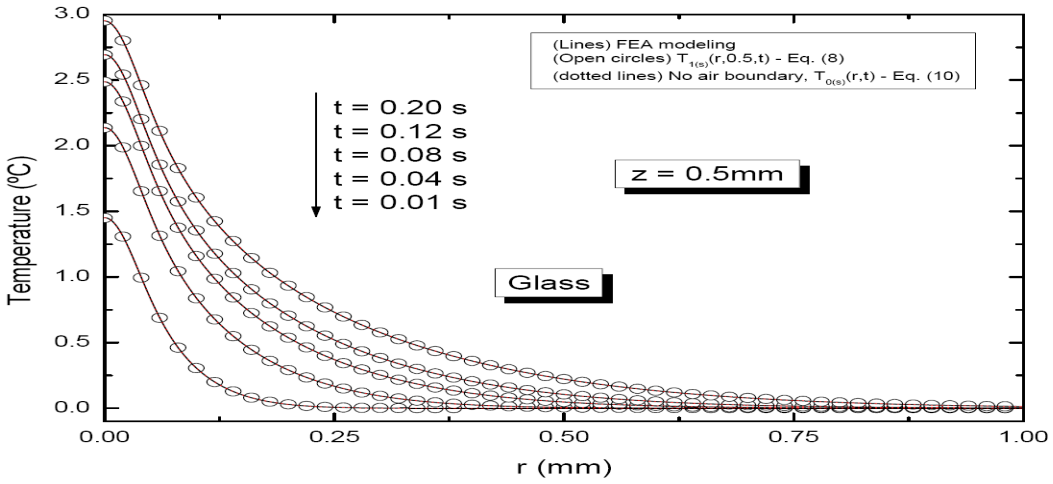

Figure 6-2. Temperature profile in the glass sample at $z = 0.5\,mm$ using the FEA modeling, the solution considering heat flux to air, Eq. (8), and the solution with no transfer of heat from glass to air, Eq. (10), at different exposure times.

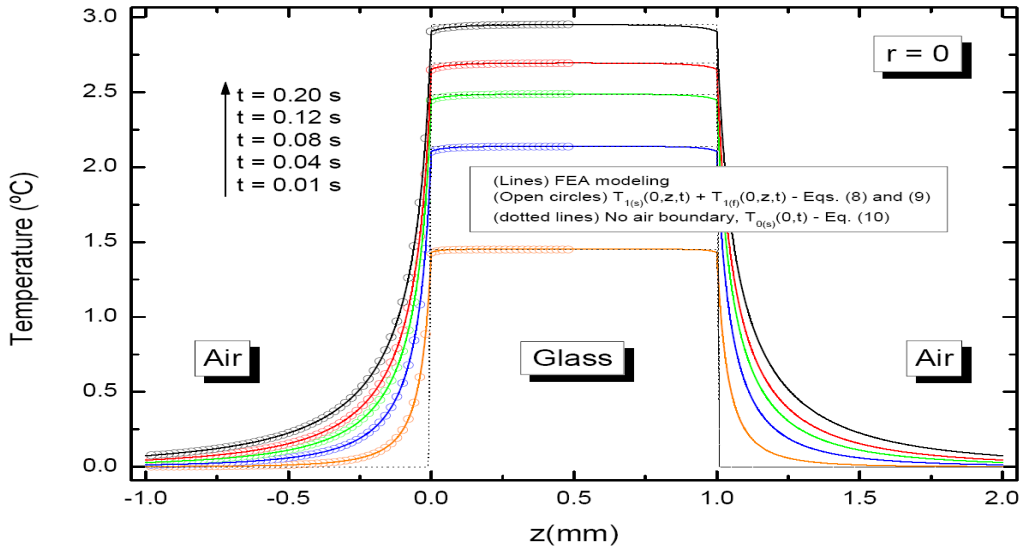

Figure 6-3. Temperature profile along the z direction (air-glass-air) using the FEA modeling, the solution considering air surroundings, Eqs.(8) and (9), and the solution with no transfer of heat from glass to air, Eq. (10), at different exposure times. $r = 0$ was used in the simulations.

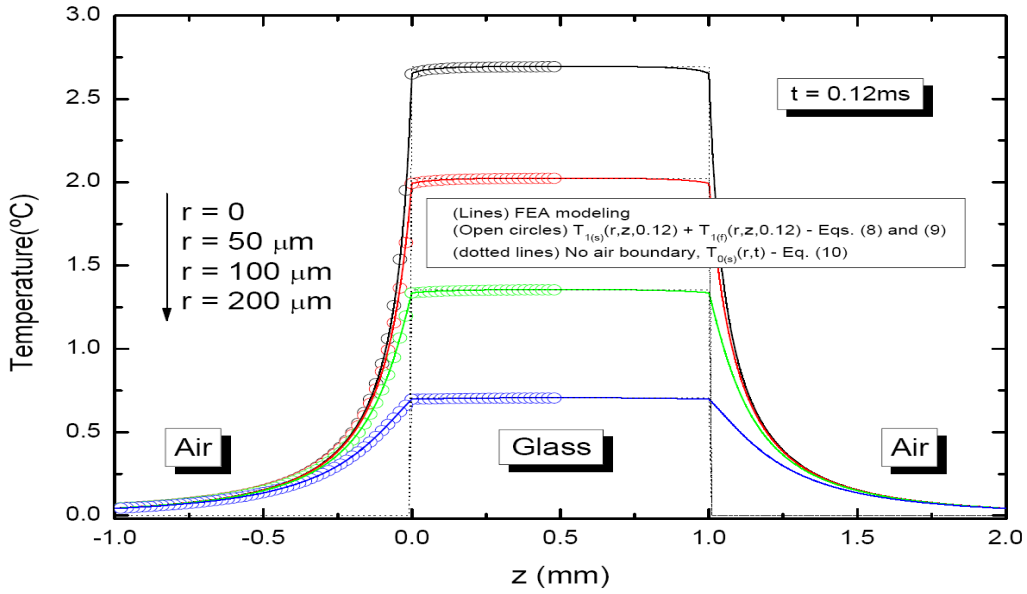

Figure 6-4. Temperature profile along the z direction (air-glass-air) using the FEA modeling, the solution considering air surroundings, Eqs. (8) and (9), and the solution with no transfer of heat from glass to air, Eq. (10), for different radial positions.

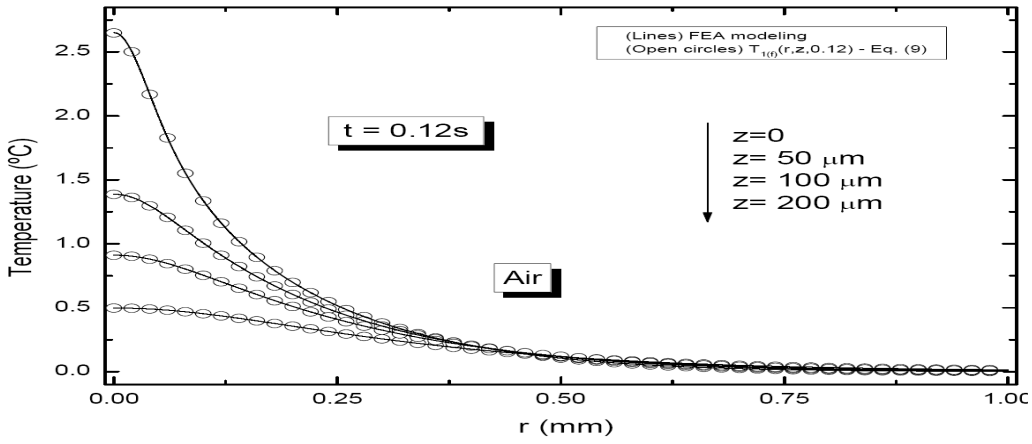

Figure 6-5. Radial temperature profile in the air surroundings at $t = 0.12s$ using the FEA modeling, the solution for the air fluid, Eq. (9), at the sample surface in the air side, $z = 0$, and up to $200\mu m$ distant from there.

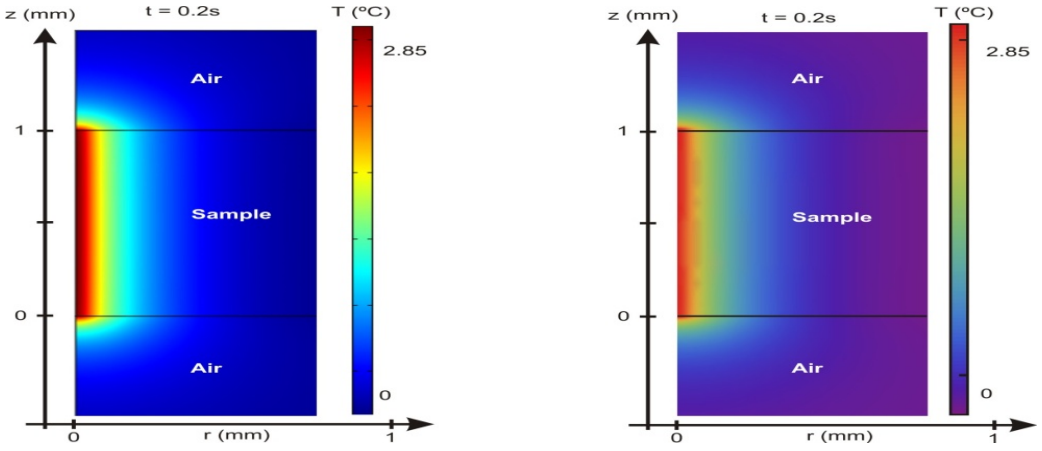

(a) (b)

Figure 6-6. Density plot using (a) the FEA and (b) the analytical approximation models.

In the case of glass-air interface, the characteristic length is around z=0.2 mm into the sample. Deeper than that the temperature is the same as that one with no axial heat fluxes as long as the excitation beam waist is small relative to sample thickness. This shows that the interfaces do not affect each other if the sample is thick relative to the beam waist. Subsequently, the single-surface approximation used for the analytical model is valid for these conditions.

The same behavior is also observed for different radial positions, as shown in Fig. 6-4 at t=0.12 s. It is interesting to note the excellent agreement between FEA modeling and the analytical solution, Eqs. (8) and (9).

Figure 6-5 displays the radial temperature profile in the air using the FEA modeling and the solution for air, Eq. (9), at the sample surface in the air side from z=0 to 200 m. The exposure time was t=0.12 s. Again, agreement between both the FEA and

analytical modeling predictions is good. The results obtained using the FEA model show that the first order analytical approximation presented in this work can be used to describe the temperature profile in the sample and in the air surrounding it, at least in cases where binomial expansion is valid. In addition, the order zero approximation also represents quite well the temperature in the sample for thick samples. The density plot illustrated in Fig.6- 6 shows the complete solution for both the FEA and analytical approximation models within both air and sample.

PROBE BEAM PHASE SHIFT AND THERMAL LENS INTENSITY

The temporal and radial distribution of the temperature rise inside the sample and in the air induce a refractive index gradient, acting as an optical element, causing a phase shift Φ to the probe beam. The solutions presented in Eqs. (8) and (9) can be analytically used to describe theoretically the TL effect, by calculating the phase shift of the probe beam after passing thought the TL region and, therefore, to express the TL intensity signal.

For low optical absorbing samples, we can use our semi-infinite solution for the temperature, given by Eq. (8), to obtain the phase shift for finite sample of thickness *l* by the following equations

$$\Phi_s(r,t) = \frac{2\pi}{\lambda_P}\frac{ds}{dT} 2\int_0^{l/2}\left[T(r,z,t) - T(0,z,t)\right]dz \tag{13}$$

where the integration is from $0 < z < l/2$, however multiplied by a factor 2 .*ds/dT* is the temperature coefficient of the optical path length at the probe beam wave length λ_p For the air domain.

$$\Phi_f(r,t) = \frac{2\pi}{\lambda_P}\left(\frac{dn}{dT}\right)_f 2\int_{-\infty}^{0}\left[T_f(r,z,t) - T_f(0,z,t)\right]dz \tag{14}$$

Here the factor of 2 accounts for the layers of air on both sides of the sample and $(dn/dT)_f$ is the temperature coefficient of the refractive index of the air. The total phases shift, $\Phi(r,t) = \Phi_{(s)}(r,t) + \Phi_{(f)}(r,t)$ describes the distortion of the probe beam caused by the temperature change in the medium.

Substituting Eq. (8) into (13), and performing the z integration, one gets the first order phase shift in the sample as

$$\Phi_{1(s)}(g,t) = \theta_s\int_0^{\infty}\frac{-e^{-\omega^2\alpha^2/8}\omega^2}{4}\frac{\sqrt{D}}{\alpha D}\frac{k_f\sqrt{D}}{k\sqrt{D_f}}\int_0^t\left\{\left[e^{-D(t-\tau)\alpha^2}\,\mathrm{erf}\left[l/\left(4\sqrt{D}\sqrt{t-\tau}\right)\right]\left(\sqrt{D_f}\,\mathrm{erf}\left(\sqrt{\tau}\alpha\sqrt{D_f}\right) - \right.\right.\right.$$
$$\left.\left.\left. - e^{-D\tau\alpha^2}\sqrt{\mathrm{D_f} - D}\,\mathrm{erf}\left(\sqrt{\tau}\alpha\sqrt{D_f - D}\right)\right)\right]d\tau + \frac{e^{-\omega^2\alpha^2/8}\omega^2}{4}\frac{l}{2}e^{-D\tau\alpha^2}\right\}\alpha\left[\mathrm{J}_0\left(\alpha\omega\sqrt{mg}\right) - 1\right]d\alpha \tag{15}$$

Alternatively, Eq. (9) into (14), and performing the z and the time integrations, one gets the first order phase shift in the air as

$$\Phi_{1(f)}(g,t)=\theta_f\int_0^{\infty}\frac{e^{-\omega^2\alpha^2/8}\omega^2}{4}\left[\frac{\sqrt{D_f}}{\alpha D}\left(\frac{\operatorname{erf}\left(\sqrt{t}\alpha\sqrt{D_f}\right)}{\alpha^2\sqrt{D_f}}-\frac{e^{-Dt\alpha^2}\sqrt{t}\,\operatorname{erfi}\left(\sqrt{t}\alpha\sqrt{D-D_f}\right)}{\alpha^2 D\sqrt{D-D_f}}\right)-\right.$$
$$\left.-\sqrt{D_f}\frac{k_f\sqrt{D}}{k\sqrt{D_f}}\left(\frac{-2\alpha\sqrt{D/\pi}e^{-Dt\alpha^2}\sqrt{t}+\operatorname{erf}\left(\sqrt{t}\alpha\sqrt{D}\right)}{D^{3/2}\alpha^3}\right)\right]\alpha\left[\mathrm{J}_0\left(\alpha\omega\sqrt{mg}\right)-1\right]d\alpha \tag{16}$$

$\operatorname{erfi}(x)$ is the imaginary error function, $g=(r/\omega_{1P})^2$, $m=\omega_{1P}^2/\omega^2$, $\theta_f=(4\pi/\lambda_p)(dn/dT)_f Q_0$ and $\theta_s=(4\pi/\lambda_p)(ds/dT)Q_0$. Using Esq. (10) and (11) one can write the zero order approximation for the phase shift in the air and sample as

$$\Phi_{0(s)}(g,t)=\theta_s\frac{l\omega^2}{16D}\left[\operatorname{Ei}(-2mg)-Ei\left(-\frac{2mg\omega^2}{\omega^2+8Dt}\right)+Log\left(\omega^2\right)-Log\left(\omega^2+8Dt\right)\right] \tag{17}$$

in which $\operatorname{Ei}(x)$ is the exponential integral function, and

$$\Phi_{0(f)}(g,t)=\theta_f\int_0^{\infty}\frac{e^{-\omega^2\alpha^2/8}\omega^2}{4}\left[\frac{\sqrt{D_f}}{\alpha D}\left(\frac{\operatorname{erf}\left(\sqrt{t}\alpha\sqrt{D_f}\right)}{\alpha^2\sqrt{D_f}}-\frac{e^{-Dt\alpha^2}\sqrt{t}\,\operatorname{erfi}\left(\sqrt{t}\alpha\sqrt{D-D_f}\right)}{\alpha^2 D\sqrt{D-D_f}}\right)\right]\alpha\left[\mathrm{J}_0\left(\alpha\omega\sqrt{mg}\right)-1\right]d\alpha \tag{18}$$

Eq. (17) is the phase shift commonly used to describe the Thermal Lens effect [7] for low optical absorbing solids.

The complex electric field of a TEM_{00} Gaussian probe beam emerging from the sample can be expressed as [3]

$$U_P(r,Z_1)=B\exp\left[-i\left(\frac{\pi}{\lambda_P}\frac{r^2}{R_{1P}}+\Phi\right)-\frac{r^2}{\omega_{1P}^2}\right], \tag{19}$$

with $B = \omega_{1P}^{-1}\sqrt{2P_P/\pi}\exp(-i2\pi Z_1/\lambda_P)$. P_P and R_{1P} are the probe beam power and the radius of curvature of the probe beam at Z_1. The propagation of the emerged probe beam from the sample to the detector plane can be treated as a diffraction phenomenon. Using Fresnel diffraction theory, its complex amplitude at the detector plane can be obtained as described in Ref. 3. In this work only the center point of the probe beam at the detector plane is considered. Then, the complex amplitude of the probe beam at the centre, using cylindrical coordinates, is given by [3]

$$U(Z_1+Z_2,t) = C\int_0^\infty \exp\left[-(1+iV)g - i\Phi_{(s)}(g,t) - i\Phi_{(f)}(g,t)\right]dg \tag{20}$$

when $Z_2 << Z_c$. Here $V = Z_1/Z_C$, Z_C is the confocal distance of the probe beam, and $C = B\exp(-i2\pi Z_2/\lambda_P)i\pi\omega_{1P}^2/\lambda_P Z_2$. Substituting Eqs. (15)- (18) Into Eq. (20) and carrying out numerical integration over g, the intensity $I(t)$ at the detector plane can be calculated as $I(t) = \left|U(Z_1+Z_2,t)\right|^2$.

The effect of the TL on the probe beam is only to induce a phase shift. The geometrical configuration of the probe and excitation beams defines the sensitivity of the TL method by means of m. This parameter can be modified either by changing ω_{1p} or ω. When $r = \omega_{1p}$, within which more than 86% of the probe beam power is included, the time dependence of the phase shift, assuming $g = 1$, is $\Phi(1,t)$. It can be calculated using Eqs. (15) or (17) for the sample and Eqs. (16) or (18) for the air. The phase shifts

calculated using the parameters of Table 6-1 with g=1 is shown in Fig. 6- 7. Here the time scale is in units of t_c. One can see from Fig. 6-7 that the zero-order approximation for the phase shift created in the sample agrees with the first-order one. The relative difference is less than 0.3%. The air phase shift it is approximately 1.7% of that of the glass sample.

The relative difference between phase shifts calculated with zero- and first-order approximations is more important when the sample thickness is reduced. Figure 6-8 shows this difference at t=0.12 s as a function of the sample thickness. With a thin sample, boundary effects become important and the first order approximation should be used.

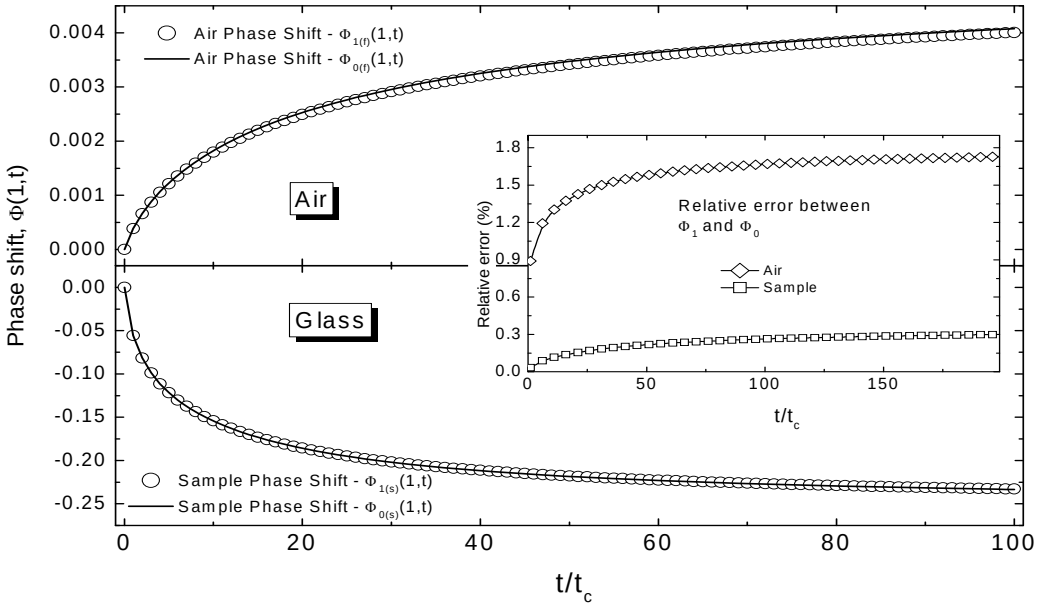

Figure 6-7. Probe beam phase shift in air and in the sample calculated using order 0 and 1 approximations as a function of time. The inset shows the relative error between both approximations.

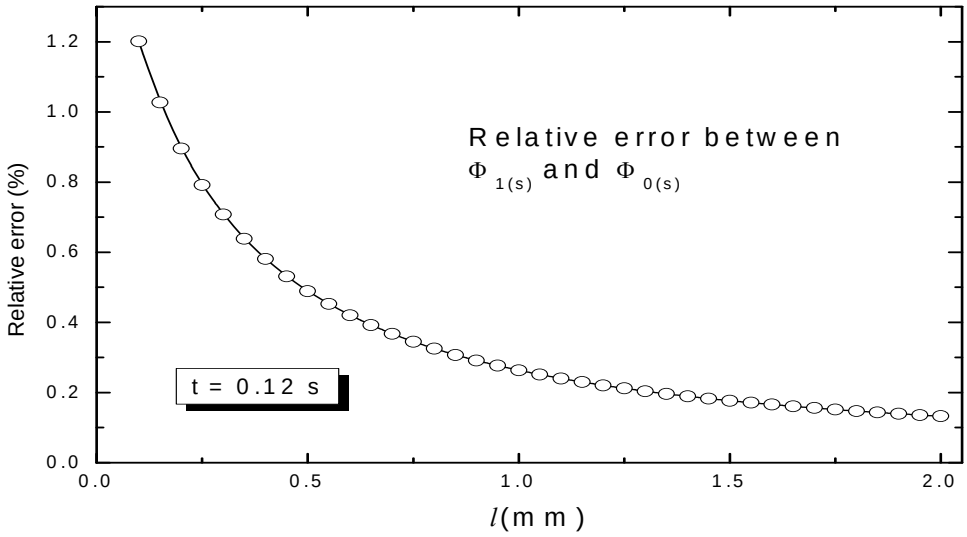

Figure 6-8. Relative difference between the zero and first order approximations for the sample phase shift at $t = 0.12s$ as a function of the sample thickness.

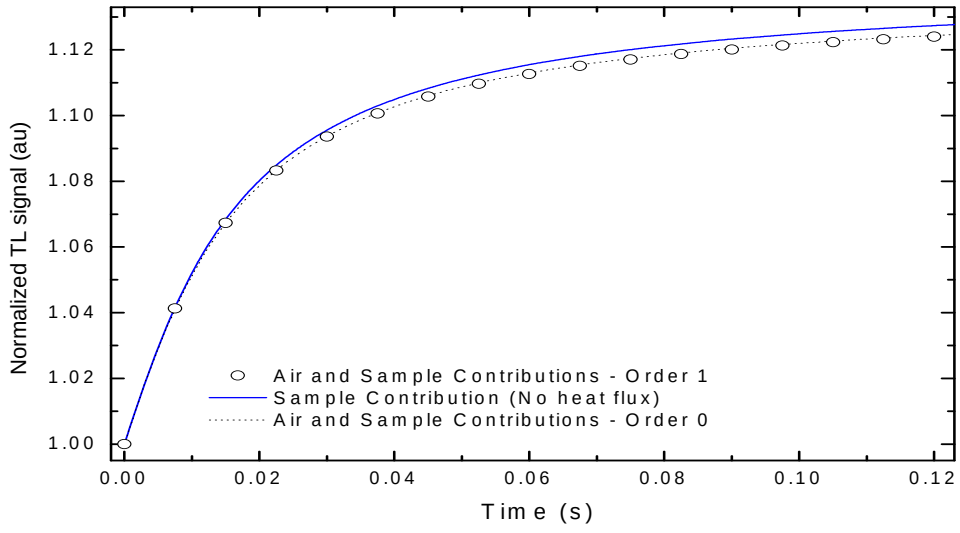

Figure 6-9. Normalized TL signal calculated using the approximations and the parameters listed in Table 6-1. The sample thickness used was $l = 1mm$.

Finally, Fig. 6-9 shows the TL signal calculated using the analytical expressions and the phase shift. The agreement between the zero and first order approximations is again good when both the TL contributions from the air and the sample elements are taken into account. For the case where no air effect is included, the intensity transient deviates a little from the expected using the air coupling solution. This difference could lead to an overestimation of the thermal diffusivity and the parameter θ of approximately 2%.

CONCLUSION

We presented analytical solutions for the temperature gradient induced by the TL effect considering both the heat transfer from sample to air and the TL generated in the air surroundings. Our analytical solution was found to agree with that of our FEA software. The results showed that heat transfer between the sample surface and the air coupling fluid does not introduce an important effect in the optical phase shift when compared with the solution obtained without considering the air-sample heat flux. On the other hand, when the TL created in the air coupling fluid is taken into account, a significant effect is introduced on the predicted time-dependent TL signals, which corresponds to approximately 1.7% of the sample's TL effect. The effect is due to finite heat transfer at the interface typically neglected in semi-infinite cylinder approximations. These solutions open up the possibility of applying the TL method for accurate prediction of the heat transfer to the coupling fluid and subsequently to study the gas surrounding the samples by using a known material solid sample.

REFERENCES

1. J. P. Gordon, R. C. C. Leite, R. S. Moore, S. P. S. Porto, and J. R. Whinnery, J. Appl. Phys. **36**, 3 (1965).
2. R. D. Snook, and R. D. Lowe, Analyst **120**, 2051 (1995).
3. J. Shen, R. D. Lowe, and R. D. Snook, Chem Phys. **165,** 385 (1992).
4. S. E. Bialkowski, *Photothermal Spectroscopy Methods for Chemical Analysis* (Wiley, New York, 1996).
5. A. Mandelis, ed., *Progress in Photoacoustic and Photothermal Science and Technology* (Elsevier, New York, 1991).
6. D. P. Almond, and P. M. Patel, *Photothermal Science and Techniques* (Chapman & Hall, London, 1996).
7. M. L. Baesso, J. Shen, and R. D. Snook, J. Appl. Phys. **75**, 3732 (1994).
8. M. Franko, and C. D. Tran, Rev. Sci. Instrum. **67**, 1 (1996).
9. J. Shen, M. L. Baesso, and R. D. Snook, J. Appl. Phys. **75**, 3738 (1994).
10. M. L. Baesso, A. C. Bento, A. A. Andrade, J. A. Sampaio, E. Pecoraro, L. A. O. Nunes, T. Catunda, and S. Gama, Phys. Rev. B **57**, 10545 (1998).
11. S. M. Lima, T. Catunda, R. Lebullenger, A. C. Hernandes, M. L. Baesso, A. C. Bento, and L. C. M. Miranda, Phys. Rev. B **60**, 15173 (1999).
12. E. Pelicon, J. H. Rohling, A. N. Medina, A. C. Bento, M. L. Baesso, D. F. de Souza, S. L. Oliveira, J. A. Sampaio, S. M. Lima, L. A. O. Nunes, and T. Catunda, J. Non-Cryst. Solids, **304**, 244 (2002).

13. N. G. C. Astrath, J. H. Rohling, A. N. Medina, A. C. Bento, M. L. Baesso, C. Jacinto, T. Catunda, S. M. Lima, F. G. Gandra, M. J. V. Bell, and V. Anjos, Phys. Rev. B **71**, 14202 (2005).

14. M. P. Belancon, L. C. Malacarne, P. R. B. Pedreira, A. N. Medina1, M. L. Baesso, A. M. Farias, M. J. Barbosa, N. G. C. Astrath, and J. Shen, Submitted to J. Physics: Conference Series (2009).

15. N. G. C. Astrath, L. C. Malacarne, P. R. B. Pedreira, A. C. Bento, M. L. Baesso, and J. Shen, Appl. Phys. Lett. **91**, 191908 (2007).

16. L. C. Malacarne, F. Sato, P. R. B. Pedreira, A. C. Bento, R. S. Mendes, M. L. Baesso, N. G. C. Astrath, and J. Shen, Appl. Phys. Lett. **92**, 131903 (2008).

17. F. Sato, L. C. Malacarne, P. R. B. Pedreira, M. P. Belancon, R. S. Mendes, M. L. Baesso, N. G. C. Astrath, and J. Shen, J. Appl. Phys. **104**, 053520 (2008).

18. N. G. C. Astrath, F. B. G. Astrath, J. Shen, J. Zhou, P. R. B. Pedreira, L. C. Malacarne, A. C. Bento, and M. L. Baesso, Opt. Lett. **33**, 1464 (2008).

19. O. O. Dada and S. E. Bialkowski, Appl. Spectrosc. **62**, 1326 (2007).

20. O. O. Dada, M. R. Jorgensen, and S. E. Bialkowski, Appl. Spectrosc. **61**, 1373 (2007).

21. P. R. Joshi, O. O. Dada, and S. E. Bialkowski, Appl. Spectrosc. **63**, 815 (2009).

22. D. R. Lide, *CRC Handbook of Chemistry and Physics* (88th Ed., CRC Press Cleveland, 1977).

CHAPTER 7

PULSED-LASER EXCITED THERMAL LENS SPECTROSCOPY WITH SAMPLE-FLUID HEAT COUPLING [c]

ABSTRACT

Analytical and finite element analysis modeling methods of the pulsed laser excited photothermal lens signal of solids samples surrounded by air are presented. The analytical and finite element analysis solutions for the temperatures induced in the sample and in the air were found to agree for over the range of conditions in this report. Model results show that the air contribution to the total photothermal lens signal is significant in many cases. In fact, these solutions open up the possibility of applying the pulsed excited TL method for accurate prediction of the heat transfer to the coupling fluid and subsequently to study the gas surrounding the samples by using a known material solid sample.

INTRODUCTION

Photothermal (PT) effects are employed in several high-sensitivity measurement techniques used for material characterization.[1-3] Basically, light-induced heating of a sample produces the PT effect. This heating may cause a number of different effects in solid, liquid and gas samples.

---

[c]COAUTHORED BY PR JOSHI, NGC ASTRATH, LC MALACARNE, GVB LUKASIEVICZ, MP BELANCON, ML BAESSO, AND SE BIALKOWSKI. REPRODUCED WITH PERMISSION FROM THE *JOURNAL OF APPLIED PHYSICS*, 107, 083512 (2010) COPYRIGHT 2010 AMERICAN INSTITUTE OF PHYSICS (SEE APPENDIX C)

For instance, the induced temperature change: generates acoustic waves inside the sample which propagate out to the surroundings; [1] induces increased infrared emission; [1] changes the refractive index of the sample; [4-9] and creates surface deformation.[10-13]

Information on the temperature rise in the sample as well as its thermo-physical parameters can be obtained with the different detection methods. [1-16] The limits of detection for the PT methods are related to how realistically the experimental description can be theoretically modeled. [17,18] Generally, simple and applicable theoretical models are obtained by introducing modeling approximations that lead to analytical solutions. In some cases, these approximations can be accounted for by using appropriated experimental setups. However, it is not always feasible. In most practical situations, for example, heat is transferred from the sample to the surroundings along the axial dimension. This is especially true when the heated sample is in contact with the air or another coupling fluid. Recently, it has been showed that sample/air heat coupling in the Thermal Lens (TL) experiment could significantly contribute to the TL signal. [19-21] In fact, the fluid thermal coupling is always treated as a perturbation to the TL signal. This perturbation could become stronger as the sample thickness is reduced and/or depending on the thermo-optical properties of the sample/fluid system.

The theoretical modeling of the thermal lens signal is difficult to be analytically deducted assuming heat coupling with the surroundings and also adopting realistic boundary conditions. With approximations, such model can be achieved, but the lack of a more complete theory makes difficult the validation of the approximated model. In this sense, finite element methods provide numerical solutions to the heat transfer equations

with the realistic boundary conditions imposed by the experimental geometry. Finite Elemental Analysis (FEA) software has been recently [19-21] applied to describe complex heat coupling conditions on photothermal techniques. Numerical and approximated solutions have been compared to the FEA modeling. FEA has shown to be a powerful tool to model cw and pulsed photothermal methods.

This work presents an analytical theoretical description of the pulsed-laser excitation thermal lens method by taking the coupling of heat both within the sample and out to the surroundings into account. Our results are compared with finite elemental analysis solution, leading to an excellent agreement. The analytical model is then used to quantify the effect of the heat transfer from the sample surface to the air coupling fluid on the thermal lens signal. The results showed that the air signal contribution to the total photothermal lens signal is significant in many cases.

THEORY

The thermal lens effect is based on the heat deposition in a sample by non-radiative decay process following optical energy absorption by the sample. The sample is heated by the absorbed optical energy from a pulsed Gaussian profile laser, resulting in a transverse temperature gradient, which induces a refractive index gradient behaving like an optical lens. The propagation of another laser beam (the probe beam) through the TL is affected, resulting in a change in its intensity profile. By measuring the intensity variation, the information on physical properties of the sample can be obtained.[5]

The radii of the excitation and probe beams in the sample are ω_{0e} and ω_{1P}, respectively. The probe beam propagates in the z-direction, and the sample is located

at $z = 0$. The sample dimensions are large compared with the excitation beam radius to avoid edge effects, and the absorbed excitation laser energy by the sample is low so that the excitation laser can be considered to be uniform along the z-direction.

The TL signal is dependent on the spatially dependent refractive index change produced due to the temperature change in the sample. Indeed, by heat conduction, a temperature gradient in the air surrounding the sample is established. One then consider two semi-infinity spaces with boundaries at $z = 0$, with the sample in the $0 < z < \infty$ region and the fluid (air in this work) in the $-\infty < z < 0$ region. The temperature rise distributions inside the sample, $T_s(r,z,t)$, and in the fluid, $T_f(r,z,t)$, are given by the solution of the heat conduction differential equations

$$\frac{\partial T_s(r,z,t)}{\partial t} - D\nabla^2 T_s(r,z,t) = Q(r,z) \tag{1}$$

$$\frac{\partial T_f(r,z,t)}{\partial t} - D_f\nabla^2 T_f(r,z,t) = 0, \tag{2}$$

and the boundary and initial conditions are given by

$$\begin{aligned} &k\partial_z T_s(r,z,t)\big|_{z=0} = k_f \partial_z T_f(r,z,t)\big|_{z=0} \\ &T_s(\infty,z,t) = T_s(r,\infty,t) = 0 \\ &T_s(r,z,0) = T_f(r,z,0) = 0 \\ &T_s(r,0,t) = T_f(r,0,t) \\ &T_f(\infty,z,t) = T_f(r,-\infty,t) = 0 \end{aligned} \tag{3}$$

Here $D_i = k_i / \rho_i c_i$ is the thermal diffusivity of the material i (sample and fluid). c_i, ρ_i and k_i are the specific heat, mass density, and thermal conductivity of the material i, respectively. The energy absorbed by the sample, for a collimated, short-pulsed Gaussian

profile laser propagating on the z-axis direction is $Q(r,z,t) = Q_0\, Q(r)\, Q(z)\, \delta(t)$, with $Q(r) = \exp\left(-2r^2/\omega^2\right)$. $\delta(t)$ is the delta function, which is zero unless $t = 0$. $Q_0 = 2P_e A_e \phi / \pi c \rho \omega^2$ and P_e is the excitation beam power, A_e is the optical absorption coefficient at excitation beam wavelength λ_e, and ϕ is a heat yield parameter accounting for energy loss due to luminescence during sample excitation. $Q(z) = 1 - \exp(-A_e z)$ is the absorptance along z-direction. For the purposes here, the optical absorption coefficient is small and $Q(z) = 1$ can be assumed.

Using the integral transform methods, Laplace and Hankel, and the conditions described in Eq.(3), one can write the solution of the heat conduction differential equations in the Laplace-Hankel space as

$$T_s(\alpha,z,s) = -\frac{Q(\alpha)\left(k_f\sqrt{D}/k\sqrt{D_f}\right)\sqrt{s+D_f\alpha^2}}{\left(s+D\alpha^2\right)\left(1+\dfrac{k_f\sqrt{D}\sqrt{s+D_f\alpha^2}}{k\sqrt{D_f}\sqrt{s+D\alpha^2}}\right)}\frac{e^{-z\sqrt{\left(s+D\alpha^2\right)/D}}}{\sqrt{s+D\alpha^2}} + \frac{Q(\alpha)}{\left(s+D\alpha^2\right)}, \tag{4}$$

and

$$T_f(\alpha,z,s) = -\frac{Q(\alpha)\sqrt{s+D_f\alpha^2}}{\left(s+D\alpha^2\right)\left(1+\dfrac{k_f\sqrt{D}\sqrt{s+D_f\alpha^2}}{k\sqrt{D_f}\sqrt{s+D\alpha^2}}\right)}\frac{e^{-z\sqrt{\left(s+D_f\alpha^2\right)/D_f}}}{\sqrt{s+D_f\alpha^2}}. \tag{5}$$

In Esq. (4) and (5), $Q(\alpha) = Q_0 \exp\left(-\omega^2\alpha^2/8\right)\omega^2/4$ and it comes from the Hankel transform of the source term. For the glass-air system, $k_f\sqrt{D}\sqrt{s+D_f\alpha^2} << k\sqrt{D_f}\sqrt{s+D\alpha^2}$, and the term in the denominator of Eqs. (4) and (5) can be expanded in series as $(1+x)^{-1} = 1 - x + x^2 + O\left(x^3\right)$. The temperature gradients are then given by the inverse Laplace and Hankel transforms

of Eqs. (4) and (5). Taking the expansion up to the first order, that is, $\left(1-k_f\sqrt{D}\sqrt{s+D_f\alpha^2}\,\middle/\,k\sqrt{D_f}\sqrt{s+D\alpha^2}\right)$, the temperature gradient in the sample, $T_{1(s)}(r,z,t)$, is

$$T_{1(s)}(r,z,t)=\int_0^\infty T_s(\alpha,z,t)\,\alpha\,\mathrm{J}_0(\alpha r)\,d\alpha\,, \tag{6}$$

with

$$\begin{aligned} T_s(\alpha,z,t)=Q(\alpha)e^{-Dt\alpha^2}-Q(\alpha)\frac{k_f\sqrt{D}}{k\sqrt{D_f}}\int_0^t\left(\frac{e^{-\tau\alpha^2D_f}}{\sqrt{\pi}\sqrt{\tau}}+e^{-D\tau\alpha^2}\alpha\right. \\ \left.\times\frac{\mathrm{erf}\left(\sqrt{\tau}\alpha\sqrt{-D+D_f}\right)}{\left(-D+D_f\right)^{-1/2}}\right)e^{-D\alpha^2(t-\tau)}\frac{\exp\left(-\dfrac{z^2}{4D(t-\tau)}\right)}{\sqrt{\pi(t-\tau)}}d\tau \end{aligned} \tag{7}$$

For the fluid, the first order expansion, $T_{1(f)}(r,z,t)$, is

$$T_{1(f)}(r,z,t)=\int_0^\infty T_f(\alpha,z,t)\,\alpha\,\mathrm{J}_0(\alpha r)\,d\alpha \tag{8}$$

with

$$\begin{aligned} T_f(\alpha,z,t)=Q(\alpha)\int_0^t\left[\left(\frac{e^{-\tau\alpha^2D_f}}{\sqrt{\pi}\sqrt{\tau}}+e^{-D\tau\alpha^2}\alpha\,\mathrm{erf}\left(\sqrt{\tau}\alpha\sqrt{-D+D_f}\right)\sqrt{-D+D_f}\right)-\right. \\ \left.-\left(\frac{k_f\sqrt{D}}{k\sqrt{D_f}}\frac{e^{-D\tau\alpha^2}\left(1-2D\tau\alpha^2+2\tau\alpha^2D_f\right)}{\sqrt{\pi}\sqrt{\tau}}\right)\right]e^{-D_f\alpha^2(t-\tau)}\frac{e^{-z^2/4D_f(t-\tau)}}{\sqrt{\pi(t-\tau)}}d\tau \end{aligned} \tag{9}$$

$\mathrm{J_n}(x)$ is the Bessel function of the first kind and $\mathrm{erf}(x)$ is the error function.

The strength of the photothermal lens element is found from the second radial derivative, evaluated on-axis. Integration over the path length in the sample and in the surrounding air results in the inverse focal length [15]

$$\frac{1}{f(t)} = \left(\frac{dn}{dT}\right)_f \int_{path} \left|\frac{d^2}{dr^2} T_{1(f)}(r,z,t)\right|_{r=0} dz + \left(\frac{ds}{dT}\right)_s \int_{path} \left|\frac{d^2}{dr^2} T_{1(s)}(r,z,t)\right|_{r=0} dz \tag{10}$$

As $J_0(r=0)=1$, we can rewrite Eq. 10 as

$$\frac{1}{f(t)} = \frac{1}{f_f(t)} + \frac{1}{f_s(t)} = 2\left(\frac{dn}{dT}\right)_f \int_{-\infty}^{0} \left|\int_0^{\infty} T_f(\alpha,z,t)\left(-\alpha^2/2\right)\alpha d\alpha\right| dz + 2\left(\frac{ds}{dT}\right)_s \int_0^{L/2} \left|\int_0^{\infty} T_s(\alpha,z,t)\left(-\alpha^2/2\right)\alpha d\alpha\right| dz \tag{10}$$

The space and time dependences of the temperature equations for the air and samples media, Eqs. (6) to (9), and the inverse focal length, Eq. (10), will be compared to the FEA modeling solutions for a system with glass sample of thickness l surrounded by air. The numerical integrations in these equations are performed by using standard command in the software Mathematica (version 7.0).

To compare the analytical solutions presented previously, FEA software was used to perform numerical solutions to the heat transfer equations with the realistic boundary conditions. Comsol Multiphysics 3.5 analysis is carried out on a Dell Studio XPS 435, i7 940 processor, using MS Windows Vista. The Comsol Multiphysics software in conduction and convection mode solves the heat diffusion equation given as

$$\rho c \frac{\partial T(r,z,t)}{\partial t} - k\nabla^2 T(r,z,t) = \rho c Q(r,z,t) - \cancel{\rho c u \cdot \nabla T(r,z,t)} \tag{11}$$

in which u is the flow velocity. All other symbols are the same as those introduced above. Note that Eqs. (1), (2) and (11) differ only by the second term on the right side of the equation. This term can account for convection or mass flow heat transfer, which is not important for the sample investigated in this work: glass.

A detailed description of FEA modeling can be found elsewhere. [16,20,21] Briefly, it consists of drawing the sample geometry and specifying material boundary conditions, heat sources, and sinks. The problems are then solved with rough finite element definition and further refinement of elements and domain are made. The element mesh is refined until model results become independent of mesh size. Finally, the temperature profile can be obtained either at a single time, over a time series, or at steady state, for the sample and air domain. The model solid absorbing media was cylindrical plate of 10 mm in diameter and 1mm thick. Optical excitation was along z-axis.

The values of the thermal, optical and mechanical parameters used for the analytical and FEA modeling simulations are shown in Table 7-1.

Table 7-1. Parameters used for the simulations. The thermal, optical and mechanical properties listed below are associated to characteristics values found in glasses [13]and for the surrounding medium we use the air properties. [22]

Parameters	(units)	Glass sample	Air
D	($10^{-7}m^2/s$)	5.0	2.2
k	(W/mK)	1.4	0.026
ρ	(kg/m^3)	933	1.18
c	(J/kgK)	3000	1005
ds/dT	(10^{-6} K^{-1})	10.0	-1.0
ω	(μm)	50	
$t_c = \omega^2/4D$	(ms)	1.25	

RESULTS AND DISCUSSION

Figure 7-1 shows the normalized radial temperature, $T_{1(s)}(r,0.5,t)/T_{1(s)}(r,0.5,0)$ within the glass sample at its center, $z=0.5mm$. The results by the FEA model are compared to the temperature solution considering heat flux from glass to air, Eq. (6) at different exposure times. One can see that there is almost no difference between the FEA model and the semi-infinite approximation with glass-air heat coupling.

Figure 7-2 shows the normalized temperature profiles along the z direction, from air to glass domain, using the FEA modeling, the solution considering air surroundings, Eq. (6), and the solution with no transfer of heat from glass to air, Eq. (8), at different exposure times at $r=0$. It clearly shows an excellent agreement between the analytical solutions considering air coupling and the FEA model.

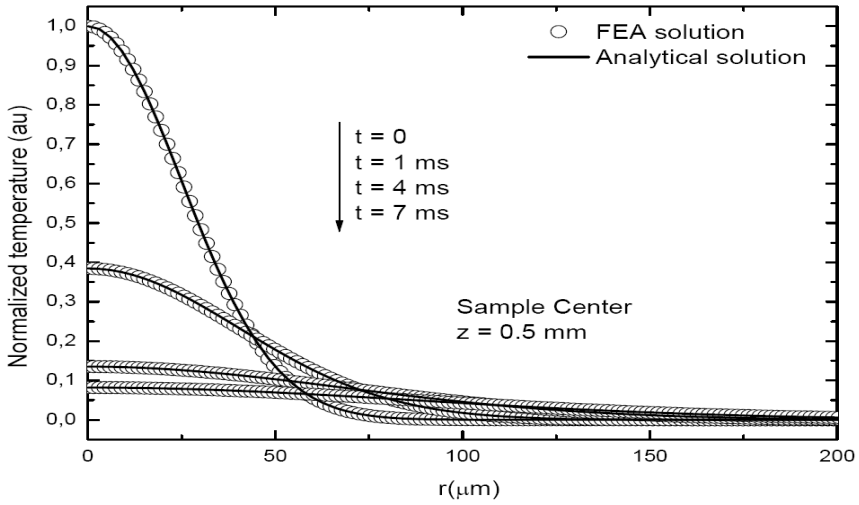

Figure 7-1. Normalized temperature profile in the glass sample at $z=0.5mm$ using the FEA modeling, the solution considering heat flux to air, Eq. (6) at different exposure times.

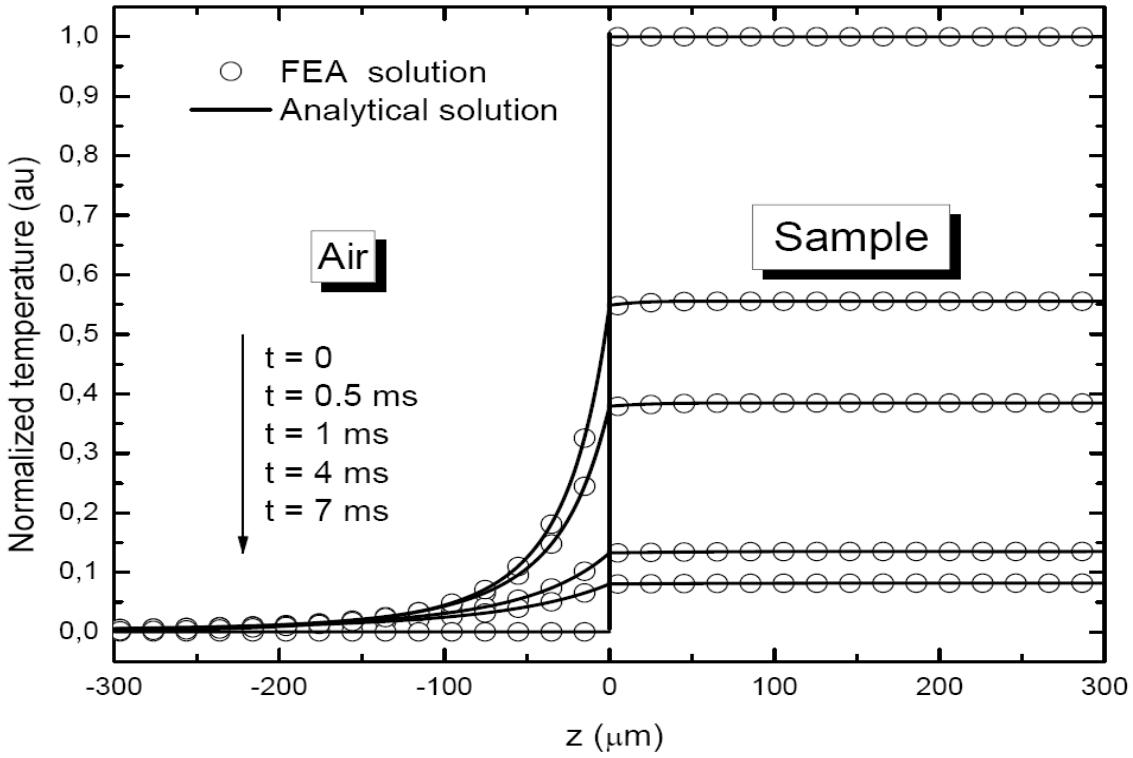

Figure 7-2. Normalized temperature profile along the z direction (air-glass) using the FEA modeling and the solution considering air surroundings, Eqs. (6) and (8), at different exposure times. $r = 0$ was used in the simulations.

As displayed by Fig.7-3, the agreement between both predictions is also very good for the normalized radial temperature profile in the air surroundings using the FEA modeling and the solution for the air fluid, Eq. (8), at the sample surface on the air side, $z = 0$, and up to $0.2mm$ distant. The exposure time was $t = 1ms$.

The results obtained using FEA model show that the first order analytical approximation presented in this work can be used to describe the temperature profile in the sample and in the air surrounding it.

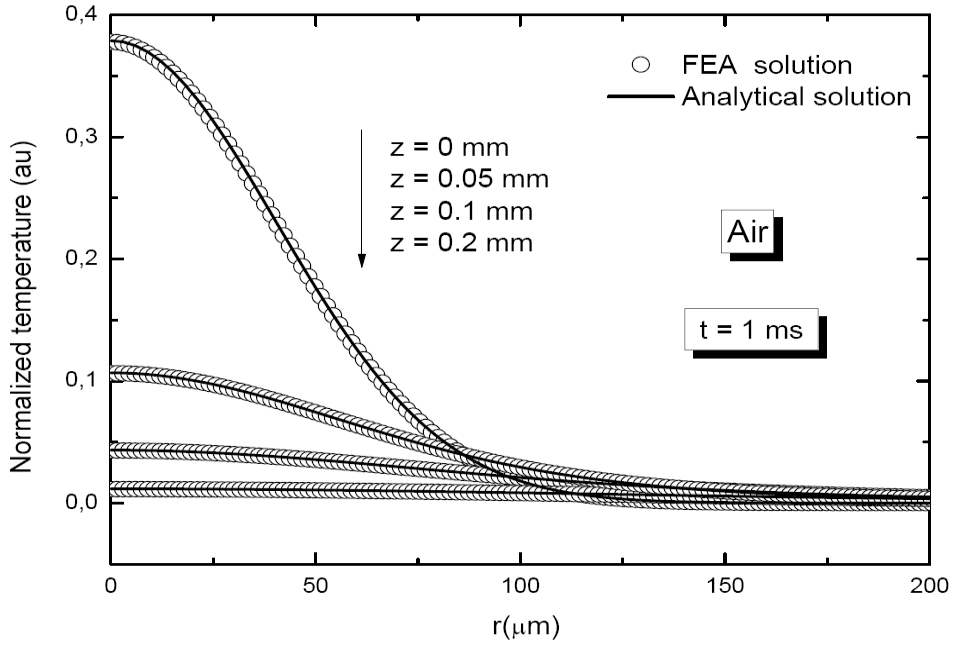

Figure 7-3. Radial temperature profile in the air surroundings at $t = 1ms$ using the FEA modeling and the solution for the air fluid, Eq. (8), at the sample surface in the air side, $z = 0$.

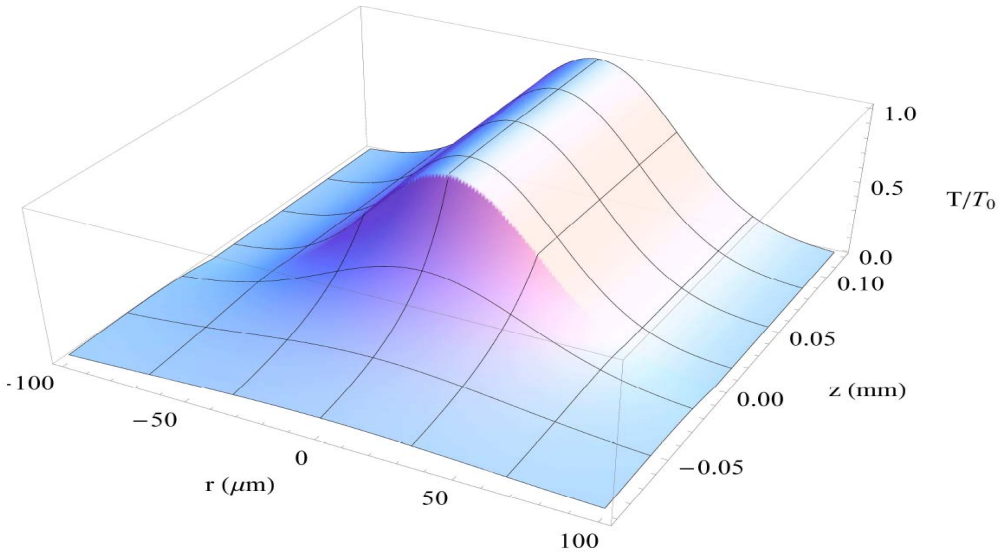

Figure 7-4. Normalized radial temperature profile in the sample and in the air surroundings at $t = 0.5ms$ using Eqs. (6) and (8).

Figure 7-4 shows a complete picture of the normalized radial temperature gradient along the z-direction at $t = 0.5ms$.

The solutions presented in Eqs. (6) and (8) can be analytically used to describe theoretically the thermal lens effect, by calculating the inverse focal length of the probe beam after passing thought the TL region, Fig. 7-5. The air and samples absolute contributions are normalized by the sample $f_s(0)^{-1}$ inverse focal length at $t = 0$. The results are then compared to the FEA modeling. For the FEA solutions for the inverse focal length, one performed the integration over the second radial derivative of the temperature change evaluated on $r = 0$.

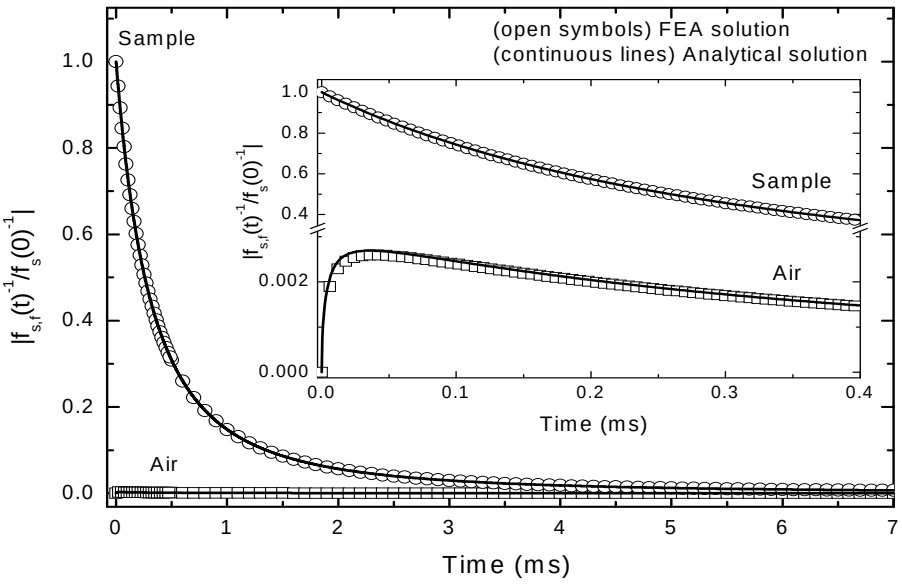

Figure 7-5. FEA and analytical solution using Eq. (10) for the normalized inverse focal length for the 1mm thick sample. We used $(dn/dT)_f = -1\times10^{-6}K^{-1}$ and $(ds/dT)_s = 10\times10^{-6}K^{-1}$.

The time dependent thermal lens signal calculated using FEA and the analytical solutions are in good agreement. $(ds/dT)_s = 10\times10^{-6}K^{-1}$ was used for the glass sample and $(dn/dT)_f = -1\times10^{-6}K^{-1}$ for the air. For a relatively thick sample, 1mm, both the FEA and analytical solutions for the inverse focal length showed no significant difference. Fig. 7-5 shows that the magnitude of the signal of glass is more than three orders greater than that of the air. This is because the temperature change with pulsed laser excitation is much faster than the heat diffusion to the surroundings. However, this result is highly dependent on the thermo-optical parameters of the sample and heat coupling fluid and the sample thickness. It can be exemplified by performing a relative change of the air and sample signals for different sample thickness. Fig.7- 6 shows the absolute ratio between the air and sample signals in function of the sample thickness.

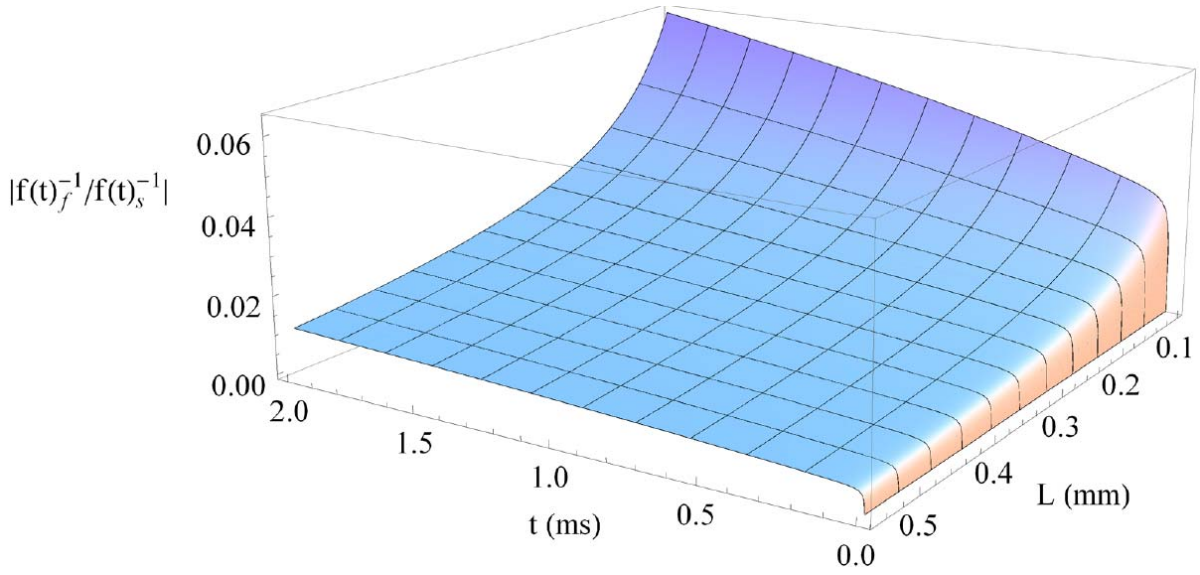

Figure 7-6. Absolute ratio between the air and sample signal, $\left|f(t)_f^{-1}/f(t)_s^{-1}\right|$, in function of the sample thickness with $(dn/dT)_f = -1\times10^{-6}K^{-1}$ and $(ds/dT)_s = 10\times10^{-6}K^{-1}$.

From Fig.7-6 one can see that the effect of the air on the sample signal is very small for thick samples. On the other hand, as the thickness decreases, the air photothermal signal becomes stronger and it has a significant contribution to the total inverse focal length. In fact, the air signal contribution is about 6% of the sample signal. It is important to note that the air signal is a negative contribution to the total inverse focal length, $(dn/dT)_f < 0$.

This behavior is also observed even with thick samples when $(dn/dT)_f$ presents values of the same order of $(ds/dT)_s$. Experimentally, it can be obtained by using a heat coupling fluid with higher $(dn/dT)_f$ an/or by using different semitransparent samples with smaller $(ds/dT)_s$. To illustrate this, Fig. 7- 7 shows the absolute ratio between the air and sample signals in function of the $\left|(dn/dT)_f/(ds/dT)_s\right|$ ratio. If the absolute value of $\left|(dn/dT)_f\right|$ is small compared to $(ds/dT)_s$, one have the case considered previously, where the effect of the air on the sample signal is very small. However, if they become comparable or if $\left|(dn/dT)_f\right| > (ds/dT)_s$, the effect of the air on the photothermal signal ensues significant.

Figure 7-8 shows the normalized inverse focal length for a typical glass-air system in function of the sample thickness. $(dn/dT)_f = -1\times10^{-6}K^{-1}$ and $(ds/dT)_s = 10\times10^{-6}K^{-1}$ were used in the numerical calculations using Eq. (10). For thin samples, there is an initial rapid decrease in inverse focal length.

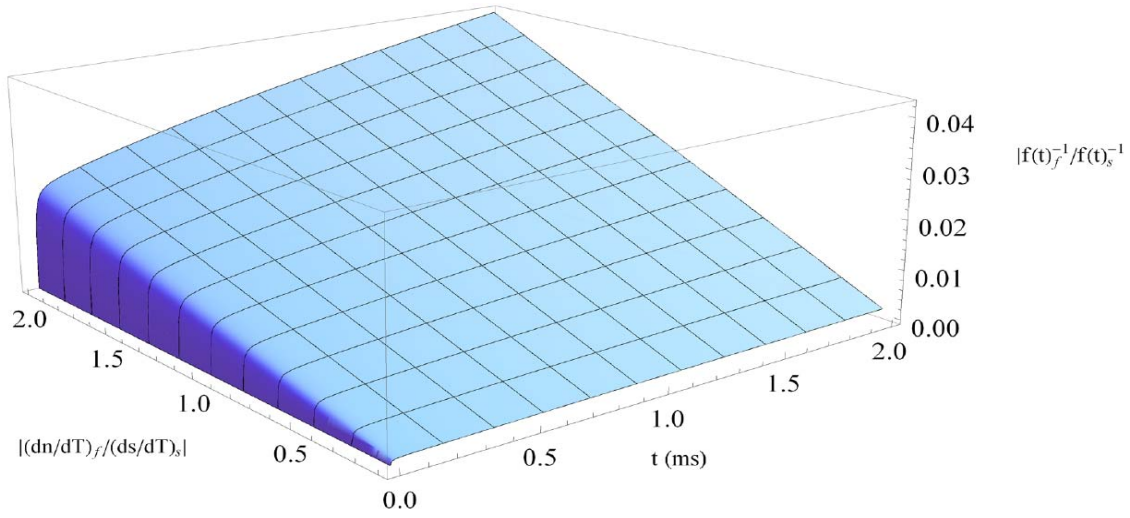

Figure 7-7. Absolute ratio between the air and sample signal, $\left| f(t)_f^{-1} / f(t)_s^{-1} \right|$, in function of the $\left| (dn/dT)_f / (ds/dT)_s \right|$ ratio.

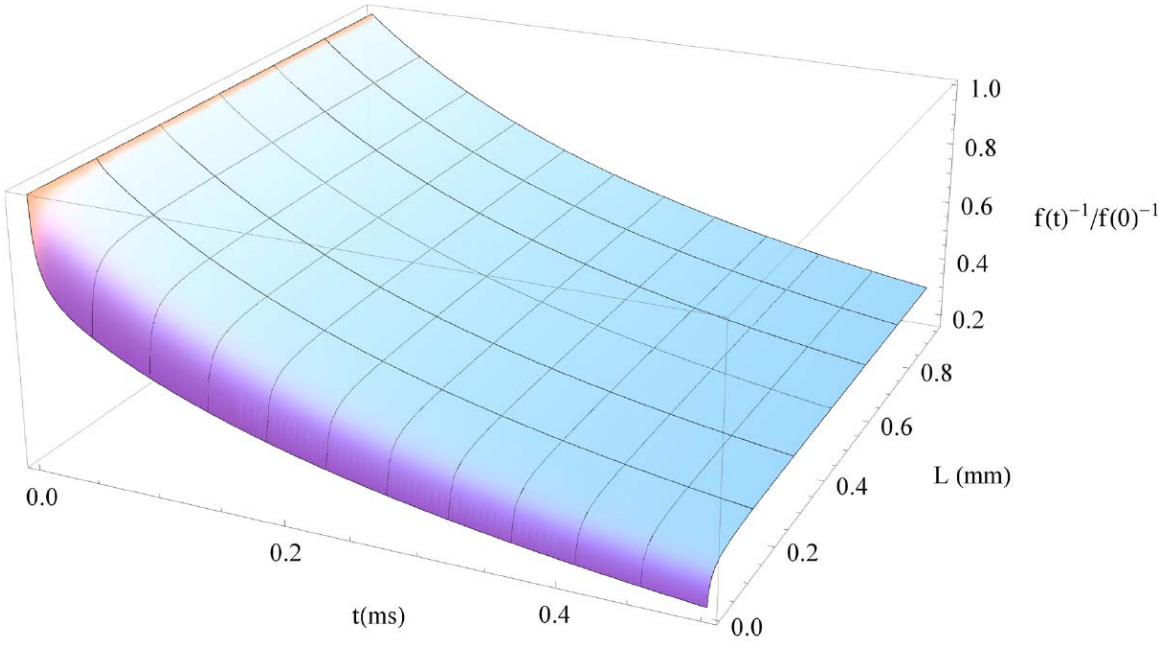

Figure 7-8. Analytical solution using Eq. (10) for the normalized inverse focal length as a function of the sample thickness with $(dn/dT)_f = -1 \times 10^{-6} K^{-1}$ and $(ds/dT)_s = 10 \times 10^{-6} K^{-1}$.

This rapid decay is due to heat loss to the air at the surfaces, which decreases the length of the photothermal lens. This effect is less pronounced as the thickness increases due to the fact that border effects are less important for thick samples. The fact that the air signal contribution to the inverse focal length becoming significant for some cases, for instance, when the sample thickness is reduced and/or $\left|(dn/dT)_f\right|$ is comparable to $(ds/dT)_s$, or $\left|(dn/dT)_f\right| > (ds/dT)_s$, turns out to be an interesting point for this technique. It could be used to determine thermo-optical properties of the surrounding media providing the physical parameters of the sample are known.

CONCLUSION

Analytical and finite element analysis modeling were used to describe the pulsed laser excited photothermal lens signal by considering both the heat transfer from sample to air and the TL generated in the air surroundings. The analytical solutions for the temperatures induced in the sample and in the air were found to agree with that of the FEA software. The results showed that the air signal contribution to the total photothermal lens signal is significant in many cases, mainly for those where the absolute value of $\left|(dn/dT)_f\right|$ is comparable to that of $(ds/dT)_s$ and also $\left|(dn/dT)_f\right| > (ds/dT)_s$. In fact, these solutions open up the possibility of applying the pulsed excited TL method for accurate prediction of the heat transfer to the coupling fluid and subsequently to study the gas surrounding the samples by using a known material solid sample. Finally, on one side, the analytical solutions presented here are in complete agreement with the FEA modeling and it could be used for material parameter determination. On the other hand,

FEA modeling opens up numerous possibilities of analyzing theoretically different samples at different external conditions.

REFERENCES

1. A. Mandelis, ed., *Progress in Photoacoustic and Photothermal Science and Technology* (Elsevier, New York, 1991).
2. S. E. Bialkowski, *Photothermal Spectroscopy Methods for Chemical Analysis* (Wiley, New York, 1996).
3. D. P. Almond, and P. M. Patel, *Photothermal Science and Techniques* (Chapman & Hall, London, 1996).
4. J. P. Gordon, R. C. C. Leite, R. S. Moore, S. P. S. Porto, and J. R. Whinnery, J. Appl. Phys. **36**, 3 (1965).
5. J. Shen, R. D. Lowe, and R. D. Snook, Chem Phys. **165,** 385 (1992).
6. M. L. Baesso, J. Shen, and R. D. Snook, J. Appl. Phys. **75**, 3732 (1994).
7. M. L. Baesso, A. C. Bento, A. A. Andrade, J. A. Sampaio, E. Pecoraro, L. A. O. Nunes, T. Catunda, and S. Gama, Phys. Rev. B **57**, 10545 (1998).
8. S. M. Lima, T. Catunda, R. Lebullenger, A. C. Hernandes, M. L. Baesso, A. C. Bento, and L. C. M. Miranda, Phys. Rev. B **60**, 15173 (1999).
9. N. G. C. Astrath, J. H. Rohling, A. N. Medina, A. C. Bento, M. L. Baesso, C. Jacinto, T. Catunda, S. M. Lima, F. G. Gandra, M. J. V. Bell, and V. Anjos, Phys. Rev. B **71**, 14202 (2005).
10. N. G. C. Astrath, L. C. Malacarne, P. R. B. Pedreira, A. C. Bento, and M. L. Baesso, and J. Shen, Appl. Phys. Lett. **91**, 191908 (2007).

11. L. C. Malacarne, F. Sato, P. R. B. Pedreira, A. C. Bento, R. S. Mendes, M. L. Baesso, N. G. C. Astrath, and J. Shen, Appl. Phys. Lett. **92**, 131903 (2008).

12. F. Sato, L. C. Malacarne, P. R. B. Pedreira, M. P. Belancon, R. S. Mendes, M. L. Baesso, N. G. C. Astrath, and J. Shen, J. Appl. Phys. **104**, 053520 (2008).

13. N. G. C. Astrath, F. B. G. Astrath, J. Shen, J. Zhou, P. R. B. Pedreira, L. C. Malacarne, A. C. Bento, and M. L. Baesso, Opt. Lett. **33**, 1464 (2008).

14. A. Marcano, O. L. Rodriguez, and Y. Alvarado, J. Opt. A: Pure Appl. Opt. **5**, S256 (2003).

15. W. B. Jackson, N. M. Amer, A. C. Boccara, and D. Fournier, Appl. Opt. **20**,1334 (1981).

16. O. O. Dada, M. R. Jorgensen, and S. E. Bialkowski, Appl. Spectrosc. **61**, 1373 (2007).

17. A. Chartier, and S. E. Bialkowski, Opt. Eng. **36**, 303 (1997).

18. J. R. Whinnery, Acc. Chem. Res. **7**, 225 (1974).

19. L. C. Malacarne, N. G. C. Astrath, P. R. B. Pedreira, R. S. Mendes, M. L. Baesso, P. R. Joshi, and S. E. Bialkowski, Submitted to J. Appl. Phys. (2009).

20. O. O. Dada, and S. E. Bialkowski, Appl. Spectrosc. **62**, 1326 (2008).

21. P. R. Joshi, O. O. Dada, and S. E. Bialkowski, Appl. Spectrosc. **63**, 815 (2009).

22. D. R. Lide, *CRC Handbook of Chemistry and Physics* (88^{th} Ed., CRC Press, Cleveland, 1977).

CHAPTER 8

SUMMARY

The research work outlined in this dissertation focuses on pulse-laser excited photothermal lensing effect on glasses and a small size cylindrical sample cell. The COMSOL multiphysics finite element analysis software modeling of the pulse-laser excited glass shows that there is: (1) heat transfer between the glass surface and the air coupling fluid, (2) fast heat transfer along the axial direction which is the direction of propagation of the excitation source, and (3) glass surface deformation due to pulse-laser heating. These issues have been addressed for the application of photothermal lens spectroscopy to the study of glass correctly.

First, finite elemental analysis software is used to model the photothermal effect by simulating the coupling of heat both within the sample and out to the surroundings. Modeling shows that there is significant amount heat transfer from the glass surface to the air. And at the same time the air signal contribution to the total photothermal lens signal is significant. Although heat transfer between the glass surface and the air coupling fluid has a significant effect on the predicted time dependent photothermal lens signals, a pulse-laser excitation has been found to be a better option in comparison to continuous laser excitation for photothermal lens spectroscopy of glass surrounded by air. This is because of the slower heat transfer from the glass to the air surrounding than the time dependent photothermal lens signals decay in sample for pulse-laser excitation.
For comparison with experimental signals, a simple equation based on the finite element analysis result is proposed for accounting for the variance of experimental data where this

type of heat coupling situation occurs. Experimental results for photothermal lens measurements are compared to finite elemental analysis models for commercial colored glass filters. The colored glass filters are found to have positive thermo-optical coefficients and considered to be the consequence of counteracting factors: optical nonlinearity, stress-induced birefringence, and the structural network of glass.

Secondly, the fast initial signal decay in glass, which is shown by the FEA modeling of photothermal lens signal of colored silica glass surrounded by air, is interpreted as due to the diffusion of heat from the surface of glass. This is because when the heated sample is direct in contact with air or another coupling fluid, heat is transferred from sample to the surroundings along to the axial dimension. And this problem is more severe, particularly when the sample is thin and insulated. The fast signal decay is detected by using fast response detector in transmission and reflection photothermal lens experiments. FEA modeling is used to evaluate the time constant of slow and fast components and corrections are made for the prediction of material properties.

Finite heat transfer at the interface is typically neglected in semi-infinite cylinder approximations. In order to address the issue of heat coupling between the sample and its immediate surrounding an analytical and finite element analysis modeling were used to describe the pulsed and continuous laser excited photothermal lens signal by considering both the heat transfer from sample to air and the thermal lens generated in the air surroundings. The analytical solutions for the temperatures induced in the sample and in the air were found to agree with that of the FEA modeling. The results showed that the air signal contribution to the total photothermal lens signal is significant in many cases,

mainly for those where the absolute value of $\left|(dn/dT)_f\right|$ is comparable to that of $(ds/dT)_s$ and also $\left|(dn/dT)_f\right| > (ds/dT)_s$.

Third, The FEA modeling shows that there is surface deformation due to pulse laser heating of colored glass filters, and consequently the optical path length of them changed. The modeling also shows that the extent of deformation increases with absorption coefficient of glass. It has been found that the photothermal lens signals and thermal expansion are affected due to air environment around the solid sample. The surface deformation phenomenon can be exploited for the measurement of thermal and physical properties of solid materials. In short, FEA modeling can be used to better understand the pulsed laser excited photothermal spectroscopy signals by correctly accounting for the heat transfer of the sample to the surroundings where the absorbing material is in direct contact with the coupling fluid surroundings. The cylindrical approximation is not valid in these cases.

The fluid thermal coupling is treated as a perturbation to the thermal lens signal. FEA modeling could be used to correct the perturbation to the thermal lens signal for material parameter determination. These studies open up the new avenues of application of FEA modeling and the pulsed excited thermal lens method for accurate prediction of the heat transfer to the coupling fluid and subsequently to study the gas surrounding the samples by using a known material solid sample. However, a comparative study of different materials of different optical and thermal properties is required with the help of these methods for the best results.

Lastly, realizing the advantages of cylindrical sample cell over conventional cell, a novel apparatus for performing photothermal lens spectroscopy with pulsed excitation laser is described. When the whole sample cell volume is irradiated with constant irradiance beam produced by an excitation laser, the photothermal lens element is formed by thermal diffusion from the irradiated sample volume through the sample cell walls. The parabolic-form photothermal lens produced by thermal diffusion is aberration free. A low-volume cylindrical sample cell requires a little sample and signals produced by thermal diffusion through the sample wall are less susceptible to the bulk heat transfer effects due to convection. The apparatus is found to work with cells designed to contain sample volumes to nL level.

FEA modeling is used to examine the temperature profile and the photothermal signal and result of it is compared with the experimental result. The experimental photothermal lens enhancement is found to be that predicted from theory within experimental error. A best advantage of cylindrical sample cell is that it circumvents the large temperature changes by heat transport to the surrounding. However, further study to optimize the apparatus and the experiment is required for the best performance.

APPENDIXES

APPENDIX A:

Figure and Data

All figure data are stores in the "MGD" media device that accompanies this dissertation.

APPENDIX B:

Comsol Multiphysics Files

Comsol Multiphysics files for finite element analysis modeling results are stored in "MGD" media device that accompanies this dissertation.

APPENDIX C:

Permission letters

From: Prakash Joshi [p.r.joshi@aggiemail.usu.edu]
Sent: Wednesday, March 24, 2010 4:05 PM
To: office@s-a-s.org
Subject: Re: Permission letter

Dear Bonnie Saylor,

I am in the process of preparing my dissertation in the department of chemistry and biochemistry at Utah State University, which is expected to be completed by the end of spring of 2010.
I am writing to request SAS permission to include the manuscript of my paper entitle "Pulsed Laser Excited Photothermal Lens Spectrometry of CdSxSe1-x Doped Silica Glasses" in its entirety in my dissertation. The paper was published in Applied Spectroscopy Volume 63, number 7, 2009. In addition a copy of the permission letter shall be printed in an Appendix to my dissertation.

I will be happy to answer any question or request regarding this letter.

Thank you for your consideration

Permission granted for the use requested above:
Permission granted this 6th day of April 2010. Full citation required.

Bonnie Saylor, Executive Director, SAS

Prakash Raj Joshi
Department of Chemistry and Biochemistry
Utah State University
Logan, Utah 84322-0300

05 January 2010

Dr. Oluwatosin O. Dada
Department of Chemistry
University of Washington
Seattle, WA 98195-1700 USA

Prakash Raj Joshi
Department of Chemistry and Biochemistry
Utah State University
Logan, Utah 84322-0300

Dear Dr. Oluwatosin O. Dada,

I am in the process of preparing my dissertation in the department of chemistry and biochemistry at Utah State University, which is expected to be completed by the end of spring of 2010.

You were a co-author with me on the manuscript entitled "Pulsed Laser Excited Photothermal Lens Spectrometry of CdS_xSe_{1-x} Doped Silica Glasses". I am writing to request your permission to include the manuscript in its entirety in my dissertation. I will include acknowledgement of your contributions as an author to this manuscript as part of a footnote on the page of that chapter. In addition, a copy of this letter will be printed in an Appendix to my dissertation.

Please indicate your approval of this request by signing the endorsement below. I will be happy to answer any question or special request regarding this letter.

Think you for your time and consideration.

Prakash Raj Joshi

I hereby give my permission to Prakash Raj Joshi to reprint the manuscript entitled "Pulsed Laser Excited Photothermal Lens Spectrometry of CdS_xSe_{1-x} Doped Silica Glasses", co-authored by Oluwatosin O.Dada, and Stephen E. Bialkowski.

Signed 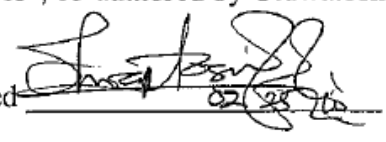 Date 02/25/2010

From: RIGHTS <Rights@aip.org>
Date: Wed, Apr 7, 2010 at 10:13 AM
Subject: Re: Fwd: copyright permission
To: p.r.joshi@aggiemail.usu.edu

Dear Dr. Joshi:

Thank you for requesting permission to reproduce material from American Institute of Physics publications.

Permission is granted – subject to the conditions outlined below – for the following:

"Analytical solution for mode-mismatched thermal lens spectroscopy with sample-fluid heat coupling,"
Journal of Applied Physics Volume 107, Issue 5, 053104 (2010).

To be used in the following manner:

Reproduced in your dissertation to be submitted to the Department of Chemistry and Biochemistry at Utah State University.

The American Institute of Physics grants you the right to reproduce the material indicated above on a one-time, non-exclusive basis, solely for the purpose described. Permission must be requested separately for any future or additional use.

Please let us know if you have any questions.

Sincerely,

Susann Brailey
~~~~~~~~~~~
Office of the Publisher, Journals and Technical Publications
Rights & Permissions
American Institute of Physics
Suite 1NO1
2 Huntington Quadrangle
Melville, NY 11747-4502
516-576-2268 TEL
516-576-2450 FAX
~~~~~~~~~~~

from: RIGHTS <Rights@aip.org>
to: Prakash Joshi <p.r.joshi@aggiemail.usu.edu>

date: Mon, May 17, 2010 at 12:04 PM
subject: Re: Permission letter
mailed-byaip.org

Dear Dr. Joshi:

Thank you for requesting permission to reproduce material from American Institute of Physics publications.

Permission is granted – subject to the conditions outlined below – for the following:

Journal of Applied Physics, Volume 107, Issue 8, 083512 (2010).

To be used in the following manner:

Reproduced in your dissertation for submission to the department of chemistry and biochemistry at Utah State University.

The American Institute of Physics grants you the right to reproduce the material indicated above on a one-time, non-exclusive basis, solely for the purpose described. Permission must be requested separately for any future or additional use.

Please let us know if you have any questions.

Sincerely,
Susann Brailey

~~~~~~~~~~~

Office of the Publisher, Journals and Technical Publications
Rights & Permissions
American Institute of Physics
Suite 1NO1
2 Huntington Quadrangle
Melville, NY 11747-4502
516-576-2268 TEL
~~~~~~~~~~~

516-576-2450 FAX
rights@aip.org

from: Gustavo Lukasievicz <lbgustavo@hotmail.com>
to: p.r.joshi@aggiemail.usu.edu

date: Wed, Apr 28, 2010 at 9:14 PM
subject: Permission to reprint the manuscripts
mailed-byhotmail.com

Dear Prakash,

I hereby give my permission to Prakash Raj Joshi to reprint the manuscript entitled “Pulsed-Laser Excited Thermal Lens Spectroscopy With Sample-Fluid Heat Coupling” co-authored by Nelson G. C.Astrath, Luis C. Malacarne, Gustavo V. B. Lukasievicz, Marcos P. Belancon, Mauro L. Baesso, Prakash R. Joshi, and Stephen E.Bialkowski

Regards,

Gustavo

Gustavo V. B. Lukasievicz
Universidade Estadual de Maringá
Av. Colombo 5790, CEP 87020-900
Maringá - Paraná - Brasil

---

from: lcmala@dfi.uem.br
to: Prakash Joshi <p.r.joshi@aggiemail.usu.edu>

date: Tue, Apr 20, 2010 at 6:58 AM
subject: Re: Permission letter request
mailed-by: dfi.uem.br

Dear
Prakash Raj Joshi

I hereby give my permission to Prakash Raj Joshi to reprint the manuscripts entitled "Analytical Solution For Mode-Mismatched Thermal Lens Spectroscopy with Sample-Fluid Heat Coupling", co-authored by Luis C. Malacarne, Nelson G. C. Astrath, Paulo R. B. Pedreira, Mauro L. Baesso, Renio S. Mendes, Prakash R. Joshi and Stephen E. Bialkowski and "Pulsed-Laser Excited Thermal Lens Spectroscopy With Sample-Fluid Heat Coupling" co-authored by Nelson G. C. Astrath, Luis C. Malacarne, Gustavo V. B. Lukasievicz, Mauro L. Baesso, Marcos P. Belancon, Prakash R. Joshi, and Stephen E.Bialkowski

Dr. Luis C. Malacarne
Departamento de Física
Universidade Estadual de Maringá
Maringá-PR, 87020-900, Brazil

from :Marcos Paulo Belançon <marcosbelancon@gmail.com>
to :p.r.joshi@aggiemail.usu.edu

date :Thu, Apr 15, 2010 at 1:13 AM
subject Fwd: Permission letter
mailed-bygmail.com
signed-bygmail.com

Dear Prakash,
I hereby give my permission to Prakash Raj Joshi to reprint the manuscript entitled "Pulsed-Laser Excited Thermal Lens Spectroscopy With Sample-Fluid Heat Coupling" co-authored by Nelson G. C. Astrath, Luis C. Malacarne, Gustavo V. B. Lukasievicz, Mauro L. Baesso, Marcos P. Belancon, Prakash R. Joshi, and Stephen E.Bialkowski

Regards,

Marcos Paulo Belançon
Universidade Estadual de Maringá
Departamento de Física
Av. Colombo 5790, CEP 87020-900
Fone: +55(44)3261-4330
Maringá - Paraná - Brasil

Marcos Paulo Belançon
Universidade Estadual de Maringá
Curso de Doutorado em Física
Université Claude Bernard Lyon I
LPCML - (+33) 04 72 43 29 71
Celular - (+33) 0633220268

from: Mauro Luciano Baesso (UEM) <mlbaesso@uem.br>
to: p.r.joshi@aggiemail.usu.edu

date:Thu, Apr 15, 2010 at 4:50 AM
subject ENC: Permission letter
mailed-byuem.br

Dear Prakash,
I hereby give my permission to Prakash Raj Joshi to reprint the manuscripts entitled "Analytical Solution For Mode-Mismatched Thermal Lens Spectroscopy with Sample-Fluid Heat Coupling", co-authored by Luis C. Malacarne, Nelson G. C. Astrath, Paulo R. B. Pedreira, Mauro L. Baesso, Renio S. Mendes, Prakash R. Joshi and Stephen E. Bialkowski and "Pulsed-Laser Excited Thermal Lens Spectroscopy With Sample-Fluid Heat Coupling" co-authored by Nelson G. C. Astrath, Luis C. Malacarne, Gustavo V. B. Lukasievicz, Mauro L. Baesso, Marcos P. Belancon, Prakash R. Joshi, and Stephen E.Bialkowski

Best regards,
Mauro L Baesso

XXXX
Universidade Estadual de Maringá
Departamento de Física
Av. Colombo 5790, CEP 87020-900
Fone: +55(44)3261-4330
Maringá - Paraná - Brasil

from :Nelson G. C. Astrath <astrathngc@pq.cnpq.br>
to :Prakash Joshi <p.r.joshi@aggiemail.usu.edu>

date :Wed, Apr 14, 2010 at 9:53 PM
subject :Permission letter
mailed-bypq.cnpq.br

Dear Prakash,

I hereby give my permission to Prakash Raj Joshi to reprint the manuscripts entitled “Analytical Solution For Mode-Mismatched Thermal Lens Spectroscopy with Sample-Fluid Heat Coupling”, co-authored by Luis C. Malacarne, Nelson G. C. Astrath, Paulo R. B. Pedreira, Mauro L. Baesso, Renio S. Mendes,Prakash R. Joshiand Stephen E. Bialkowski and“Pulsed-Laser Excited Thermal Lens Spectroscopy With Sample-Fluid Heat Coupling” co-authored by Nelson G. C. Astrath, Luis C. Malacarne, Gustavo V. B. Lukasievicz, Mauro L. Baesso, Marcos P. Belancon, Prakash R. Joshi, and Stephen E.Bialkowski

Regards,

Nelson

Nelson Guilherme Castelli Astrath
Universidade Estadual de Maringá
Av. Colombo 5790, CEP 87020-900
Fone: +55(44)3041-5910,+55(44)9944-9570
Maringá - Paraná - Brasil
---

from :Paulo Roberto Borba Pedreira <prbpedreira@gmail.com>
to :p.r.joshi@aggiemail.usu.edu

date :Wed, Apr 14, 2010 at 10:53 PM
subject :Permission to reprint
mailed-bygmail.com
signed-bygmail.com

Dear Prakash,

I hereby give my permission to Prakash Raj Joshi to reprint the manuscript entitled "Analytical Solution For Mode-Mismatched Thermal Lens Spectroscopy with Sample-Fluid Heat Coupling", co-authored by Luis C. Malacarne, Nelson G. C. Astrath, Paulo R. B. Pedreira, Mauro L. Baesso, Renio S. Mendes, Prakash R. Joshi, and Stephen E.

Regards,

Paulo Roberto Borba Pedreira
Universidade Estadual de Maringá
Departamento de Física
Av. Colombo 5790, CEP 87020-900
Fone: +55(44)3261-4330
Maringá - Paraná - Brasil

---

from; Renio dos Santos Mendes <rsmendes@dfi.uem.br>
to: p.r.joshi@aggiemail.usu.edu

date: Thu, Apr 22, 2010 at 5:12 AM
subject: Permission letter]
mailed-by: dfi.uem.br

Dear Prakash,

I hereby give my permission to Prakash Raj Joshi to reprint the manuscripts entitled "Analytical Solution For Mode-Mismatched Thermal Lens Spectroscopy with Sample-Fluid Heat Coupling", co-authored by Luis C. Malacarne, Nelson G. C. Astrath, Paulo R. B. Pedreira, Mauro L. Baesso, Renio S. Mendes, Prakash R. Joshi, and Stephen E. Bialkowski.

Regards,

Renio dos Santos Mendes
Universidade Estadual de Maringa
Departamento de Fi-sica
Av. Colombo 5790, CEP 87020-900
Fone: +55(44)3261-4330
Maringa - Parana - Brasil

CURRICULUM VITAE

Prakash Raj Joshi

Utah State University

Department of Chemistry and Biochemistry

Logan,Utah. 84322-0300

PROFESSIONAL STATUS: PhD Analytical Chemistry

PHONE : 435-797-6278

E-MAIL: p.r.joshi@aggiemail.usu.edu
: prjoshidu@yahoo.com

AREAS OF INTEREST

- Photothermal spectroscopy
- Synthesis and characterization of nanoparticles
- Raman, Fluorescence, IR Absorption and Emission Spectroscopy
- GC and HPLC
- Atomic Absorption and Emission Spectroscopy

EDUCATION

- Ph.D., Analytical Chemistry, Utah State University, US (2010)
- Dissertation: *Pulsed-Laser Exited Photothermal Study of Glasses and Nanoliter Cylindrical Sample Cell Based on Thermal Lens Spectroscopy*
- M. Phil., Physical Chemistry, Kathmandu University, Nepal (1999)
- Dissertation: *Synthesis, Characterization, and thermal studies of complexes of Copper (II), Mercury (II) and Cobalt (II) with sulfur and Nitrogen containing ligands.*
- M. Sc., Physical Chemistry, Tribhuwan University, Kathmandu, Nepal (1994)
- Dissertation: *Spectroscopic studies on Methylineblue crystal violet and complexes with Montmorillonite.*
- B. Sc., (Major: Chemistry, Zoology & Botany) Tribhuwan University, Kathmandu, Nepal (1989)

PROFESSIONAL EXPERIENCE

- Graduate research and teaching assistant, Department of Chemistry and Biochemistry, Utah State University (2005-2010)
- In-charge, Headed the department, Chemistry Department, Kathmandu University (2002-2005)
- Assistant professor, Kathmandu University, Nepal (2000-2005)
- Lecturer, Chemistry Department, Kathmandu University (1994-2000)
- Instructor, Chemistry Department, Kathmandu University (1993-1994)
- High School Science Teacher, Trinagar High School, Nepal (1989-1990)
- Member, Chemistry Subject Committee**,** Kathmandu University (1994-2002)
- Chairman, Chemistry Subject Committee**,** Kathmandu University (2002-2005)
- In-charge, Instrumentation Laboratory, Chemistry Department, Kathmandu University (2002-2005)
- Member, Faculty-Recruiting Committee, Chemistry Department, Kathmandu University (2002-2005)
- Expert Member of Arsenic Monitor for Water, Royal Nepal Academy of Science and Technology, RONAST (2002-2003)

COMPUTATIONAL SKILLS

Comsol Multiphysics (Finite element analysis modeling software)
Code V (Optical design software)

PROFESSIONAL SOCIETY AFFILIATIONS

American Chemical Society
Society for Applied Spectroscopy

AWARDS

National Education Award, 2002, Education Ministry, His Majesty Government of Nepal

PUBLICATION

- Prakash R. Joshi,Oluwatosin O. Dada, and Stephen E. Bialkowski "Pulsed Laser Excited Photothermal Lens Spectrometry of CdS_xSe_{1-x} Doped Silica Glasses" *Applied Spectroscopy*, **63** (7) 815-821(2009)

- Prakash R. Joshi, Oluwatosin O. Dada, and Stephen E. Bialkowski "Pulsed Laser Excited Photothermal Lens Spectrometry of Cadmium Sulfoselenide Doped Silica Glasses" *Journal of Physics: Conference Series* **214** (2010) 012117

- Luis C. Malacarne, Nelson G. C. Astrath, Paulo R. B. Pedreira, Renio S. Mendes, Mauro L. Baesso, Prakash R. Joshi, and Stephen E. Bialkowski "Analytical solution for mode-mismatched Thermal Lens spectroscopy with sample-fluid heat coupling" *Journal of Applied Physics,* **107** , 053104 (**2010)**

- Nelson G. C. Astrath, Luis C. Malacarne, Gustavo V. B. Lukasievicz, Marcos P. Belancon, Mauro L. Baesso,Prakash R. Joshi, and Stephen E. Bialkowski, "pulsed-laser excited thermal lens spectroscopy with sample-fluid heat coupling" *Journal of Applied Physics* **107,** 083512 (**2010**)

SCIENTIFIC MEETING AND PRESENTATIONS

- "Pulsed Laser Excited Photothermal Lens Spectrometry of CdS_xSe_{1-x} Doped Silica Glasses", Prakash R. Joshi Oluwatosin O. Dada, and Stephen E. Bialkowski. *237th American Chemical Society, ACS, National Meeting & Exposition March 22-26, 2009 Salt Lake City, UT*

- "Photothermal Lens Spectrometry in Nanoliter Cylindrical Sample Cells" Prakash R. Joshi, and Stephen E. Bialkowski *238th American Chemical Society, ACS, National Meeting & Exposition August 16-20, 2009 Washington, DC*